

GEO-INFORMATION IDENTIFICATION FOR EXPLORING NON-
STATIONARY RELATIONSHIPS BETWEEN VOLCANIC
SEDIMENTARY FE MINERALIZATION AND CONTROLLING
FACTORS IN AN AREA WITH OVERBURDEN IN EASTERN
TIANSHAN REGION, CHINA

JIE ZHAO

A DISSERTATION SUBMITTED TO
THE FACULTY OF GRADUATE STUDIES
IN PARTIAL FULFILLMENT OF THE REQUIREMENTS
FOR THE DEGREE OF
DOCTOR OF PHILOSOPHY

GRADUATE PROGRAM IN EARTH AND SPACE SCIENCE
YORK UNIVERSITY
TORONTO, ONTARIO

August 2013

© Jie Zhao, 2013

Abstract

GIS-based spatial analysis has been a common practice in mineral exploration, by which mineral potentials can be delineated to support following sequences of exploration. Mineral potential mapping is generally composed of geo-information extraction and integration. Geological anomalies frequently indicate mineralization. Volcanic sedimentary Fe deposits in eastern Tianshan mineral district, China provide an example of such an indication. However, mineral exploration in this area has been impeded by the desert coverage and geo-anomalies indicative to the presence of mineralization are often weak and may not be efficiently identified by traditional exploring methods. Furthermore, geological guidance regarding to spatially non-stationary relationships between Fe mineralization and its controlling factors were not sufficiently concerned in former studies, which limited the application of proper statistics in mineral exploration. In this dissertation, geochemical distributions associated with controlling factors of the Fe mineralization are characterized by various GIS-based spatial analysis methods. The singularity index mapping technique is attempted to separate geochemical anomalies from background, especially in the desert covered areas. Principal component analysis is further used in integrating the geochemical anomalies to identify geo-information of geological bodies or geological activities associated with Fe mineralization. In order to delineate mineral potentials, spatially weighted principal component analysis with more geological guidance is tried to integrate these identified controlling factors. At the end, as the first time been introduced to mineral exploration, a geographically weighted regression method is currently attempted investigate spatially non-stationary interrelationships presented across the space. Based on the results, superimposition of these controlling factors can be qualitatively and quantitatively summarized that provides a constructive geo-information to Fe mineral exploration in this area. From the practices in this dissertation, GIS-based mineral exploration will not only be efficient in mapping mineral potentials but also be supportive to strategies making of following mineral exploration. All of these experiences can be suggested to future mineral exploration in the other regions.

Acknowledgements

I would like to take this opportunity to express my sincere appreciation to my supervisor, Dr. Qiuming Cheng, for his academic guidance, patience, encourages, and most importantly, his moral role model during my doctoral study. He led me to not only reach the academic goal but also grow as an independent thinker which might be more significant for me to continue my study.

Besides, I would like to thank my supervisory committee members Dr. Gary T. Javis and Dr. Costas Armenakis at the Department of Earth and Space Science, York University. Their critical comments and constructive advises on my study had sufficiently improved this work. Thanks are also given to the colleagues Yinhuan Yuan, Linhai Jing, Xitao Xing, Jiangtao Liu, Ji Zhang, Lei Wang, and Zhijing Wang in my study group for their selfless help and time consuming on my study.

Last, I would like to thanks my beloved husband, Wenlei Wang who always encourages me to overcome any difficulties in both graduate study and life. His unwavering love and care had supported me to go through the extremely hard time. Thanks are also given to my mother Xiumei Xu and father Baoguo Zhao for their continuous understandings and encouragements.

Table of Contents

| | |
|---|-----|
| Chapter 1. Introduction | 1 |
| 1.1. Mineral potential mapping | 1 |
| 1.2. Spatial non-stationarity | 5 |
| 1.3. Fe mineralization and exploration in eastern Tianshan district, China | 8 |
| 1.4. Objectives | 11 |
| 1.5. Data employment | 14 |
| 1.6. Scope of dissertation | 17 |
| Chapter 2. Geological background | 23 |
| 2.1. Tectonic evolution of the study area | 23 |
| 2.2. Geological environment of Fe mineralization | 27 |
| 2.2.1. Tectonic settings | 27 |
| 2.2.2. Magmatism | 29 |
| 2.2.3. Stratigraphic framework | 30 |
| 2.2.4. Metallogeny of typical deposit | 33 |
| Chapter 3. Methodology | 37 |
| 3.1. Logratio transformation | 37 |
| 3.2. Singularity index mapping technique | 40 |
| 3.3. PCA and SWPCA | 43 |
| 3.3.1. Ordinary PCA | 43 |
| 3.3.2. SWPCA | 46 |
| 3.4. Student's <i>t</i> -value | 49 |
| 3.5. OLS and GWR | 51 |
| Chapter 4. Identification of fault systems | 55 |
| 4.1. Closure effect of geochemical data | 57 |
| 4.2. Identification of fault systems with logratio transformed geochemical data | 59 |
| 4.3. Identification of fault systems with Singularity mapping technique | 63 |
| 4.4. Summary and discussions | 70 |
| Chapter 5. Identification of felsic igneous rocks | 72 |
| 5.1. Identification of felsic igneous rocks with logratio transformed geochemical data | 75 |
| 5.2. Identification of felsic igneous rocks with Singularity mapping technique | 84 |
| 5.3. Conclusions | 88 |
| Chapter 6. Identification of the Yamansu Formation | 90 |
| 6.1. Identification of the Yamansu Formation with logratio transformed geochemical data | 91 |
| 6.2. Identification of the Yamansu Formation with singularity mapping technique | 98 |
| 6.3. Discussions | 102 |
| Chapter 7. Recognition of Fe mineralization | 103 |

| | |
|---|-----|
| 7.1. Geochemical signatures of Fe mineralization mapping | 104 |
| 7.1.1. Geochemical signatures of Fe | 104 |
| 7.1.2. Fe anomalies mapping | 105 |
| 7.2. Geochemical signatures of Fe mineralization associated elements mapping | 107 |
| 7.2.1. Geochemical signatures of element association | 108 |
| 7.2.2. Anomaly mapping | 109 |
| 7.3 Discussions | 112 |
| Chapter 8. Geo-information integration for mineral potential mapping by SWPCA model | 126 |
| 8.1. SWPCA model and definition of weighting factor | 128 |
| 8.2. Mapping of Fe mineralization by SWPCA | 130 |
| 8.3. Discussions | 132 |
| Chapter 9. Identification of spatially non-stationary relationships between Fe mineralization and its controlling factors | 139 |
| 9.1. Regression analysis | 142 |
| 9.1.1. OLS model | 142 |
| 9.1.2. GWR model | 145 |
| 9.2. Improvement of GWR to OLS | 147 |
| 9.3. Suggestions on Fe mineral exploration in eastern Tianshan mineral district | 149 |
| 9.4. Discussions | 152 |
| Chapter 10. Summary and conclusions | 166 |
| References | 172 |

List of Figures

| | |
|--|----|
| Fig.2. 1 Simplified geological maps. a. The study area and its tectonic settings (Modified from Yang et al., 1996 and Mao et al., 2005). A = the Kanggurtag-Harlik area. B = the Qiugemingtashi-Huangshan ductile shear zone. C = the Aqishan-Yamansu volcanic basin. (1) = the Kanggurtag-Huangshan fault. (2) = the Yamansu fault. (3) = the Aqikekuduke-Shaquanzi fault. (4) = the Toksun-Gangou fault. (5) = the Xingxingxia fault. (6) = the south-edge fault of middle Tianshan. b. The distribution of the lithologic units of the study area. | 26 |
| Fig.2. 2 Tectonic evolution model (Neoproterozoic-Early Permian) for eastern Tianshan mineral district (Modified from Su et al., 2011). | 35 |
| Fig.2. 3 Ore textures observed in the Yamansu Fe deposit. a. banded Fe ore composed of magnetite (black), pyrite (yellow) and garnet (reddish brown) (by Jie Zhao, summer 2010); b. massive Fe ore composed of magnetite (by Jie Zhao, summer 2010); c. disseminated Fe ore composed of magnetite (black), pyrite (yellow), quartz and feldspar (off-white) (by Jie Zhao, summer 2011); d. The mining pit of the Yamansu deposit. This picture was taking from the east to the west (by Jie Zhao, summer 2010). | 36 |
| Fig.3. 1 Schematic diagram of eigenvectors of principal components (PCs) and spatially weighted principal components (SWPCs) in 2-dimensional scenario. Blue area denotes the plot of observations on two variables X and Y. In this demonstration, the information contained by the first principal component is supposed to be enhanced. The comparison between these two methods can be extended to n-dimensional scenario. | 49 |
| Fig.4. 1 Scree plots of eigenvalues of PC1s of the four cases to recognize fault systems. | 66 |
| Fig.4. 2 Loading of PC1s of the four cases to recognize fault systems. | 66 |
| Fig.4. 3 Score maps of obtained PC1s to delineate spatial distributions of fault systems. a: Case 1; b: Case 2; c: Case 3; d: Case 4. | 68 |
| Fig.4. 4 PC1 scores of singularity indices of 4 selected geochemical signatures (i.e., Au, As, Hg, and Sb) for identification of fault systems. Fault traces and known Fe deposits are shown for reference. | 69 |
| Fig.5. 1 Scree plots of eigenvalues of PCs of the three cases to recognize felsic igneous rocks. | 78 |
| Fig.5. 2 Loading of PC1s and PC2s of the three cases to recognize felsic igneous rocks. a: Case 1. b: Case 2. c: Case 3. | 79 |
| Fig.5. 3 Score maps of obtained PCs to delineate spatial distributions of felsic igneous rocks. a: PC1 of log-transformed geochemical data in case 1. b: PC2 of alr transformed geochemical data in case 2. c: PC2 of alr transformed geochemical data in case 3. | 81 |
| Fig.5. 4 Score maps of obtained PCs to indicate changes of rock types. a: PC2 of log-transformed geochemical data in case 1. b: PC1 of alr transformed geochemical data in case 2. c: PC1 of alr transformed geochemical data in case 3. | 83 |

| | |
|--|-----|
| Fig.5. 5 PCA results using singularity indices of geochemical data. a: Scree plot of eigenvalues of principal components of singularity indices of geochemical data; b: Loadings of geochemical variables on PC1 of singularity indices of geochemical data. | 85 |
| Fig.5. 6 PC1 score maps of singularity indices of geochemical data. | 86 |
| Fig.6. 1 Scree plots of eigenvalues of PC1s of the two cases to recognize the Yamansu Formation. | 94 |
| Fig.6. 2 Loading of PC1s of the two cases to recognize the Yamansu Formation. | 95 |
| Fig.6. 3 Score maps of obtained PC1s to delineate spatial distributions of the Yamansu Formation. a: Case 1. b: Case 2. Outcrops of the Yamansu Formation and known Fe deposits are shown for reference. | 96 |
| Fig.6. 4 PC1 scores of singularity indices of 11 selected geochemical signatures for identification of the Yamansu Formation. Outcrops of the Yamansu Formation and known Fe deposits are shown for reference. | 101 |
| Fig.7. 1 Spatial distributions of Fe ₂ O ₃ concentration in eastern Tianshan mineral district. High values are corresponding to high Fe concentration. 7 subareas are circled in red color. From the west to the east, they are (1) the Xiaorequanzi volcanic basin, (2) the Aqishan-Bailingshan subarea, (3) the Kanggurtag-Tuwu subarea, (4) the east district of the Kumtag sand ridge, (5) the Yamansu volcanic basin, (6) the Shaquanzi subarea, and (7) the Jing'erquan subarea. | 113 |
| Fig.7. 2 Spatial distribution of singularity indices of Fe ₂ O ₃ concentration describing geochemical behaviors caused by Fe accumulation. Black triangles indicate the location of known Fe deposits and occurrences. | 114 |
| Fig.7. 3 PCA results for identifying geochemical signatures of element association related to Fe mineralization. a. Scree plots of eigenvalues of PCs; b. Loading of 8 selected geochemical signatures on PC1; c. Score map of obtained PC1 to delineate spatial distribution of geochemical signatures of element association. Known Fe deposits are shown for reference. | 116 |
| Fig.7. 4 PCA results for identifying singularity indices of geochemical signatures of element association related to Fe mineralization. a. Scree plots of eigenvalues of PCs; b. Loadings of singularity indices of 8 selected geochemical signatures on PC1; c. PC1 scores of singularity indices of geochemical signatures of element association. Known Fe deposits are shown for reference. | 118 |
| Fig.7. 5 Student's <i>t</i> -values calculated for measuring spatial relationship between known Fe deposits and a. the spatial distribution of Fe ₂ O ₃ concentration demonstrated in Fig. 7.1; b. the spatial distribution of singularity indices of Fe ₂ O ₃ concentration demonstrated in Fig. 7.2; c. PC1 of geochemical signatures of element association demonstrated in Fig. 7.3c; and d. PC1 of singularity indices of geochemical signatures of element association demonstrated in Fig. 7.4c. | 121 |
| Fig.7. 6 Optimum targets with highest probability of being underlain by known Fe deposits. The grey patterns in a. are derived based on thresholds of the 13 th class of the spatial distribution of Fe concentration demonstrated in Fig. 7.1; in b. are based on the 10 th class of spatial distribution of singularity indices of Fe concentration demonstrated in Fig. 7.2; in c. are based on the 21 st class of PC1 | |

| | |
|---|-----|
| scores demonstrated in Fig. 7.3c; and in d. are based on the 10 th class of PC1 scores demonstrated in Fig. 7.4c, respectively. The thresholds are determined by the Student's <i>t</i> -values illustrated in Fig. 7.5. | 125 |
| Fig.8. 1 SWPCA model. In the SWPCA model, controlling factors (i.e., fault systems, the Yamansu Formation and felsic intrusions) and geochemical signatures of the element association derived in the previous chapters are currently used as input variables. Weighting factor is defined in Fig. 8.2. | 134 |
| Fig.8. 2 Spatial distribution of the spatially weighting factor. The Euclidian distance of pixels from the intersections between the Yamansu Formation and felsic intrusions is currently used as the weighting factor in SWPCA model. The farther the pixel away from the intersection, the lower weighting value is assigned to the pixel. The pixels located out of the extent of the Yamansu Formation are weighting 0. Intersections between the Yamansu Formation and felsic intrusions are displayed for reference. | 135 |
| Fig.8. 3 Comparison of the statistics of PCA and SWPCA results. a: Scree plots of eigenvalues of PCs and SWPCs. b: Loadings of input variables on PC1 and SWPC1. | 136 |
| Fig.8. 4 Spatial distribution of interactions of fault systems, felsic igneous rocks, the Yamansu Formation and geochemical signatures of element association indicating favorable locations for Fe mineralization by a. PC1 scores and b. SWPC1 scores. Known Fe deposits are shown for reference. | 138 |
| Fig.9. 1 Regression coefficients estimated by GWR model. a, c, and e represent spatial distributions of non-stationary relationships between accumulation of element association and fault systems, felsic igneous rocks and the Yamansu Formation, respectively; b, d, and f represent the relationships limited to the target areas of Fe mineralization. | 159 |
| Fig.9. 2 R^2 values estimated by GWR model. a: Non-stationary distribution of R^2 value calculated by GWR model; b: A binary map of R^2 distribution defined by using the R^2 value of OLS model (i.e., $R^2 = 0.576$) as the threshold. | 161 |
| Fig.9. 3 Several other results of OLS. a: Predicted spatial distribution of $PC_{\text{association } i}$ by OLS model; b: The spatial distribution of residuals by OLS model. | 163 |
| Fig.9. 4 Several other results of GWR. a: Predicted spatial distribution of singularity indices of Fe_2O_3 concentration by GWR model; b: The spatial distribution of residuals by GWR model. | 165 |

List of Tables

| | |
|--|-----|
| Table 4. 1 Correlation coefficient matrixes calculated for 4 trace elements by logratio transformations using various dividers. a: log-transformation; b: sum of weight percent of all 4 oxides as the divider; c: weight percent of SiO ₂ as the divider; d: weight percent of Ba as the divider. | 60 |
| Table 4. 2 PCA results of singularity indices of 4 selected geochemical signatures for recognition of fault systems. | 64 |
| Table 5. 1 The properties of typical igneous-sedimentary related iron deposits in the eastern Tianshan district, China (modified from BGEDXP, 2009). | 74 |
| Table 5. 2 Correlation coefficient matrixes calculated for 7 oxides by logratio transformations using various dividers. Negative values are labeled in bold. a: log-transformation; b: sum of weight percent of all trace elements (i.e., 1-∑Oxide) as the divider; c: sum of weight percent of Ba, Be and Li as the divider. | 76 |
| Table 6. 1 Correlation coefficient matrix calculated for a: 11 log-transformed trace elements and b: 11 alr transformed trace elements using the weight percent of SiO ₂ as the divider. Negative values (in Table 6.1a) and the increased correlation coefficients (in Table 6.1b) are labeled in red. | 92 |
| Table 6. 2 PCA results of singularity indices of 11 selected geochemical signatures for recognition of the Yamansu Formation. | 101 |
| Table 7. 1 Statistical results showing the comparison of the efficiency in delineating the potential areas of Fe mineralization based on the spatial distribution of Fe ₂ O ₃ concentration (Fig. 7.1), singularity indices of Fe ₂ O ₃ concentration (Fig. 7.2), PC1 scores of geochemical signatures of element association (Fig. 7.3c) and PC1 scores of singularity indices of geochemical signatures of element association (Fig. 7.4c). | 119 |
| Table 9. 1 Depiction of four geo-variables employed in regression analysis. | 155 |
| Table 9. 2 Diagnostic parameters calculated by OLS and GWR models. | 156 |

Chapter 1. Introduction

1.1. Mineral potential mapping

Mineral exploration objective to discover mineral deposits involves a series of procedures which are area reduction, reconnaissance exploration, preliminary follow-up and detailed follow-up (Hodgson, 1990; Moon et al., 2009). The area reduction to depict areas with mineral potentials is among the most important, since all following sequences are based on the delineation to the target of interesting (Hodgson, 1990; Haldar, 2102; Carranza et al., 2009). In practice, mineral potentials are mapped based on the knowledge of objective mineral deposits. The knowledge are descriptive features of the deposit types, controlling factors of mineralization, spatial distributions of indicators to deposits, and other useful geo-information in support of mineral exploration (Cheng, 2012; Hodgson, 1990). In general, main criteria selected for mineral potential mapping are based on conceptual and empirical models (Woodall, 1994). The conceptual model is derived from geological theories, while the empirical model is dependent on experiments. Nowadays, development in computer sciences and Earth observation techniques has greatly facilitated broad utilization of geographic information system (GIS)-based spatial analysis. Well performed in data capture, manipulation, visualization, analysis, and sharing GIS has become one of the main approaches in support of mineral exploration (Bonham-Carter, 1994; Carranza,

2008; Chung and Agterberg, 1980; Chung and Moon, 1990; Haldar, 2012; Harris, 1989; Harris et al., 2001; Moon et al., 2006; Pan and Harris, 2000; Singer and Kouda, 1997).

Benefiting from the construction of geo-database worldwide (Darnley, 1995), more and more ground and underground properties can be investigated that provides multisource geo-information indicative to mineralization. The most commonly used geo-datasets are geochemical, geophysical, geological and other remotely sensed observations. In practice, potential mapping or mineral exploration model is composed of two principal modules.

The first module is geo-information or geo-anomaly extraction. Geological model (i.e., conceptual and/or empirical model) delivering informative characteristics and reliable interpretation to metallogeny of objective deposits (Bonham-Carter, 1994; Hodgson, 1990; Moon et al., 2006) serves as criteria for selecting potential areas. According to the model, geological issues associated with mineralization, so-called as controlling factors can be determined, properties of which are the geo-information of interest. Mineralization is a cascade geo-process (Cheng, 2007, 2012; Cheng and Agterberg, 2009). Its associated geo-activities (e.g., tectonism, magmatism, alteration, etc.) cause the formation of certain geological features or bodies (e.g., faults or folds, igneous intrusions or extrusions, ore bodies etc.) and accompanied presences of geo-anomalies. Due to the physical or chemical differences with their surrounding, geo-anomaly is

identifiable. Fortunately, the geo-anomaly termed as geo-information can be used to indicate occurrences of these geological activities (Zhao, 1999). In general, geo-information extracted from geological map is indicative to spatial locations of geological occurrences (e.g., mineral occurrences, igneous rocks, fault traces), appropriate spatial analysis (e.g., buffer analysis) on the geo-information can assist to determine mineralization favored spaces (Agterberg et al., 1990; Bonham-Carter, 1994). Since some of geological data were collected from filed surveys, geological units of some inaccessible areas might not be informative. Therefore, newly received exploratory datasets (e.g., geochemical and geophysical data) can be supplementary geo-information resources to the location information. Commonly used methods to extract geo-anomalies are spatial statistics and frequency analysis (Cheng, 2007; Cheng et al., 2009). Since the introduction of fractal and multifractal theory by Mandelbrot (1972), fractal and multifractal approaches have been extensively accepted by its advantages to consider both frequency and spatial properties of geo-issues (Cheng, 2012; Wang et al., 2012, 2013; Zhao et al., 2012; Zuo et al., 2009b). In Cheng et al (1994), a concentration-area (C-A) model was proposed and used to separate geochemical anomalies from background according to fractality of geochemical distributions. After that, a fractal and multifractal based singularity index mapping technique proposed by Cheng (1999) has been introduced to extract geo-anomalies from various sources of observational datasets. A series of practices had proved the efficiency of singularity index mapping technique in identification of

weak anomalies from a strong variance of background (Ali et al., 2007; Bai et al., 2010; Cheng, 2007; Wang et al., 2011, 2012, 2013; Zhao et al., 2012; Zuo et al., 2009a).

The second module is geo-information integration. Since mineralization is caused by the interactions of associated geological factors across the space, the integration is to delineate the combining effects of these factors the spatial distribution of which is consequently believed as favorable spaces of mineralization (Bonham-Carter, 1994). In real practice, the integration is the weighted sum of all geo-information. Although numerous methods assigning weights to these factors have been broadly introduced in many references, the three main types of integration methods consisting of data-driven, knowledge-driven and hybrid are still valuable to be repeated in all related documents. Data-driven methods assign weights to predictor maps according to their significance to training data (e.g., known mineral occurrences), results of which are dependent on calculation rather than theories or experience. Some commonly employed data-driven methods are weights of evidence (WofE) (Bonham-Carter, 1994), neural networks (Singer and Kouda, 1996; Harris and Pan, 1999), and principal component analysis (Jolliffe, 2002). On the contrary, knowledge-driven methods require experts assign weights to predictor maps. Practiced knowledge-driven methods include Index overlay (Renez et al., 1994; de Araujo and Macedo, 2002), Fuzzy logic (An et al., 1991; Brown et al., 2003; Knox-Robinson, 2000), and Analytical hierarchy process (AHP) (Harris et al., 1995). Although

knowledge-driven methods are dependent on theories and experiences, the assigned weights without appropriate quantification are somehow subjective. In recent decades, geological interpreters have been noticed the importance of joint usages of both data- and knowledge-driven methods. In Cheng and Agterberg (1999), a fuzzy weights of evidence method was introduced as a hybrid of both data- and knowledge-driven methods to map mineral potentials. The weights assigned to predictor maps are based on considerations of both quantification and geological experiences. Furthermore, in Cheng (2006) a spatially weighted principal component analysis (SWPCA) method was proposed, by which a weighting factor can be used to highlight the objective geo-information by modifying the correlation coefficient matrix of input variables. The weighting factor serving geological guidance makes the integration more informative to the targets of interest. More detailed introductions to integration methods can be found in Bonham-Carter (1994) and Harris and Sanborn-Barrie (2006).

1.2. Spatial non-stationarity

Spatial non-stationarity describes location-dependent relationships between variables (Brunsdon et al., 1996; Fotheringham et al., 1996a). Inherited from natural processes and/or human activities, it is broadly existed (Gao and Li, 2011). For examples, due to some specific reasons (e.g., degrees of urban development, population, transportation, etc.), relationships between agreed sale price and floor area of a house may vary

significantly in different cities (Brunsdon et al., 1999, 2002); caused by geographical variations (e.g., topography, landform, vegetation, etc.), relationships between rainfalls and altitude are varying across the space (Brunsdon et al., 2001); and relationships between urban temperature and land surface can be varied by both environmental (e.g., elevation and slope orientation) and human factors (e.g., highway infrastructure and greenbelt construction) (Li et al., 2010). In geological exploration, mineralization produced by a series of geological activities is a complex geo-process. The relationships existed between mineralization and associated geological activities present spatial non-stationarity as well. It explains why mineralization can only occur at limited locations. Being an integral concept, a deposit model is a gross functional form, according to which relationships between mineralization and its controlling factors are described and measured as general trends which may mis-specify localized reality and incorrectly represent relevant variables at different locations. In this study, a new deposit model which allows relationships between mineralization and its controlling factors to be described and measured at localized scale is proposed. This model is mean to calibrate the errors existed in the integral model generated by previous researches.

In the second module of mineral exploration modeling, mineralization caused by the interactions of its controlling factors can be depicted by the weighted sum of predictor maps (i.e., geo-information of controlling factors), the result of which is suggestive to following mineral exploration sequences. However, many delineated target areas are

not completely or well coincident with known mineral occurrences. It might be due to the data quality or method limitation. Since the data quality is an uncontrollable issue for geological interpreter, current study only discusses the limitations of integration methods. As described in geological references, the interactions of the controlling factors are spatially varied across the space that is spatial non-stationarity, and caused by interactions of various controlling factors, different types of mineralization occurred at specific locations. It indicates that the spatially varied (i.e., non-stationary) interactions across the space might be the reason why different types of mineral deposits can be discovered within an area. By the integration model, weight with constant value is assigned to a predictor map that cannot represent its spatially non-stationary controlling effects to mineralization. Consequently, the integration results will be coincident with a certain mineral types rather than comprehensively indicative. The former integration only provides a spatial distribution of mineral potentials according to recognition of a certain metallogeny (i.e., geological model), which was spatially stationary. More improved understandings to the mineralization cannot be achieved. If spatial variations of interactions of controlling factors can be interpreted in a spatial scenario, then not only the prediction will become comprehensive but also the following exploration sequences will be benefitted significantly.

1.3. Fe mineralization and exploration in eastern Tianshan district, China

The Tianshan region produced by a Palaeozoic orogeny extends east-west for more than 2,500 km in central Asia (Allen et al., 1992; Windley et al., 1990). The study area of current research located in the east part of the Tianshan region, so-called as eastern Tianshan region, with the longitude of 88°30'-96°30' and the latitude of 41°30'-42°30'. The study area is sparsely populated. Except desert regions, transportations are convenient. LanXin railway and highways stretching across the study area are the primary channels connecting Xinjiang province and eastern of China. Geographically, eastern Tianshan is a typical Gobi desert covered gently hilly area, where relative elevation differences are within a few tens of meters. Diurnal temperature swings can reach 50°C that causes serious physical denudation of exposed rocks. Sand storms occur frequently due to the extremely dry climate with an average annual precipitation less than 48 mm. Produced by seasonal mountain floods, rivers in the study area present temporarily. All of these severe climatic conditions had greatly impeded the geological exploration in this area.

Being one of the most productive mineralization districts in China, eastern Tianshan mineral district which possesses extraordinary preserves of metallic resources, including copper, nickel, gold, silver, molybdenum, rhenium, etc. has long been a focus of geological concerns (BGEDXP, 2009; Ma et al., 1993, 1997; Mao et al.,

2005). Particularly, with the proceeding of mineral exploration in this area, marine volcanic sedimentary Fe deposits with great production and abundance have become a focus of study in recent decades (BGEDXP, 2009). Although metallogeny of typical Fe deposits (e.g., Yamansu, Hongyuntan, Bailingshan, Tieling, etc.) were studied by geologists in China for a long time, arguments on it were common. Accompanied with the development of techniques and the knowledge, different opinions on the metallogeny of Fe deposits reached to the unity, gradually. In recent years, geologists in an growing number held that Fe mineralization is mainly associated with complex tectono-magmatism, including fault activities triggered by Palaeozoic plate collision between the Junggar and the Tarim plates, the volcanic eruption in the Early Carboniferous accompanied with sedimentation of bimodal volcanic strata and primary Fe ores, the Late Carboniferous emplacement of granitoid intrusions into volcanic strata, and the alteration of primary Fe ores by hydrothermal fluids differentiated from granitoid intrusions (BGEDXP, 2009; Ding, 1990). Based on this geological model of volcanic sedimentary Fe deposits, main components of traditional mineral exploration are composed of fault systems, the Carboniferous volcanic strata, volcanic edifices, and alteration zones (BGEDXP, 2009).

Following the mineral potential mapping strategies introduced in last section, geo-information of these controlling factors need to be extracted from various observational datasets and integrated by the three types of methods. However, current

study area is located in the Gobi desert where the Fe exploration was significantly impeded by ground coverage (e.g., regolith, tepetate and aeolian sand) (Xie and Wang, 2003; Zhuang et al., 2003). The location-based spatial analysis is difficult to interpret mineralization associated geological features in this area due to the deficiency of outcrops. Consequently, extracting geo-information or geo-anomaly from secondary exploratory datasets (e.g., geochemical and geophysical data) rather than observations seems more helpful to support mineral potential mapping. Nevertheless, the real practice is still facing problems of ground cover effects. Due to ground coverage, geo-anomalies coincident with mineralization might be hidden in a strong variance of background (Cheng et al., 2012; Zhao et al., 2012). Traditionally used geo-information extraction methods such as delineating target areas based on concentration values (e.g., weight percent, quantile, and mean \pm standard deviation) of elements or element assemblages cannot satisfy Fe exploration in these covered areas, because the values are frequently very low. Therefore, advanced approaches to enhance weak anomalies are necessary to be employed. In addition, spatial distributions of controlling factors should be concerned by various observational datasets and advanced spatial analysis as well, since their location information masked by ground coverage may mislead the exploration modeling. In the aspect of geo-information integration for mapping mineral potentials, more geological guidance should be involved to calibrate the shortages of former implementations.

Moreover, in order to enhance the low degrees of exploration in this area, the spatially non-stationary influences of controlling factors on Fe mineralization should be appropriately investigated. According to the knowledge regarding to the spatially varying relationships, exploration strategies within reduced areas (i.e., target areas) can be suggested to following sequences of mineral exploration that is hitherto unobserved geo-information.

1.4. Objectives

For the Fe exploration in eastern Tianshan mineral district, China, the latest exploration model is the integration of geo-information extracted from location information, geochemical and geophysical anomalies (BGEDXP, 2009). Efficiency of indication of Fe mineral potentials is highly reduced by effects of ground coverage. Furthermore, the results from geo-information integration can only present target areas where following exploration procedures can be carried out; other information regarding to exploration strategies (e.g., spatial distribution of controlling factors and their spatially non-stationary influences on Fe mineralization) will not be informed. This dissertation has three main objectives:

First of all, current study intends to achieve better knowledge regarding to the controlling factors of volcanic sedimentary Fe mineralization in eastern Tianshan mineral district. In this desert covered area, geo-anomalies associated with the Fe mineralization have been concerned by advanced spatial analysis techniques in a long

time; whereas, analysis of controlling factors of the mineralization (e.g., geological activities or processes) are still relied on location information (i.e., geological map) which are greatly impeded by the effects of ground coverage. In eastern Tianshan mineral district, physical transport (e.g., by aeolian and fluvial processes) of weathering products in the study area results lateral drift of overburden (e.g., regolith and exotic sediments). Mechanical dispersion of exposed rocks can produce high regional elemental background in their surrounding areas (Wang et al., 2003). In contrast, dispersion of exotic materials may produce low regional elemental background above covered rocks (Wang et al., 2001). From a geological point of view, formation of fault systems, igneous rocks, and deposits are accompanied by enormous energy release and material accumulation, which may be identified by singular differences with their surroundings (Cheng, 2007; Wang et al., 2011). Tracked in stream sediments (Rose et al., 1979; Davenport, 1990; Harris et al., 2001; Rencz et al., 2002), the singular differences can be recognized as geo-anomalies in stream sediment geochemical data. Therefore, it is important that spatial analysis of geochemical data allows removal of the influences of overburden on bedrock signal and identification of not only strong anomalies but also weak anomalies from background. In this dissertation, advanced geo-anomaly extraction methods consisting of the singularity index mapping technique and principal component analysis (PCA) are jointly used to separate weak geo-anomalies from background for characterization of the Fe mineralization associated geo-processes (i.e., controlling factors).

Second of all, current study intends to provide a more reliable and improved geo-information integration for Fe mineral potential mapping. As discussed in former section, both data- and knowledge-driven integration methods might be subjective or arbitrary in many cases. In this dissertation, a hybrid geo-information integration method, SWPCA is applied which employs a spatially weighting factor with geological significance highlighted to estimate weights of all predictor maps. In comparison with data- or knowledge-driven methods, current result will be more powerful in geo-information integration due to the addition of geological significance based on specific mineralization model.

Thirdly, current study intends to provide a new geo-information to enhance the knowledge of spatially non-stationary relationships between Fe mineralization and its controlling factors. In addition to mapping mineral potentials, there are more necessary concerns to interactions or relationships between geological activities or processes, knowledge of which will not only improve mineral potential mapping but also enhance understanding of metallogeny. Regression analysis is one of the commonly used methods to examine relationships among geo-variables. Relationships between each pair of geo-variables can be estimated and described by a regression coefficient and further used to determine the influence of independent variables on dependent variable. As described in former sections, the influences of controlling factors on mineralization exhibit spatial heterogeneity and non-stationarity. In order to

enhance the efficiency of Fe mineral exploration in this area, knowledge regarding to the spatially varied (spatially non-stationary) relationships between Fe mineralization and its controlling factors are necessary. Reviewing former GIS-based mineral exploration modeling, only target areas with higher possibility of mineralization can be suggested to the follow-up. Location information available to later exploration requires more detailed investigation on metallogeny to determine exploration strategies. In this dissertation, geo-information characterizing Fe mineralization and three controlling factors (i.e., fault systems, felsic intrusions, and volcanic strata) are assigned to be the dependent variable and independent variables, respectively; furthermore, both ordinary least square (OLS) regression and geographically weighted regression (GWR) are applied to investigate the objective relationships. Achieved results will provide more important and informative guidance to following sequences of the Fe exploration in this area.

1.5. Data employment

Exploratory geo-datasets employed in this research which are produced by China Geology Survey include stream sediment geochemical data in a scale of 1:200,000 and geological data acquired from 1:200,000 geological databases.

Recording geochemical signatures inherited from bedrocks, geochemical data are commonly used to identify geochemical anomalies associated with various geological bodies and to interpret geological phenomena (Bogoch et al., 1993; Brantley and

White, 2009; Cheng, 2007; Hao et al., 2007; Wang et al., 2011, 2012; Zhao et al., 2012). As part of the “Regional Geochemistry National Reconnaissance (RGNR) Project”, the stream sediment geochemical data used in this research were collected and analyzed by Chinese National Geochemical Mapping Project. The severe blowing transportation and accumulation related to strong wind in this area cause the stream sediment at/near surface to be diluted by mixing of aeolian sand, and the dilution can greatly change and blur the elemental concentration in stream sediments (Ren et al., 1989). In order to reduce the impact of aeolian sand, the samples in the size greater than 2 mm are ideal for geochemical analysis because most of the aeolian materials are smaller than this size. The coarse-grained materials can be migrated by the seasonal floods within the watercourses and finally deposited in drainage basins. The samples were collected along the watercourses and drainage basins in an interval of 1-4 km². Tepetate is another dominating cover type in the study area, which can block off the realistic elemental concentration in stream sediments. Samples in tepetate covered area are mainly collected from elurium under the tepetate layers in an interval of 1-2 km² (Xie et al., 2009). Within the samples, 39 major, minor, trace and subtrace elements/compounds were mainly analyzed by means of X-ray Fluorescence (Xie et al., 1997; Zhuang et al., 2003). The concentration of these elements/compounds is further smoothed by averaging all samples within each 2×2 km² cell. Detail information about the RGNR can be found in Xie et al. (1997).

Based on Zavaritskii geochemical classification of the elements, the 39 elements/compounds can be classified into 8 categories: (1) rock-forming elements (i.e., Li, Be, Na, Mg, Al, Si, K, Ca, Sr, and Ba); (2) volatile elements (i.e., B, F and P); (3) iron family elements (i.e., Ti, V, Cr, Mn, Fe, Co, and Ni); (4) rare elements (i.e., Y, Zr, Nb, and La); (5) radioactive elements (i.e., U, and Th); (6) group 6 elements (i.e., Mo, W); (7) metal metallogenic elements (i.e., Cu, Ag, Au, Zn, Cd, Hg, Sn, and Pb); (8) semimetal and heavy mineralizer elements (i.e., As, Sb, and Bi). Element associations are frequently used as indicators to identify geologic units (e.g., granite with radioactivity caused by the containment of U and Th, and mafic-ultramafic igneous rocks characterized by enrichment of iron family elements, etc.) and further benefit mineral exploration (Cheng et al., 2011; Zhao et al., 2012).

The earliest geological mapping in the study area can be dated back to late 1950's. Revisions of these maps had been finished until early 1990's. The revised geological maps perform better in depicting the geological setting of the study area, which had been widely used in scientific researches in China. The construction of digital geologic map database had been started from 1996 and ended by 2001. All data were digitized from the geologic maps achieved previously. After that, the database was maintained during 2002 to 2003. The current research involves fifteen 1:200,000 map sheets, and spatial distributions of tectonic settings, lithological units, ore deposits, geographical features, etc. are characterized (BGEDXP, 2009).

1.6. Scope of dissertation

This dissertation is composed of ten chapters, for each chapter, discussion on a specific topic will be delivered.

In chapter 2, detailed geological background of the study area and metallogeny of typical Fe deposits (i.e., Yamansu deposit) are introduced. Literatures regarding to major faults, felsic igneous rocks, and lithology of strata formed in this area and their influences on Fe mineralization are reviewed.

In chapter 3, detailed explanations of employed methods to identify geochemical signatures of controlling factors of Fe mineralization are provided. Development and utilization of these methods in other researchers are briefly reviewed. Logratio transformation and singularity mapping technique is used to extract geo-information from stream sediment geochemical data sets. The derived geo-information will further be integrated to identify the spatial distribution of Fe mineralization related geological bodies (i.e., controlling factors) by principal component analysis (PCA) and spatially weighted principal component analysis (SWPCA). The Student's *t*-test in the context of weights of evidence (WofE) is employed to delineate potential areas of Fe mineralization. At the end, regression analysis including ordinary least square (OLS) and geographically weighted regression (GWR) are used to estimate spatially non-stationary relationships existed between Fe mineralization and its controlling factors.

In chapter 4, geo-information of fault systems in eastern Tianshan mineral district are extracted from stream sediment geochemical data. Stream sediment geochemical data is a compositional data or closed system. Confined by a constant sum (e.g., 1 and 100%), element concentration is recorded in weight percent rather than absolute values. In order to open the closed system and analyze geochemical data with standard statistical methods (e.g., PCA), the logratio transformation is employed to preprocess element concentrations. 4 case studies of the logratio transformation with different dividers are demonstrated. After that, geochemical anomalies of element association composed of logratio transformed Au, As, Sb and Hg are assigned as the indicator of fault systems. On the other hand, the singularity index mapping technique is applied to characterize enrichment or depletion of a certain element, results of which are used to indicate the geochemical behaviors of elements in space. Combining singularity indices of Au, As, Sb and Hg with PCA, the result characterizing geochemical behaviors of element association is accepted as the indicator of fault activities. Comparing the two multivariate processes, the PCA result of singularity indices of element association depicting not only spatial presence of geochemical signatures of fault systems but also geochemical behaviors of element association is prior to the PCA result of logratio transformed geochemical data in indicating fault activities.

In chapter 5, similar data processing procedures as chapter 4 are applied to

geochemical data to derive geochemical signatures related to felsic igneous rocks. For identification of felsic igneous rocks, the element association consisting of SiO_2 , Al_2O_3 , K_2O , Na_2O , CaO , MgO , Fe_2O_3 , Ba, Be, and Li are employed. In order to decompose the closed system, 3 case studies of logratio transformation with different dividers are demonstrated. After that, PCA is applied to integrate the logratio transformed geochemical data to indicate the geochemical signatures of felsic igneous rocks. Since the formation of igneous rocks is a singular geo-process, singularity index mapping technique is currently applied to characterize singularly distributed element concentrations. By PCA, singularity indices of 10 selected element concentrations are integrated to demonstrate geochemical signatures of element association related to felsic igneous rocks. The result representing felsic activities are preserved for further analysis in latter chapters.

In chapter 6, geochemical signatures of the Carboniferous Yamansu volcanic strata are identified by PCA results of both logratio transformed and singularity indices of geochemical signatures of the element association. The element association related to the Yamansu Formation is composed of Cu, Pb, Zn, Au, Ag, Bi, Mo, W, As, Hg, and Sb. Based on the conclusion derived from chapters 4 and 5, the logratio transformation with SiO_2 as the divider is applied to geochemical data before PCA. Furthermore, the PCA result of singularity indices of element association performs better than of the logratio transformed element association in depicting the spatial

distribution of Yamansu volcanic strata. The former one is consequently kept for further usage of mineral exploration modeling.

In chapter 7, singularity index mapping technique is applied to depict spatial variations of geochemical signatures associated with Fe mineralization, the result of which can eliminate influences of both Fe-rich rocks and sandy coverage. In addition, compared to a single element, the element association with more reliable geo-information of Fe mineralization is analyzed to depict potential areas. The Student's *t*-test is applied to delineate the favorable places of Fe mineralization. By comparing the statistics of each evidence layers in mapping target areas, the PC1 score map of singularity indices of the element association with more confidence in indicating geo-information of Fe mineralization and higher efficiency in delineating target areas are retained for the usage of following chapters.

In chapter 8, as a PCA extension, spatially weighted principal component analysis (SWPCA) is applied to integrate Fe mineralization associated geo-information derived from previous chapters (i.e., chapters 4, 5, 6 and 7). By this method, a spatially weighing factor objective to highlight favorable spaces of the Fe mineralization is applied to calculate correlation coefficient matrix. In comparison with the results of ordinary PCA, it can be found that SWPCA can generate more geologically reliable integration results for mineral exploration.

In chapter 9, spatially non-stationary relationships between Fe mineralization and it

controlling factors are investigated. Both ordinary least square (OLS) and geographically weighted regression (GWR) models are employed. Results by GWR quantitatively depict non-stationary influences of tectono-magmatism on Fe accumulation in spatial scenario, which demonstrate the significant improvement in parameter estimation. Examining regression coefficients, it can be inferred that Fe mineralization at different locations in eastern Tianshan mineral district was caused by interactivities of multiple geo-processes to different degrees, and these variations can be demonstrated by the GWR results as well.

In chapter 10, the proposed exploration model of volcanic sedimentary Fe deposits in eastern Tianshan mineral district in this dissertation is reviewed. In addition, experiences through this study are summarized and discussed. Future works regarding to mineral exploration modeling are suggested to following Fe exploration sequences in eastern Tianshan mineral district.

Regarding to the researches introduced in this dissertation, a list of papers had been published or submitted:

1. One paper in respect to the identification of felsic igneous rocks had been published in the Journal of Geochemical Exploration:

Zhao, J., Wang, W., Dong, L., Yang, W., Cheng, Q., 2012. Application of geochemical anomaly identification methods in mapping of intermediate and

felsic igneous rocks in eastern Tianshan, China. *Journal of Geochemical Exploration* 122, 81-89.

2. One paper in respect to the logratio transformation had been submitted to the *Journal of Geochemical Exploration*:

Wang, W., Zhao, J., Cheng, Q., Liu, J., (Under review) Mapping of Fe mineralization-associated geochemical signatures using logratio transformed stream sediment geochemical data in eastern Tianshan, China.

3. Two papers in respect to GWR had been submitted to the *Journal of Geochemical Exploration* and *Ore Geology Review*, respectively:

Zhao, J., Wang, W., Cheng, Q., 2013a. Investigation of spatially non-stationary influences of tectono-magmatism on Fe mineralization in eastern Tianshan, China with geographically weighted regression. *Journal of Geochemical Exploration* (2013), doi: 10.1016/j.gexplo.2013.07.008.

Zhao, J., Wang, W., Cheng, Q., 2013b. Application of spatially weighted principal component analysis in support of Fe exploration in eastern Tianshan mineral district, China. *Ore Geology Reviews* (2013), doi: 10.1016/j.oregeorev.2013.08.005.

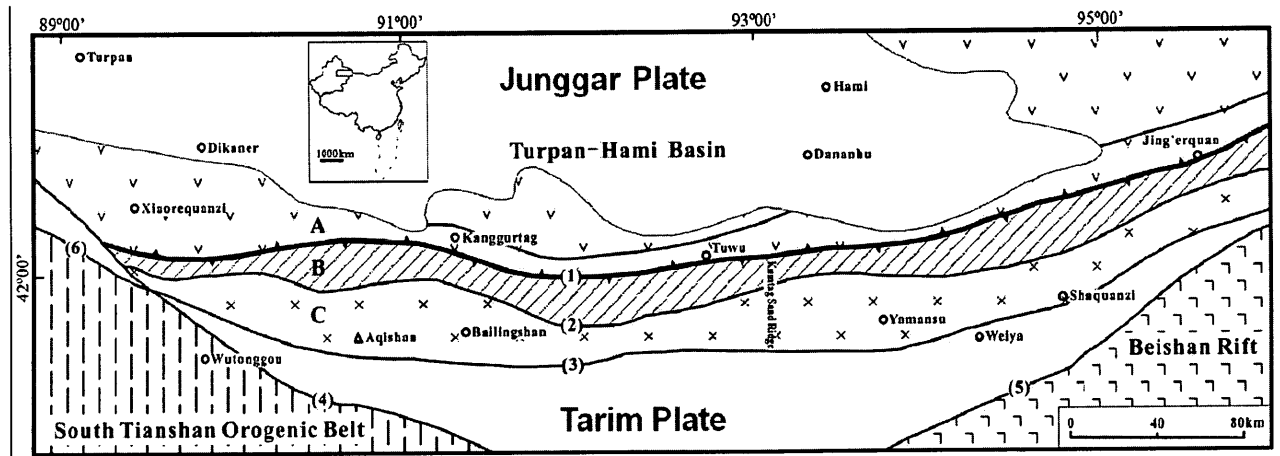
Chapter 2. Geological background

The study area, eastern Tianshan mineral district is a strip area bounded to the west by the Xiaorequanzi area, to the east by the Late Paleozoic Beishan rift, to the north by the Turpan-Hami basin, and to the south by the Aqikekuduke-Shaquanzi fault zone (Mao et al., 2005; Wang et al., 2006). It is a typical Gobi desert region with intensive physical and chemical weathering (BGEDXP, 2009). Complex geo-processes within the study area during the geological history produced favorable environment for Fe mineralization. Previous literatures illustrate that volcanic sedimentary Fe mineralization in eastern Tianshan mineral district is genetically related to a series of tectono-magmatism consisting plate collision and expansion, volcanism, emplacement of magmatic intrusion, hydrothermal alteration, etc.

2.1. Tectonic evolution of the study area

From former researches (Feng et al., 2002; Ma et al., 1993; Su et al., 2011; Wang et al., 1994; Zhang et al., 2005), complex plate tectonic evolution in this area was developed through a long geological history. In the Ordovician, due to the *B* type subduction of the ancient Tianshan oceanic crust (north) under the Tarim crust (south), magmatism, metamorphism and migmatism were intensively occurred along the northern edge of the Tarim continental crust. In the Silurian, plate tectonic activities became complex. Following the *B* type subduction in the Ordovician, the

Turpan-Hami micro-continent situated in the Tianshan oceanic crust collided and collaged onto the Tarim crust (i.e., the *A* type subduction). After that, accompanying with formations of the Bogurda-Harlik and the Aqishan-Yamansu volcanic arcs, a new *B* type subduction zone along the north edge of the Turpan-Hami continent was developed. Meanwhile, influenced by the rift expansion between these two arcs, the Kanggur inter-arc basin was produced. In the Late Carboniferous, the continuous *B* type subduction of the Tianshan oceanic crust triggered closure of the Kanggur basin which led to the *A* type subduction of these two arcs. Consequently, granitoid magmatism (e.g., emplacement, differentiation, and hydrothermal alteration) was spreading over the suture zone. At the end of the Late Carboniferous, the Tianshan oceanic crust moved underneath the Tarim crust, and the collision between the Junggar crust and the Turpan-Hami continent occurred.



a

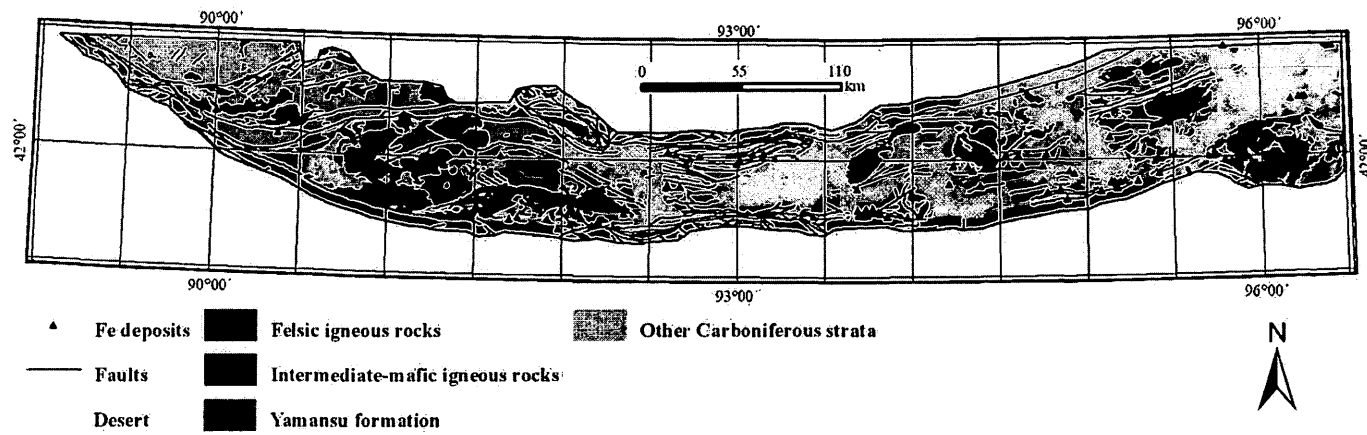


Fig.2. 1 Simplified geological maps. **a.** The study area and its tectonic settings (Modified from Yang et al., 1996 and Mao et al., 2005). A = the Kanggurtag-Harlik area. B = the Qiugemingtashi-Huangshan ductile shear zone. C = the Aqishan-Yamansu volcanic basin. (1) = the Kanggurtag-Huangshan fault. (2) = the Yamansu fault. (3) = the Aqikekuduke-Shaquanzi fault. (4) = the Toksun-Gangou fault. (5) = the Xingxingxia fault. (6) = the south-edge fault of middle Tianshan. **b.** The distribution of the lithologic units of the study area.

2.2. Geological environment of Fe mineralization

2.2.1. Tectonic settings

The southward subduction of the Tianshan ocean crust (as a part of the Junggar plate) to the Tarim crust in the period of the Ordovician to the Late carboniferous produced the generally EW trending structural framework of this district (Wang et al., 1994). Three EW trending faults including the Kanggurtag-Huangshan fault, the Yamansu fault, and the Aqikekuduke-Shaquanzi fault constituted the main regional faults (Fig. 2.1a).

The fault system is one of the most important factors to Fe mineralization in eastern Tianshan mineral district. First of all, EW-trending faults confine boundaries of the volcanic strata which are believed as host rocks of Fe ores (Fig. 2.1a) (BGEDXP, 2009; Li et al., 2002; Mao et al., 2005; Yang et al., 1996). Consequently, the volcanic strata, especially the Fe ore-bearing strata (i.e., the Yamansu Formation) are mainly spreading along EW direction within the Jueluotag aulacogen (Fig. 2.1b). Secondly, intersections of NE- and NW-trending faults dominate the spatial distribution of eruption centers of volcanoes. They could therefore control spatial distributions of both the Yamansu Formation and Fe ores (BGEDXP, 2009). Thirdly, the fault system performed as conduits associated with emplacement of granitoid and migration of differentiated hydrothermal fluids (Ma et al., 1993; Wang et al., 1994; Zhang et al., 2005). The general properties of the three major faults are introduced as follow:

1. Kanggurtag-Huangshan fault

Being the largest tectonic settings in dividing geological environment in eastern Tianshan mineral district, the Kanggurtag-Huangshan fault is the boundary of the Junggar crust in the north and the Tarim crust in the south. The west end of this fault is connected with the north edge of southern Tianshan district and the east end of this fault reaches territory of Mongolia. The southward-convex fault trace is striking through the entire study area from the west to the east. The fault is steeply dipping southward (Zhou et al., 1996; BGEDXP, 2009).

2. Yamansu thrust nappe belt

The Yamansu thrust nappe belt is the second largest tectonic setting in the study area. It is the boundary of the Qiugemingtashi-Huangshan shear zone in the north and the Aqishan-Yamansu volcanic arc in the south. EW trending secondary imbricate thrust systems are commonly existed within the nappe belt. Strata within the Yamansu nappe belt are generally middle metamorphosed. In the study area, it is an important mineralization zone for ductile shear zone type gold deposits (Ma et al., 1997).

3. Aqikekuduke-Shaquanzi fault

The Aqikekuduke-Shaquanzi fault was the frontier of subduction of the ancient Tianshan oceanic crust to the Tarim crust in the Ordovician and was developed into a right lateral strike-slip fault in the Mesozoic (Ma et al., 1993; Wang et al., 1994; Zhang et al., 2005; Han and Zhao, 2003; Mao et al., 2002; Zhou et al., 1996). Separating eastern Tianshan from middle Tianshan, this southward-convex fault is southward dipping and trending from the west to the east across the study area. Lithologically, this fault is the line separating the Precambrian metamorphosed strata

in the south caused by upthrust of hanging-wall block and the Late Paleozoic volcanic strata in the north (Zhou et al., 1996).

2.2.2. Magmatism

Most of the Fe deposits are formed within the extent of Late Paleozoic Jueluotag aulacogen, where volcanic edifices produced by a series of geological activities are linearly distributed (Han and Zhao, 2003; Hou et al., 2006). Previous researches indicated that the tension period of Jueluotag aulacogen is the main period of the Fe mineralization. Bimodal volcanic eruptions were widely spread during the tension period starting from the Early Carboniferous. Along with the migration of magma towards the earth surface, Fe ore materials were erupted, transported and finally solidified in lower marine basins in layer and/or layer-like forms within the Carboniferous Yamansu volcanic strata (Han et al., 2002; Ma et al., 1993; Wang et al., 2006). After the tension period, intensive emplacement of granitoid caused by the compression of Jueluotag aulacogen in Late Carboniferous (i.e., middle-late Hercynian period, $318.1 \pm 1.3 \sim 250$ Ma) played an important role in altering and enriching the previously precipitated Fe ores (Jiang et al., 2002; Wang et al., 2007; Ding, 1990). First of all, the intrusions of felsic magma can be sources of ore-forming materials. Differentiated from the magma, ore-forming materials contained in the hydrothermal fluids were retained for mineralization while non-metallogenic materials (e.g., SiO_2 , Mg^{2+} , Ca^{2+}) were consumed during the processes of silicification, diopsidization, actinolitization. Second of all, heat provided by the intrusions could hydrothermally alter previously formed Fe ore bodies. Magnetization and garnetization of existing Fe ore rocks driven by the heat resulted that the

magnetite in the ore rocks were interbanded with pyrite and garnet (BGEDXP, 2009; Li et al., 2002; Yang et al., 1996). In summary igneous rocks in the eastern Tianshan district, either extrusive/intrusive or mafic/felsic, are not only main products of magmatism but also primary components of regional lithologic strata (Li et al., 2002; Zhang et al., 2004; Wang et al., 2006).

In eastern Tianshan mineral district, felsic intrusions emplaced during middle Hercynian period are widespread. Two granitoid belts (i.e., Kanggurtag-Harlik belt in the north and Aqishan-Yamansu belt in the south) are separated by the Huangshan-Jing'erquan late Hercynian mafic/ultramafic complex. Bounded to the Kanggurtag region and Kumtag Sand Ridge (Fig. 2.1a), the study area can be divided into the west, the middle and the east subareas. The large-scale felsic intrusions are mainly distributed in the west end of Aqishan-Yamansu belt and east ends of both granitoid belts. Magmatism in the middle range of the study area was not that concentrated. The felsic intrusions are mainly composed of monzogranite, granodiorite, plagiogranite, moyite, quartz diorite, and diorite. A small number of tonalite, plagiogranite porphyry, diorite porphyrite, granite porphyry, and quartz monzodiorite can also be observed in limited places (BGEDXP, 2009; Li et al., 2002).

2.2.3. Stratigraphic framework

Due to the collision between Junggar oceanic crust and Tarim continental crust, the study area was formed by the Late Paleozoic orogeny. The outcropping strata in the study area are mainly composed of thick layers of low grade-non metamorphic Carboniferous marine volcanic sedimentary rocks. Strata deposited during Ordovician,

Silurian, Devonian, Permian and Mesozoic are scattered in the study area.

Lithologic units in the eastern Tianshan district (Fig. 2.1a) are mainly located in three E-W trending areas, which area juxtaposed from the north to the south (Li et al., 2002; Mao et al., 2005): (A) the Kanggurtag-Harlik area; (B) the Qiugemingtashi-Huangshan area; and (C) the Aqishan-Yamansu area. Areas A and C are composed of igneous rocks deposited during the Middle Ordovician-Upper Carboniferous and the Lower Carboniferous-Middle Permian, respectively. In area C Permian granitic intrusions are widely distributed (Mao et al., 2002). The Yamansu Formation (C_{1y}) is the primary ore-hosting strata in area C (Fig. 2.1b). Influenced by intensive tectonic activities, the area B clamped between areas A and C is a series of highly deformed and metamorphic volcanic-sedimentary strata.

The strata outcropping over the study area include following units (BGEDXP, 2009; Li et al., 2002; Ma et al., 1997; Wang et al., 2006; Yang et al., 1996):

Middle Ordovician Daliugou Formation (O_{2-3d}): intermediate-felsic volcanoclastics, continental clastics, carbonate rocks and volcano lava;

Upper Silurian-Lower Devonian Hongliugou group (S_3D_1H): non-metamorphic continental clastics, tuffaceous clastics, and marine volcanoclastics layered with volcanoclastic sedimentary rocks;

Lower Devonian Dananhu Formation (D_1d): submarine intermediate-mafic volcanoclastics, tuff, and clastics layered with intermediate-mafic volcanic rocks;

Middle Devonian Tousuquan Formation (D_2t): marine siliceous volcanoclastic

sediments layered with mafic-felsic lava and marble.

Carboniferous:

Area (A):

Lower Carboniferous Xiaorequanzi Formation (C_{1xr}): intermediate-felsic volcanic rocks layered with volcanoclastics, clastics and limestone lens;

Upper Carboniferous Dikan'er Formation (C_{2d}): continental clastics, tuffaceous clastics and carbonate rocks;

Area (B):

Lower Carboniferous Gandun Formation (C_{1g}): Siliceous rocks, quartz sandstone layered with felsic volcanoclastics (protolith);

Upper Carboniferous Wutongwozi Formation (C_{2w}): clastics layered with intermediate-felsic tuff (lower member) and volcanoclastics, andesite, basalt, and felsophyre layered with clastics (upper member);

Area (C):

Lower Carboniferous Aqishan Formation (C_{1a}): intermediate-felsic volcanic rocks and volcanoclastics;

Lower Carboniferous Yamansu Formation (C_{1y}): Biolithite limestone, continental fine-grained clastics, volcanoclastics, and carbonate rocks layered with tuffaceous clastics, volcanoclastics and mafic-felsic lava (i.e., bimodal volcanic rocks);

Upper Carboniferous Shaquanzi Formation (C_{2sh}): laminated limestone and clastics layered with volcanic rocks and volcaniclastics;

Upper Carboniferous Matoutan Formation (C_{2m}): intermediate-mafic volcanic rocks and volcaniclastics;

Middle Permian Aqikebulak Formation (P_{2a}): marine-land interchanging facies of volcanic sedimentary series.

2.2.4. Metallogeny of typical deposit

The Yamansu deposit with an average grade of 51% Fe is the largest volcanic sedimentary Fe deposits in the study area, the ores of which are mainly hosted by the potash-felsophyre in Carboniferous Yamansu Formation (Mao et al., 2005; Han and Zhao, 2003). Undergone complex tectonic activities along the boundary of Junggar and Tarim plates, the formation of this type of Fe deposits (e.g., the Yamansu, Baishanquan, Bailingshan and Hongyuntan deposits) were caused by multi-stage geo-processes (Ma et al., 1993; Qin et al., 2005; Shu et al., 1997; Wang et al., 1994; Zhang et al., 2005, 2008). Being the most representative volcanic sedimentary Fe deposit in the study area, its mineralization process can be divided into two stages. The first stage is volcanic extrusion and sedimentation stage. Fe ions were dissolved out of magma chambers at low-oxygen fugacity condition and further oxidized due to the participation of underground water during upwelling (Han et al., 2002; Lu et al., 1995; Zhang and Xie, 2001). Meanwhile, ore-bearing fluids were formed and extruded along with intermediate-mafic magma in the early Carboniferous and precipitated in sea basins (Han et al., 2002). The Fe ore bodies were arranged in

stratoid and lenticular posture with the attitude in accordance with their host (i.e., the Yamansu volcanic and volcanoclastic rocks). The second stage involves magmatic-hydrothermal transformation (BGEDXP, 2009). After solidification, the Fe ore bodies were further enriched by either contact metamorphic or regional metasomatic processes (Guilbert and Park, 1986; Misra, 2000). Thermal sources of these two processes were gas/liquid mixture produced in the later stages of volcanic eruption and the hydrothermal fluids extracted from the Late Carboniferous granitoid intrusions, respectively. They both intensively altered (i.e., albitization, chloritization, epidotization, diopsidization and garnetization, etc.) the country rocks and previously formed Fe ores (BGEDXP, 2009; Ding, 1990; Han and Zhao, 2003; Li et al., 2002; Shu et al., 1997; Yang et al., 1996; Wang, 2005). The banded texture (Fig. 2.3) constituted by ore minerals (e.g., magnetite and pyrite) and gangue minerals (e.g., garnet) is common in the Fe ores, which is comparable to most of banded iron formations (BIFs) witnessed around the world (Edwards and Atkinson, 1986; Guilbert and Park, 1986). Other ore textures including massive and disseminated textures can be observed in the Fe ores as well. The magnetite and pyrite were formed at a temperature of 330-340°C and 150-220°C, respectively (Liu et al., 1996).

In this chapter, geological background of eastern Tianshan mineral district is briefly introduced. Through previously discussed geological background of this area, it can be noticed that the Fe mineralization was under the control of a series of geological processes consisting of tectonic and magmatic activities. The formation of Fe deposits can be considered as end products of interactions of these activities. Therefore, in order to improve the Fe exploration in this area, geological features associated with

the tectono-magmatism are necessary to be identified; meanwhile, the relationships between these geo-processes and Fe mineralization should be interpreted by quantitative evaluation in spatial scenario.

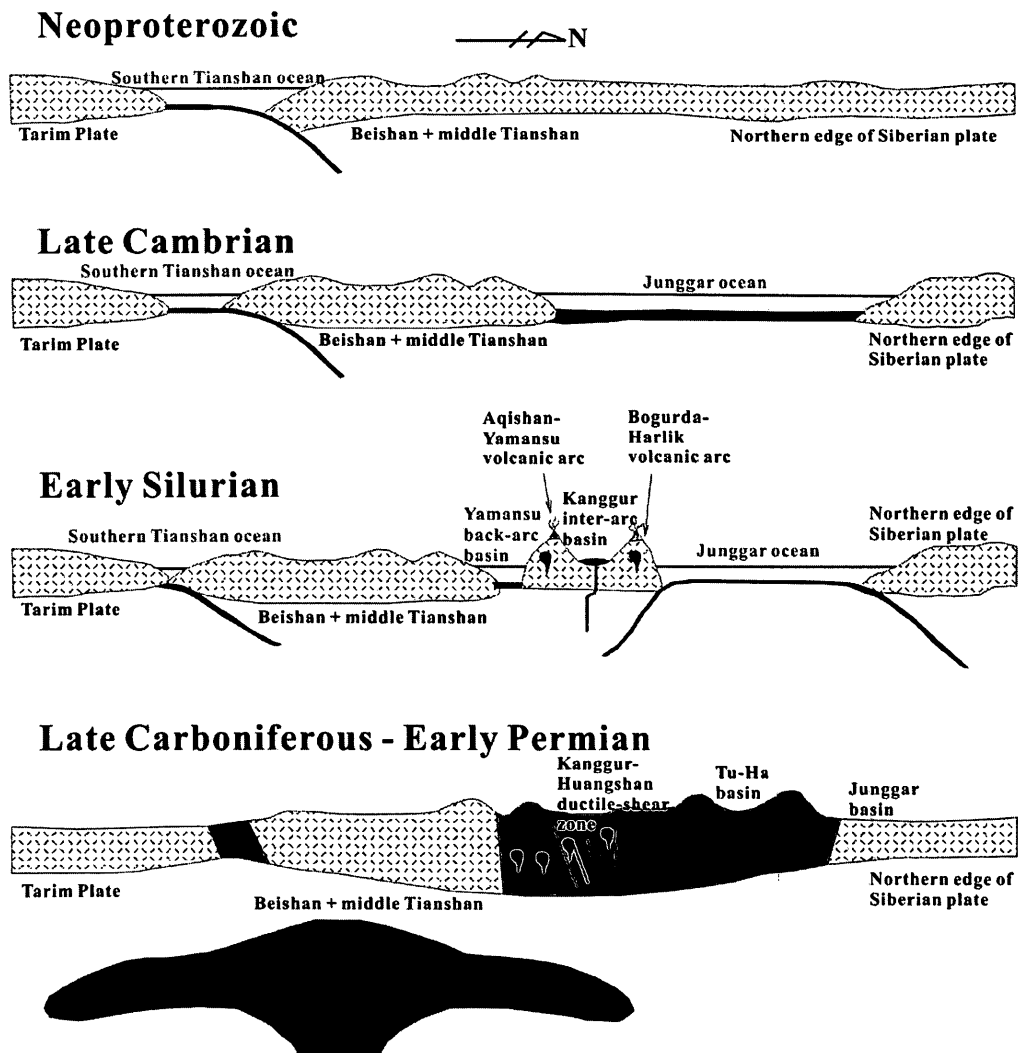


Fig.2. 2 Tectonic evolution model (Neoproterozoic-Early Permian) for eastern Tianshan mineral district (Modified from Su et al., 2011).

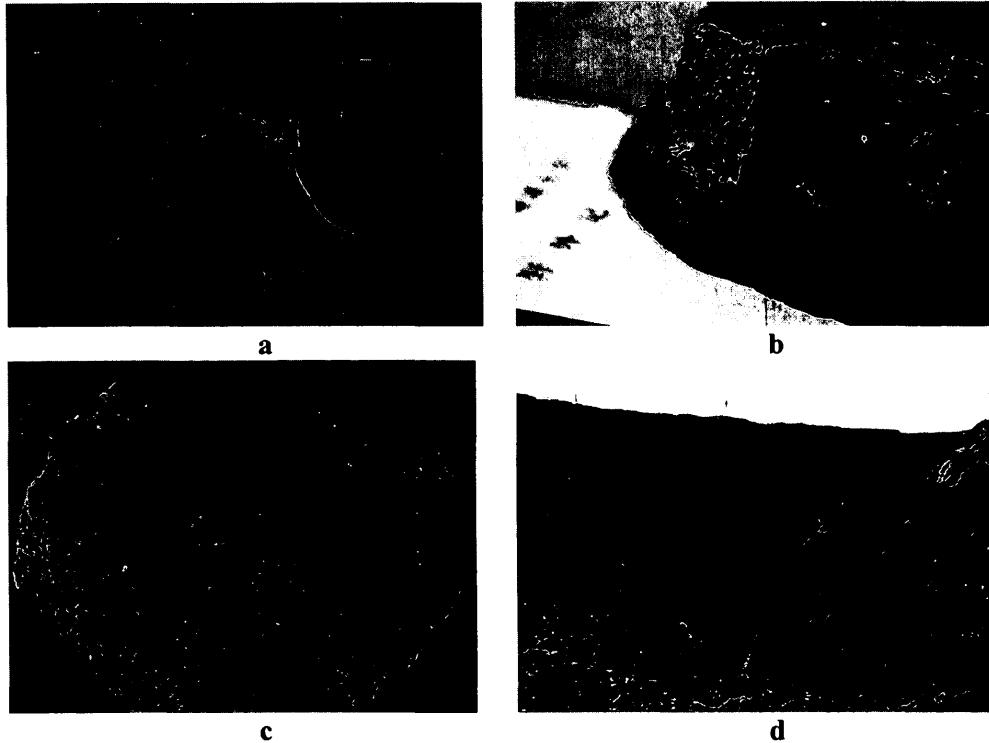


Fig.2. 3 Ore textures observed in the Yamansu Fe deposit. **a.** banded Fe ore composed of magnetite (black), pyrite (yellow) and garnet (reddish brown) (by Jie Zhao, summer 2010); **b.** massive Fe ore composed of magnetite (by Jie Zhao, summer 2010); **c.** disseminated Fe ore composed of magnetite (black), pyrite (yellow), quartz and feldspar (off-white) (by Jie Zhao, summer 2011); **d.** The mining pit of the Yamansu deposit. This picture was taking from the east to the west (by Jie Zhao, summer 2010).

Chapter 3. Methodology

3.1. Logratio transformation

Confined by the constant sum, compositional data (e.g., raw geochemical data) lies in a restricted space where data are recorded as proportion rather than absolute values (Pawlowsky-Glahn and Egozcue, 2006). Being relative proportions, none of the compositions can vary between $(-\infty, +\infty)$ independently. For example, if SiO_2 contained in a sample of igneous rock accounts for 69% of the total weight, then the content of another constituent like MgO can only take values less than 31%. In the restricted space or so-called simplex, data are following Aitchison geometry where D -part compositions only contain $D-1$ dimensional information since the residual composition can be expressed by the difference between constant unity and the sum of $D-1$ compositions (Egozcue and Pawlowsky-Glahn, 2006). In other words, the correlation and covariance matrices of compositional data are singular (Pawlowsky-Glahn and Egozcue, 2006). Since most standard statistical methods are designed for Euclidean geometry, applications of which to raw geochemical data might be inappropriate, even though the log-transformed data are normally distributed (Filzmoser et al., 2012). Therefore, logratio transformations which converts compositional data to Euclidean space can be used to open the closure effect, and the logratio transformed data will be analyzed with unconstrained multivariate statistics

(Aitchison and Egozcue, 2005; Carranza, 2011). The alr, the clr, and the ilr transformation are the three main algorithms converting compositional data to an open system by which more realistic correlations among compositions can be identified (Carranza, 2011; Pawlowsky-Glahn and Egozcue, 2006).

Suppose a set of geochemical data as a D -part compositional vector $x=(x_1, \dots, x_D)^T$ in simplex is defined as S^D . Compositions x_i ($i=1, 2, \dots, D$) (e.g., 39 elements/oxides tested in currently used stream sediment geochemical samples) are strictly positive components summing to a constant (e.g., 100%). Geochemical data as a closed system can be opened by alr (Eq. 3-1), clr (Eq. 3-2) and ilr (Eq. 3-3) transformation to a real space R , respectively (Egozcue et al., 2003; Filzmoser et al., 2009):

$$y_i = \log \frac{x_i}{x_j} \quad (i=1, 2, \dots, D-1, j=D) \quad (3-1)$$

$$y_i = \log \frac{x_i}{\sqrt[D]{\prod_{i=1}^D x_i}} \quad (i=1, 2, \dots, D) \quad (3-2)$$

$$y_i = \sqrt{\frac{D-i}{D-i+1}} \log \frac{x_i}{\sqrt[D-i]{\prod_{j=i+1}^D x_j}} \quad (i=1, 2, \dots, D-1) \quad (3-3)$$

Logratio transformation processes compositional data by two treatments: defining ratios for compositions and taking logarithm on the ratios. The former is to decompose the closure effect by selecting a common divider (e.g., one composition, geometric mean, etc.), while the latter is to make the transformed compositional data lognormally distributed (Aitchison, 1982, 1986; Filzmoser et al., 2009; Zhou, 1998).

In general, there are three main logratio transformation algorithms applied to compositional data: (1) additive logratio (alr) transformation (Aitchison, 1982, 1983, 1986); (2) centered logratio (clr) transformation (Aitchison, 1982, 1983, 1986); and (3) isometric logratio (ilr) transformations (Egozcue et al., 2003).

Through former studies on these three logratio algorithms, some properties assisting to comprehend the three forms of logratio transformation are reviewed as follow:

- (1) The algorithms of alr and clr are relatively simple. By alr transformation, one composition (i.e., denominator) is selected to divide remaining compositions (i.e., numerators) and then log-transformation is taken on the ratios (Aitchison, 1986). By clr transformation, compositions are divided by the geometric mean of all components and then log-transformation is taken on the ratios (Aitchison, 1986). Different from alr and clr, by ilr transformation the stepwise elimination of compositions is taken into the calculation of geometric mean which performs as the divider. It provides one-to-one conversion of compositions lies in Aitchison geometry into a vector in real Euclidean geometry (Filzmoser et al., 2012; Hron et al., 2010).
- (2) Both alr and ilr transformation can reduce the dimensionality of compositional data (i.e., from S^D to R^{D-1}), whereas the clr preserves D real components. The clr transformed compositions adding up to zero means that the transformed vectors

are constrained in a sub-space (Egozcue et al., 2003; Pawlowsky-Glahn and Egozcue, 2006).

(3) Both clr and ilr transformed vectors lie in orthogonal systems.

Many applications revealed that ilr transformation generating correct equivalent in real Euclidean space is ideal for decomposing the compositional data (Carranza, 2011; Filzmoser et al., 2009; Filzmoser et al., 2012); meanwhile, it is also blamed for its shortages of geological interpretability (Pawlowsky-Glahn and Egozcue, 2006). As well as ilr, the clr is commonly used in many cases especially when all compositions are necessary to be involved or of interest (Drew et al., 2010). The alr are believed as subjective and its results are dependent on the chosen denominator; however alr transformed data insist the geological meanings inherited from the compositions rather than obtain a set of unknown physical quantities (Rollinson, 1992, 1993). Therefore, compared with the clr and ilr transformation, the statistical treatment to alr transformed data and the interpretation of the statistical results can be dominated with a geological guidance.

3.2. Singularity index mapping technique

Nonlinear processes (e.g. earth quake, fault activities, emplacement of igneous rocks) occur quite often in geological domain, the products of which can present singular and non-stationary properties such as anomalous energy release and material accumulation

within a short space-temporal interval (Cheng, 2012; Wang et al., 2011, 2012, 2013; Zhao et al., 2012). Typically, mineralization caused by a series of cascade geo-processes produces abnormal geochemical signatures which can be identified by nonlinear methods (Cheng, 2007). Singularity mapping technique in the context of multifractal has become one of the most popular methods in separating the geochemical anomalies from background. Suppose the mass of metallic element contained in an area A (i.e., 2-dimensional scenario) is denoted as $\mu(A)$, and the metal concentration of the area A can be expressed as $C(A) = \mu(A)/A$. From a multifractal point of view, the changes of $\mu(A)$ and $C(A)$ depend on the variation of A by following power-law relationships:

$$\langle \mu(A) \rangle = cA^{\alpha/2} \quad (3-4)$$

$$\langle C(A) \rangle = cA^{\alpha/2-1} \quad (3-5)$$

where the coefficient c is a constant defining the magnitude of the power-law equation; the exponent α determining the shape of the power-law equation or changing behavior of the quantities of element with changes of A within the given area is termed as singularity index; and The “expectation” symbol $\langle \rangle$ explains the power-law relationships in a statistical manner. Generally, the changing behaviors of the quantities of element characterized by singularity index α can be classified two situations: (1) $\alpha = 2$ describes a non-singular distribution of element concentration which means $C(A)$ is constant in the area of A and will not change accordingly with

the variation of A ; (2) $\alpha \neq 2$ describes a singular distribution of element concentration implying changes of $C(A)$ is dependent on the variation of A . Specifically, based on the magnitude of α , positive and negative singularities can be further differentiated by $\alpha < 2$ and $\alpha > 2$, respectively. The former case shows increase of $C(A)$ with the decrease of area A , which is corresponding with the accumulation of element concentration at a given location. The latter case shows decrease of $C(A)$ with area A decreases, which is corresponding with the depletion of element concentration at a given location. Generally, geochemical anomalies produced by various geo-processes (e.g., mineralization, magmatic emplacement, fault activities) can be characterized by enrichment of element (and/or element associations) within a narrow space interval (Cheng, 2007; Zhao et al., 2012; Wang et al., 2011, 2013). By mapping the singularity indices across the space, locations with geochemical anomalies will frequently indicated by positive singularity.

To estimate the singularity index, a series of square window $A(\varepsilon)$ with various side lengths $\varepsilon_{\min} = \varepsilon_1 < \varepsilon_2 < \dots < \varepsilon_n = \varepsilon_{\max}$ centered at a given location are defined. Therefore, singularity index can be estimated by taking log-transformation on both sides of Eq. (3-5):

$$\text{Log}C[A(\varepsilon)] = \text{Log}(c) + (\alpha - 2)\text{Log}(\varepsilon) \quad (3-6)$$

where $C[A(\varepsilon)]$ is the average element concentration value within the square window $A(\varepsilon)$. $\text{Log}(c)$ is a constant value. Plotting the window size against the element

concentration on a log-log plot, the singularity index α at the given location can be achieved from the slope of the linear function (i.e., $\alpha - 2$). Therefore, singularity indices at all locations can be estimated by sliding the square windows across the space (Cheng, 2007). Detailed information about window-based method can be found in Cheng (1999). In this dissertation, calculation of singularity indices of elemental concentrations was manipulated in GeoDAS GIS environment.

3.3. PCA and SWPCA

3.3.1. Ordinary PCA

As a well known multivariate statistics, PCA has been broadly used to examine the relationships between variables. By orthogonal transformation, a series of interrelated variables can be converted into uncorrelated principal components (PCs) based on a covariance or correlation coefficient matrix (Horel, 1984; Loughlin, 1991). PCA is well performed to reduce high-dimensional information carried by original datasets to fewer PCs whose eigenvalues are descendingly ordered. In general, the first few PCs will be with most variance of original datasets (Panahi et al., 2004). Therefore, PCA is frequently utilized to increase information interpretability of targets of interest by reducing the dimensionality (Cheng et al., 2011; Christophersen and Hooper, 1992; Horel, 1984; Jolliffe, 2002; Singh and Harrison, 1985). According to the algorithm of PCA, PCs are linear combinations of original variables to represent integration results of original variables in different ways (Abdi and Williams, 2010; Nomikos and

MacGregor, 1994); meanwhile, information possessed by each PC is disintegrated from the whole datasets. In other words, PCA can perform as both integrator of fractions and decomposer of the whole.

Since introduced to geological field, PCA has been extensively employed to geochemical data for identifying geological bodies (e.g., ores, igneous rocks, strata, etc.) (Cheng 2007; Wang et al., 2011, 2012; Zhao et al., 2012). From a geochemical perspective, different geochemical distributions (i.e., elemental concentration) are caused by effects of diverse geo-processes (Jiang et al., 2006). Elemental assemblages associated with geological bodies can be characterized by different PCs (i.e., linear combination of corresponding geochemical distributions), which may represent geochemical signatures of the end products of these geo-processes.

Algorithmically, correlation coefficient matrix evaluating interrelations between variables is the foundation of PCA (Cheng, 2002; Cheng et al., 2011). According to the orthogonal transformation, eigenvectors of the matrix will construct an orthogonal Euclidian space where PCs are the axes, while the eigenvalues correspond to the variance of PCs. The PC with maximum eigenvalue (i.e., the greatest variance) is termed as the first PC (PC1). The second PC (PC2) has the second largest eigenvalue, and so forth (Christophersen and Hooper, 1992). Suppose a geochemical dataset consisting of p elemental concentrations is conducted by PCA, the correlation coefficient between any two elemental concentrations is defined by the following

formula (Cheng et al., 2006, 2011; Wang and Cheng, 2008):

$$R(A, B) = \frac{\frac{1}{mn} \sum (A_{ij} - \bar{A})(B_{ij} - \bar{B})}{\sqrt{\frac{1}{mn} \sum (A_{ij} - \bar{A})^2} \sqrt{\frac{1}{mn} \sum (B_{ij} - \bar{B})^2}} \quad (3-7)$$

where, A_{ij} and B_{ij} are the concentration values of the geochemical distributions of element A and B at location (i, j) , respectively, and m and n represent the number of rows and columns of these two variables. The correlation coefficients of these p elemental concentrations will build a $p \times p$ symmetrical correlation coefficient matrix R (Cheng, 2011).

Based on the achieved matrix, the eigenvalues and eigenvectors can be calculated by Eqs. (3-8) and (3-9), respectively:

$$\det(R - \lambda I) = 0 \quad (3-8)$$

$$(R - \lambda I)U = 0 \quad (3-9)$$

where, R is the correlation coefficient matrix of multivariate datasets, I is the $p \times p$ identity matrix, and “det” is the determinant of the matrix formed by $R - \lambda I$. λ_i ($i=1, 2, \dots, p$) calculated from the characteristic equation of R is the eigenvalue, and $U = [a_{i1}, a_{i2}, \dots, a_{ip}, i = 1, 2, \dots, p]$ is the eigenvector matrix consisting of PCs with m rows and n columns. Mathematically, each PC can be expressed as a linear combination of the p variables (i.e., X_1, X_2, \dots, X_p) as:

$$PC_i = a_{1i}X_1 + a_{2i}X_2 + \dots + a_{pi}X_p \quad (3-10)$$

Based on Kaiser's rule (Kaiser, 1960), eigenvalue of each PC should be greater than or equal to 1 to explain at least as much variance as one observed variable; otherwise they are considered to be statistically unreliable (Jolliffe, 2002). Restricted to this rule, some of the PCs with eigenvalue less than 1 will not be further used. However, the loadings of these PCs might be explainable to some physical meanings. Applications of PCA in geochemical exploration frequently encounter this problem, since the PCs with weak variance (i.e., $\lambda_i < 1$) but meaningful geo-information might be the interests of geological interpreters in many cases. Therefore, the PCA extensions which can provide more statistically acceptable PCs by increasing the eigenvalues of formerly unusable PCs will greatly benefit the understandings of geological bodies resulted from multiple geo-processes.

3.3.2. SWPCA

Proposed by Cheng (2000), SWPCA applied a spatially weighting factor to the calculation of correlation coefficient matrix (Eq. 3-7). The relative importance of geological issue-associated certain physical quantities at different locations is taken into consideration by a spatially weighting factor (Cheng, 2006, 2011; Wang and Cheng, 2008; Xiao et al., 2012). A spatially weighted correlation coefficient of two variables can be expressed as

$$R^*(A, B) = \frac{\frac{1}{mn} \sum W_{ij} (A_{ij} - \bar{A})(B_{ij} - \bar{B})}{\sqrt{\frac{1}{mn} \sum W_{ij} (A_{ij} - \bar{A})^2} \sqrt{\frac{1}{mn} \sum W_{ij} (B_{ij} - \bar{B})^2}} \quad (3-11)$$

where, W_{ij} is the spatially weighting factor. In practice, W_{ij} ranging from 0 to 1 (i.e., $0 \leq W_{ij} \leq 1$) is used. $W_{ij} = 0$ implies that the location at (i, j) is not important or irrelative to the objective geological features, which will be removed from calculation of correlation coefficient. $W_{ij} = 1$ implies that the location at (i, j) is very important or highly associated with the objective geological features, which will be highlighted during the calculation of correlation coefficient. Values of the spatially weighting factor assigned to locations ranging from $0 < W_{ij} < 1$ are based on their significance to the objective geological features. In other words, the greater the W_{ij} is, the more important the locations (i, j) are. In addition, if W_{ij} is a constant across the space, then Eq. (3-11) will be same as the ordinary formula Eq (3-7). If W_{ij} is a binary pattern with two values 1 and 0, then W_{ij} is similar to the ordinary mask. The design of mask depends on spatial locations or intrinsic properties of specific objective features.

As described above, PCs with qualified loadings can be used to describe the geological features. If a spatially weighing factor is applied to enhance the geo-information supported by the i^{th} PC (PC_i), then the SWPCA will produce new PC_i (i.e., $SWPC_i$) (Fig. 3.1); meanwhile, the eigenvector of $SWPC_i$ will be stretched along the similar but not exactly same direction as PC_i :

$$SWPC_i = b_{1i}X_1 + b_{2i}X_2 + \dots + b_{pi}X_p \quad (3-12)$$

where $[b_{1i}, b_{2i}, \dots, b_{pi}, i = 1, 2, \dots, p]^T$ forms a new eigenvector matrix. Since the observations of original variables X_p are not changed by using W_{ij} , whilst the eigenvector matrix is derived from spatially weighted correlation coefficient matrix R^* , the eigenvalues (i.e., variances) of PC i and SWPC i should be different (Fig. 3.1). As a result, the SWPC1 will not be able to retain as greatest variance as the ordinary PC1 does and the eigenvectors and eigenvalues of other newly produced SWPCs by Eq. (3-12) are varied (Fig. 3.1). SWPC1 possessing smaller eigenvalue than PC1 can be considered as a rotation of PC1 to the enhanced direction. Moreover, the eigenvector of other SWPCs perpendicular to SWPC1 will have a greater eigenvalue than ordinary PCs (Fig. 3.1). If the eigenvalues of these SWPCs are equal to or greater than 1, then more SWPCs will become reliable for interpreting than ordinary PCs. More detailed description and discussions of the SWPCA can be found in Cheng et al. (2011). In this dissertation, both PCA and SWPCA approaches were manipulated in GeoDAS GIS environment.

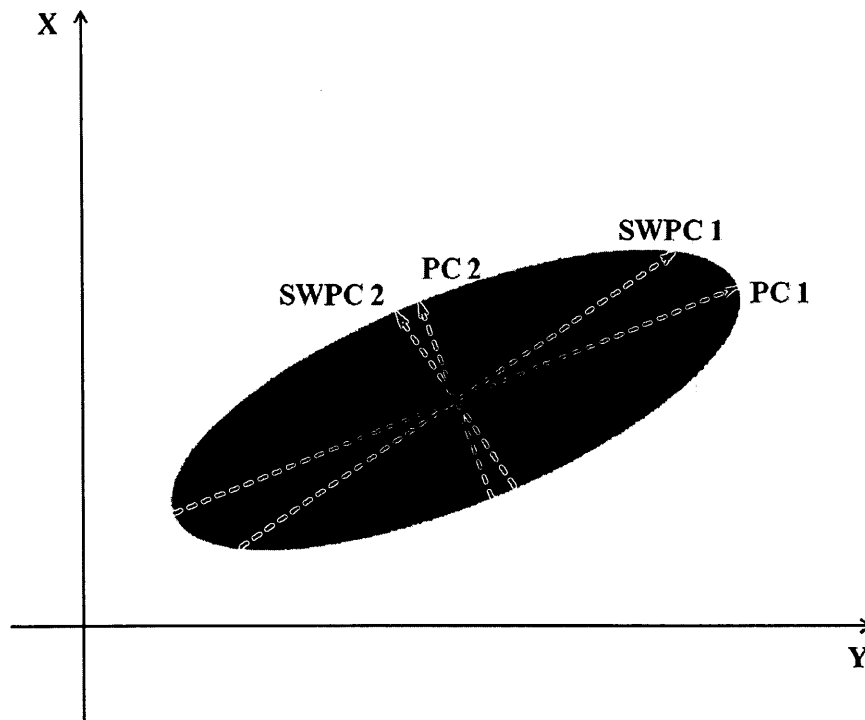


Fig.3. 1 Schematic diagram of eigenvectors of principal components (PCs) and spatially weighted principal components (SWPCs) in 2-dimensional scenario. Blue area denotes the plot of observations on two variables X and Y. In this demonstration, the information contained by the first principal component is supposed to be enhanced. The comparison between these two methods can be extended to n-dimensional scenario.

3.4. Student's *t*-value

The student's *t*-statistic involved in the weights of evidence (WofE) method has been used frequently to quantify the spatial relationship between a point pattern and a map (polygon) pattern (Bonham-Carter, 1994; Cheng and Agterberg, 2009; Cheng et al., 1994; Zuo et al., 2009). In WofE, two statistics W^+ and W^- are defined to characterize the spatial relationship between point events and a map pattern according to conditional probabilities:

$$W_j^+ = \text{Log} \frac{P(B_j|D)}{P(B_j|\bar{D})} \quad (3-13)$$

$$W_j^- = \text{Log} \frac{P(\bar{B}_j|D)}{P(\bar{B}_j|\bar{D})} \quad (3-14)$$

where D and \bar{D} represent presence and absence of point event, respectively; and B_j and \bar{B}_j stands for presence and absence of the j^{th} map pattern. The symbols $P(B|D)$, $P(B|\bar{D})$, $P(\bar{B}|D)$, $P(\bar{B}|\bar{D})$ stand for conditional probabilities of point events with respect to map patterns. W^+ is a log-transformed ratio of conditional probabilities of $P(B|D)/P(B|\bar{D})$, thus it measures the spatial relationship between point events and the presence of map pattern B . Similarly, W^- measures the spatial relationship between point events and the absence of map pattern \bar{B} . The sum of these indices, $C = W^+ - W^-$, measures the overall spatial relationship between point events and map pattern. In order to characterize the statistical significance of the spatial relationship one needs to know the standard deviation of these indices. The student's t -statistic can then be used to quantify the statistical significance of the spatial relationship:

$$t = \frac{C}{\sigma} \quad (3-15)$$

where σ is the standard deviation of C , which can be estimated according to the following approximations:

$$\sigma(W^+) = \sqrt{\frac{1}{B_j \cap D} + \frac{1}{B_j \cap \bar{D}}} \quad (3-16)$$

$$\sigma(W^-) = \sqrt{\frac{1}{B_j \cap D} + \frac{1}{B_j \cap \bar{D}}} \quad (3-17)$$

$$\sigma = \sqrt{\sigma^2(W^+) + \sigma^2(W^-)} \quad (3-18)$$

More detailed discussions and derivation of the above equations can be found in Bonham-Carter (1994) and Bonham-Carter et al. (1989). In this dissertation, *t*-values were calculated in GeoDAS GIS environment.

3.5. OLS and GWR

Suppose a dependent variable *Y* can be estimated by a linear function of a series of independent variables X_k , an OLS model can be expressed as:

$$Y_i = a_0 + \sum_k a_k X_{ik} + \varepsilon_i \quad (3-19)$$

where, Y_i is the observation value of the dependent variable at location *i*, X_{ik} is the observation value of k^{th} independent variable at location *i*, and ε_i is the independent and normally distributed error term with zero means (Brunsdon et al., 1996). The regression coefficient a_k characterizing relationships between *Y* and X_k can be derived from the following matrix manipulation:

$$a^* = (X^T X)^{-1} X^T Y \quad (3-20)$$

where, a^* denotes an estimation of coefficient *a* which evaluates the strength of influence of independent variables to the dependent variable, *X* and *Y* represent observation values of independent variables and the dependent variable, respectively

(Brunsdon et al., 1996). For the OLS model, a^* is a constant over space without implying any information for specific locations. In other words, one model fits all situations. Under some situations, it may lead great error in the estimation of relationships between variables especially when the relationships are non-stationary (Fotheringham et al., 2002).

As a localized regression model, GWR allows variables to be estimated at different locations across the space. One of superiorities of using GWR is to explore spatial non-stationary relationships among variables. By GWR, the regression model can be expressed as:

$$Y_i = a_0(u_i, v_i) + \sum_k a_k(u_i, v_i) X_{ik} + \varepsilon_i \quad (3-21)$$

where, (u_i, v_i) indicates the location of point i in Euclidean space, and $a_k(u_i, v_i)$ are the localized coefficients of the k^{th} independent variable at location i . The realistic meanings of other parameters in Eq. (3-21) are inherited from OLS model. Comparing these two regression models, OLS can only demonstrate a general trend of relationships between variables whereas GWR provides more localized inspection to the relationships between variables. In GWR, a weighting factor $w(u_i, v_i)$ is applied during parameter estimation, by which the j^{th} observation is weighted in accordance with its proximity to calibration point i . Observations close to the calibration point i will be assigned higher spatial weighting, and consequently have stronger influence on the estimation of the coefficients $a_k(u_i, v_i)$ than the locations away from i (Brunsdon et al., 1996, 2002; Fotheringham et al., 1998, 2001). The coefficients estimated for each single location can be:

$$a^*(u_i, v_i) = (X^T w(u_i, v_i) X)^{-1} X^T w(u_i, v_i) Y \quad (3-22)$$

where $w(u_i, v_i)$ is an $n \times n$ matrix. Diagonal elements of $w(u_i, v_i)$ denote the spatial weighting of observed j^{th} sample point located around calibration point i , while the other elements are zero (Brunsdon et al., 1996; Fotheringham et al., 1998; Charlton et al., 2009). The weighting matrix can be expressed as:

$$w(u_i, v_i) = \begin{matrix} w_{i1} & 0 & 0 & \dots & 0 \\ 0 & w_{i2} & 0 & \dots & 0 \\ 0 & 0 & w_{i3} & \dots & 0 \\ \cdot & \cdot & \cdot & \dots & \cdot \\ 0 & 0 & 0 & \dots & w_{ij} \end{matrix} \quad (3-23)$$

Furthermore, the spatial weighting of observed j^{th} sample point w_{ij} is designed as a piecewise function:

$$w_{ij} = \begin{cases} \exp\left(-\frac{d_{ij}^2}{\beta^2}\right) & \text{if } d_{ij} < \beta \\ 0 & \text{otherwise} \end{cases} \quad (3-24)$$

where β is the bandwidth which determines a maximum influence distance between calibration point i and observation point j . Based on the weighting function in Eq. (3-24), only points located within the bandwidth are considered in calibration of the center point i . As the distance between point i and j increases, the weighting of point j will decrease following a Gaussian curve. A greater β defining a wider boundary of Gaussian curve will have more observation point j involved that corresponds to a more global model for parameter estimation; whereas a smaller β defining a narrow

boundary of Gaussian curve will have less observation point j involved that corresponds to a more localized model for parameter estimation. It can be assume that if β tends to infinity, then the weighting of observation point j will approach to 1 and GWR becomes the OLS. Therefore, GWR can be seen as disaggregation of OLS model at different locations (Fotheringham et al., 2002), and the bandwidth β governs the decay rate of w_{ij} and the degree of locality of the regression model (Brunsdon et al., 2001, 2002; Fotheringham and Brunsdon, 1999). An appropriate bandwidth can be determined by cross-validation (*CV*) method or Akaike information criterion (*AIC*). More details of these two methods can be found in Brunsdon et al (1996, 2000) and Fotheringham et al. (2002). In this dissertation, both OLS and GWR approaches were implemented in ArcGIS GIS environment.

Chapter 4. Identification of fault systems

As introduced in Chapter 2, tectonism is significant to the Fe mineralization in eastern Tianshan mineral district, China. According to stages of mineralization, fault activities or faults can be sorted into pre-, syn-, and post-mineralization (Zhai et al., 1999; Wang et al., 2012). From former studies, there are several discussions regarding to the influence of fault activities on Fe mineralization in the study area (BGEDXP, 2009; Ma et al., 1997; Wang, 1998). First of all, the pre-mineralization latticed fault systems controlled centers of volcanic eruptions in this area. Secondly, the syn- and post-mineralization fault activities played an important role in modification of shapes and distributions of Fe ores. Finally, fault systems acted as hydrothermal fluid conduits benefitting the Fe mineralization and hydrothermal alteration. Due to controlling effects of faults on Fe mineralization, most of Fe deposits are located within the fault systems and/or their buffer zones (Fig. 2.1b). Consequently, delineating spatial distributions of fault systems and/or their associated signatures is necessary and beneficial to the Fe exploration.

Stress difference is one of the main effects enforcing hydrothermal fluid flow (Curewitz and Karson, 1997; Everett et al., 1999; Kassoy and Zebib, 1978; Kerrich, 1986; Sibson, 1996; Tan et al., 2004). Fault activities which produce local decompression environment with abrupt decrease of geo-stress within geological bodies are beneficial to the convection of hydrothermal fluids (López and Smith, 1995;

Saemundsson et al., 2009; Sibson, 1994). In the study area, latticed fault systems especially tension fractures are generally believed as mineralization favored positions (BGEDXP, 2009; Ma et al., 1993). By extracting salts (e.g., NaCl, MgCl₂, etc.) from wall rocks, hydrothermal fluids were developed into brine during migration within faulted spaces, and the increasing of salinity will boost the solubility of metals exponentially (e.g., Hg, Sb, As, U, Pb, Zn, Cu, Ag, and V, etc.) in hydrothermal fluid (Barton and Johnson, 2000; Ellis, 1968; Hemley et al., 1992). Being geochemically active fractions, Hg, Sb and As are sensitive to the variations in environment and are apt to be dissolved into or precipitated from the hydrothermal fluids. Meanwhile, As and Sb are often paragenetically associated with Au. Acting as mineralizer, geochemical behaviors of As, Sb and Hg benefit the migration of Au (Hua et al., 2002; Thornton and Farago, 1997; Yang and Blum, 1999). Influenced by variations in geo-stress, temperature, physical-chemical condition, etc., these elements tend to migrate with hydrothermal fluids toward surface and/or precipitate at favorable places. In general, the places are coincident with fracture zones or intersections of faults along different directions (Yuan et al., 1979). In eastern Tianshan district, there is a Au mineralization belt located in Kanggurtag-Huangshan shear zone (Fig. 2.1a), formation of which is accompanied with activation, migration and mineralization of Au and its paragenetic elements (As, Sb and Hg). The presence of mineralization produces geochemical anomalies of these elements at/near the surface which are linearly distributed along fault traces and/or around intersections of faults trending

along different directions (Qian, 2009). Therefore, geochemical anomalies of these four elements (i.e., Au, As, Hg, and Sb) are broadly received as indicators to faults (BGEDXP, 2009; He and Chen, 2002; Yuan et al., 1979). In this chapter, they are employed to recognize the spatial distribution of fault systems in the study area.

4.1. Closure effect of geochemical data

With development of computer sciences in past decades, exploratory datasets were frequently employed to recognize geo-anomalies (i.e., geo-information) for mapping mineral potentials. As an important source of geo-information, geochemical data has been processed by advanced spatial analysis methods to identify mineralization-associated geological bodies and delineate mineralization-favored spaces (Cheng et al., 2011; Wang et al., 2011, 2012, 2013; Zhao et al., 2012). However, commonly used geochemical data is a typical compositional data. The closure effect which may cause errors if standard statistics applied to them was concerned by only limited quantity of geological studies in China (Cheng et al., 2011; Zhao et al., 2012; Zhou, 1998; Zuo et al., 2013). Based on properties of compositional data, it is significant to pay attention to the closure effect during working on the geochemical data with statistical analysis methods.

Reviewing references regarding to the closure effect, it can be noticed that compositional data has long been concerned in the geological field (Buccianti et al., 2006; Chayes and Trochimczyk, 1978). Compositional data is not particular and

exists in various geological datasets (e.g., mineral contents of igneous rocks, elemental concentration of whole-rock geochemical samples, rock types of sediment samples, etc.) (Buccianti et al., 2006; Carranza, 2011). Representing relative information of different parts to a whole, compositional data are always summing to a unity (e.g., 1 for the case if an observed physical quantity is in parts per unit, 100 for the case if the physical quantity is in percentage, etc.) and recorded in a closed system (Filzmoser and Hron, 2009; Pawlowsky-Glahn and Egozcue, 2006). Unlike unconstrained variables whose values are free to vary from $-\infty$ to $+\infty$ in Euclidean space independently, compositional data, especially the exploratory data by geological observations are often with positive values ranging from 0 to 1 (or a constant sum) (Pawlowsky-Glahn and Egozcue, 2006). Restricted by the force of constant sum, geo-information carried by compositions is trading off each other. Taking geochemical samples as an example, increase in the proportion of one element will cause decrease of the other(s) to some degree. As a result, correlation coefficients of compositions are not free to vary from -1 to +1 independently, and there must be at least one negative correlation coefficient; furthermore, correlation coefficients are negatively biased (Pawlowsky-Glahn and Egozcue, 2006; Thomas and Aitchison, 2006). Consequently, correlations among these compositions are often spurious, misleading and/or meaningless in statistical sense (Rollinson, 1993). Standard statistical methods (e.g., principal component analysis) employed to examine relations between open variables might be inappropriate for the analysis of untransformed

compositional data (i.e., closed systems) (Aitchison, 1983). For geochemical data like whole-rock and stream sediment samples, logratio transformation is a helpful approach to open the closed system for better understandings of realistic relationships among compositions (Carranza, 2011; Egozcue et al., 2003; Felzmoser et al., 2012; Verma et al., 2006).

In this research, a geochemical exploration model to identify fault systems with stream sediment geochemical data in eastern Tianshan mineral district is demonstrated. In order to approximately depict spatial distributions fault systems, the alr transformation, prior to statistical analysis (i.e., principal component analysis, PCA), is chosen and applied to stream sediment geochemical data. Through a series of experiments, the opened geochemical data is no longer constrained by the constant sum, which can be used to explore the realistic geochemical signatures of geological bodies. Achieved principal components (PCs) reduce the inappropriate estimation resulted from the closure effect.

4.2. Identification of fault systems with logratio transformed geochemical data

Since the interpretation of results of alr transformation are considerably dependent on the divider, four practices demonstrate the delineation of fault systems by using PCA to the 4 log-transformed trace elements (i.e., case 1), to 4 alr transformed trace elements, the divider of which is the sum of weight percent of all oxides (i.e., $\sum x_i$, x_i

are the oxides) (i.e., case 2), to 4 alr transformed trace elements, the divider of which is weight percent of SiO_2 (i.e., case 3), and to 4 alr transformed trace elements, the divider of which is weight percent of trace element Ba (i.e., case 4). Among these four experiments, case 1 without opening the closure effect will be treated as a standard to evaluate the improvement of alr transformed results. The sum of weight percent of all 7 major elements (i.e., SiO_2 , Na_2O_3 , MgO , Fe_2O_3 , K_2O , CaO , and Al_2O_3) assigned as the divider in case 2, which is an intuitive divider with a general geological guidance, because weight of all the oxides may account for more than 90% of the samples. SiO_2 and Ba in case 3 and 4 are to test the differences of using a major and trace element as the divider, respectively. The content of SiO_2 is relatively stable over the space and shows high percentages in both igneous rocks and desert coverage. Ba as the divider is employed as a weighting factor to highlight the geo-information of fault systems because there is a distinct depletion and accumulation of Ba in the fault systems and the igneous rocks, respectively, in eastern Tianshan mineral district (BGEDXP, 2009). Choosing Ba as the divider is similar to the application of TM 5/7 to identify hydrothermal alteration in remote sensing. PCA results of these four cases are demonstrated in Table 4.1 and Figs 4.1 to 4.3.

Table 4. 1 Correlation coefficient matrixes calculated for 4 trace elements by logratio transformations using various dividers. **a:** log-transformation; **b:** sum of weight percent of all 4 oxides as the divider; **c:** weight percent of SiO₂ as the divider; **d:** weight percent of Ba as the divider.

| a: | Sb | Hg | Au | As |
|-----------|-------|-------|-------|-------|
| Sb | 1.000 | | | |
| Hg | 0.348 | 1.000 | | |
| Au | 0.297 | 0.182 | 1.000 | |
| As | 0.675 | 0.276 | 0.497 | 1.000 |

| b: | Sb | Hg | Au | As |
|-----------|-------|-------|-------|-------|
| Sb | 1.000 | | | |
| Hg | 0.466 | 1.000 | | |
| Au | 0.431 | 0.322 | 1.000 | |
| As | 0.750 | 0.421 | 0.595 | 1.000 |

| c: | Sb | Hg | Au | As |
|-----------|-------|-------|-------|-------|
| Sb | 1.000 | | | |
| Hg | 0.384 | 1.000 | | |
| Au | 0.321 | 0.212 | 1.000 | |
| As | 0.693 | 0.317 | 0.515 | 1.000 |

| d: | Sb | Hg | Au | As |
|-----------|-------|-------|-------|-------|
| Sb | 1.000 | | | |
| Hg | 0.414 | 1.000 | | |
| Au | 0.343 | 0.237 | 1.000 | |
| As | 0.712 | 0.354 | 0.532 | 1.000 |

Comparing with the major oxides, concentrations of the trace elements are extremely small. The trading off effects in these 4 trace elements (i.e., Au, As, Hg and Sb) may not as significant as the major oxides, and concentrations of these four trace elements in geochemical data can vary more independently, which means their concentrations have more freedom to vary across the space. Statistical results of the trace elements might consequently be influenced by the closure effect less than the major oxides.

This hypothesis can be validated by the PCA results of the four cases (Figs 4.1, 4.2 and 4.3). Although the bias to small correlations is rectified to different degrees (Tables 4.1), there is no significant difference among statistical results of the four cases (e.g., the eigenvalues, loadings and scores) can be observed. Positive loadings of elements in these four PC1s suggested that they satisfy geochemical signatures of fault systems (Fig. 4.2), by high scores of which the spatial distribution of fault systems in eastern Tianshan mineral district can consequently be indicated (Fig. 4.3). Overlaid with geological features, all PC1s well correspond to the fault traces, among which PC1 scores of case 2 and 3 (Figs 4.3b and 4.3c) show similar patterns to PC1 of case 1 (Fig. 4.3a) while PC1 of case 4 (Fig. 4.3d) demonstrates minor differences and disturbances (e.g., abnormal high values at middle to lower right). Since both numerators and denominators used in case 4 are trace elements with extremely small concentrations (i.e., ppm or ppb), the closure effects are not significant. Furthermore, the 4 logratio transformed trace elements are more influenced by the ratio effect rather than logratio transformation. Therefore, when trace elements are required to be used, dividers like major oxides with general geological meanings (e.g., SiO₂) are recommended in decomposing the closure effect.

Cross-referencing with geologic map, all PC1 scores in Fig. 4.3 show prominent coincidence between high values and fault traces. However, due to the extensive regolith coverage in eastern Tianshan region, there are still many fault traces stretching in areas with low PC1 scores. Therefore, additional treatments are

implemented (see below) to enhance delineation of fault systems associated geochemical signatures in the covered areas.

4.3. Identification of fault systems with Singularity mapping technique

Geo-processes or activities (e.g., tectonism) resulting in mineralization are frequently accompanied by intense accumulation or depletion of materials and energy within a short spatial-temporal interval (Cheng, 2007). End products of these geo-processes (e.g., faults systems) can cause geo-anomalies which are important to mineral exploration (Zhao, 1999). Separating anomalies from background is one of the top issues in geochemical exploration (Cheng, 1999a). Due to some uncontrollable issues (e.g., ground coverage and the burial depth of geological bodies), geochemical anomalies may be weak and difficult to be distinguished from background. Singularity index mapping technique developed within the context of multifractal theory has been proven to be efficient in identifying weak geo-anomalies hidden within the strong variance of background (Cheng, 2007, 2012; Wang et al., 2011, 2012, 2013; Zhao et al., 2012; Zuo et al., 2009).

By means of singularity mapping technique, both weak and strong geo-anomalies of four elements (i.e., Au, As, Hg, and Sb) can be separated from backgrounds, appropriately. After that, singularity indices (i.e., α) of these four elements are integrated by PCA to depict geochemical behaviors of element association caused by tectonism. As introduced previously, a window-based method needs to set several

parameters including windows shape and the minimum and maximum window sizes. Considering both shapes and extents of igneous rocks to be identified, square windows whose side size ranging from 2 km to 26 km with an interval of 4 km were defined. It means that these windows in areas of $2 \times 2 \text{ km}^2$, $6 \times 6 \text{ km}^2$, $10 \times 10 \text{ km}^2$, $14 \times 14 \text{ km}^2$, ... , $26 \times 26 \text{ km}^2$ will be built. For each window, the average value of element concentration $C[A(r_i)]$ is acquired by calculating the mean value of all samples located in the window. At each given location i , element concentration will be calculated for the 7 windows $A(r_i)$. Plotting the average concentrations versus window sizes on a log-log graph, a linear trend line can be draw by means of least square method. Based on Eq. (3-6), the singularity index α for the location i can be estimated by the slop of the straight line (i.e., $\alpha - 2$). By sliding the window sets, singularity indices of a certain element can be estimated for all locations in space.

As described above, geochemical concentrations are laying in a closed system, and the logratio transformation should be applied before any of the statistical treatments. Currently achieved singularity indices depict geochemical behaviors according to the spatial variations of geochemical concentrations, values of which around 2 can vary independently rather than recorded in forms of proportion. Therefore, it is not necessary to take logratio transformation on singularity indices of geochemical signatures before statistical treatments.

Table 4. 2 PCA results of singularity indices of 4 selected geochemical signatures for recognition of fault systems.

| | | | | |
|--|-------------|-------------|-------------|-------------|
| Component variance | PC1 1.92 | PC2 0.91 | PC3 0.83 | PC4 0.33 |
| Loadings of singularity indices of geochemical signatures on PC1 | As 0.62 | Au 0.38 | Hg 0.33 | Sb 0.60 |

The singularity indices calculated for each of the selected geochemical variables are integrated by PCA. Positively loaded singularity indices of four geochemical distributions suggested that PC1 scores can be used to represent the geochemical behaviors of element association (Table 4.2). Based on properties of singularity index (i.e., $\alpha < 2$ means enrichment and $\alpha > 2$ means depletion), low PC1 scores coincident with positive geochemical anomalies can be used to infer the spatial distribution of fault systems. Furthermore, the low scores illustrate precipitation of elemental association from hydrothermal fluids along the fault systems (Fig. 4.4). In addition to the well delineation of strong anomalies in exposed areas, weak anomalies hidden by the strong background (i.e., areas with overburden) are recognized successfully. In comparison with previously achieved patterns (Fig. 4.3), the PCA result by integrating singularity indices of these four elements produces a better performance in recognizing fault systems not only in exposed areas but also in the covered extents.

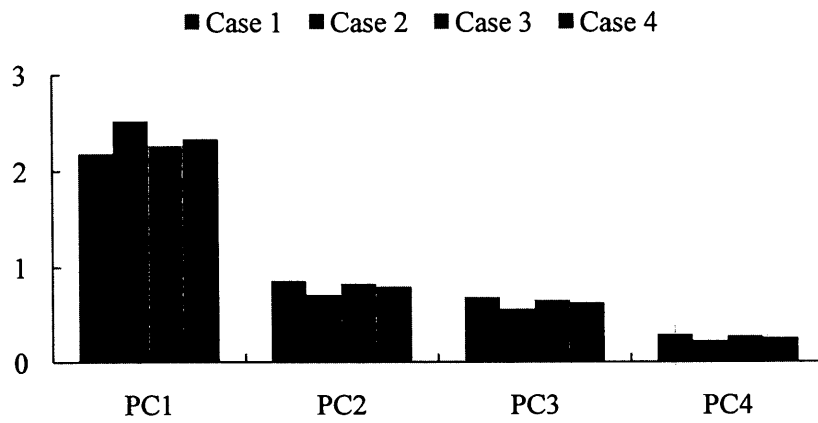


Fig.4. 1 Scree plots of eigenvalues of PC1s of the four cases to recognize fault systems.

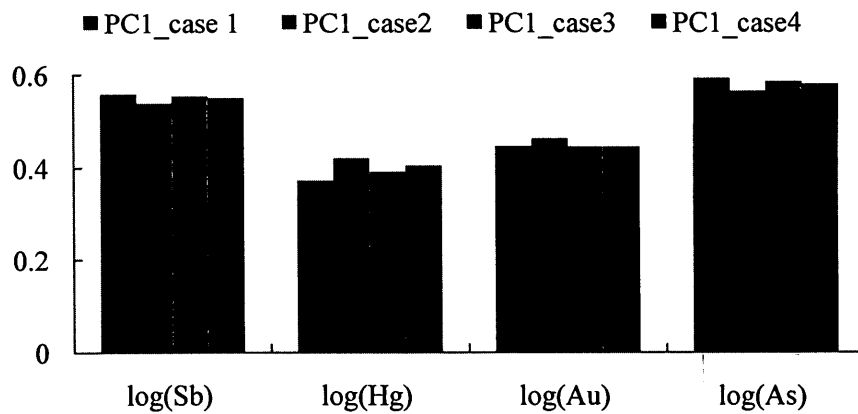
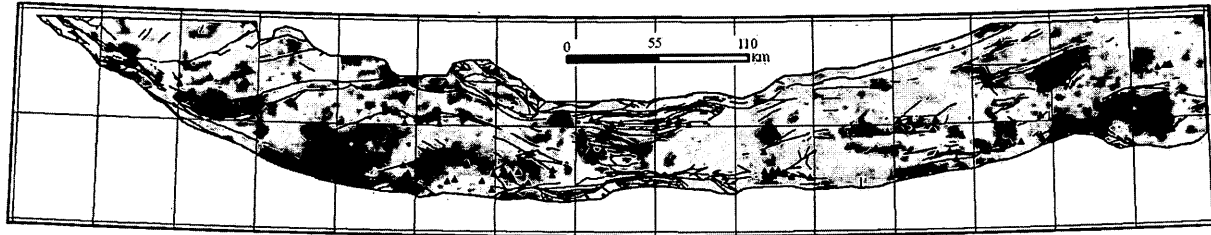


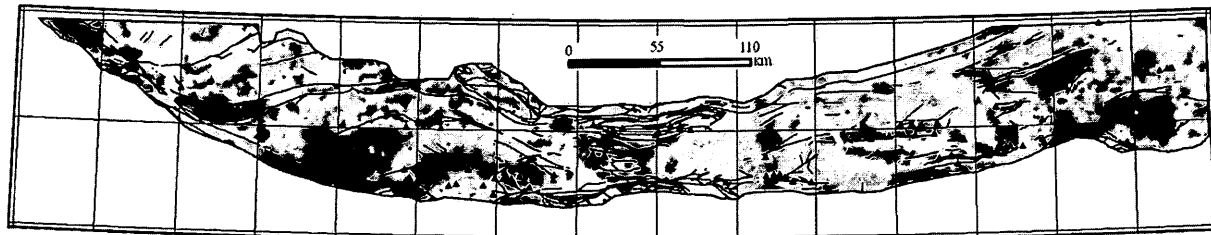
Fig.4. 2 Loading of PC1s of the four cases to recognize fault systems.



PCI: Case 1 ▲ Fe deposits
 ■ High : 6.825 — Faults
 ■ Low : -5.278



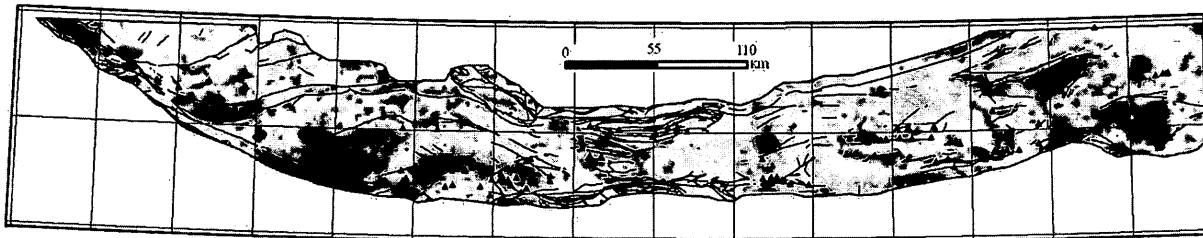
a



PCI: Case 2 ▲ Fe deposits
 ■ High : 6.595 — Faults
 ■ Low : -5.339

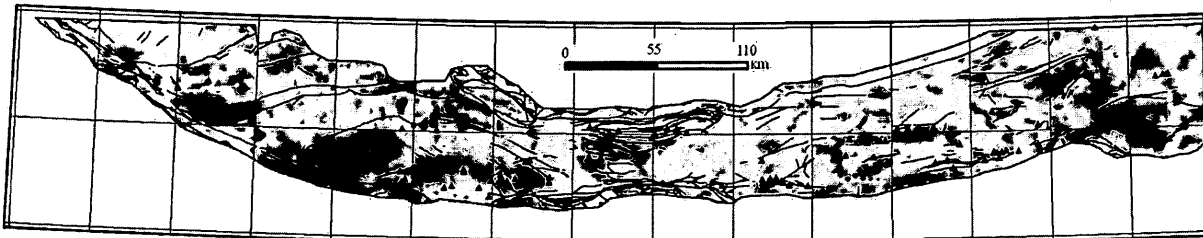


b



PC1: Case 3 ▲ Fe deposits
 High : 6.697 — Faults
 Low : -5.326

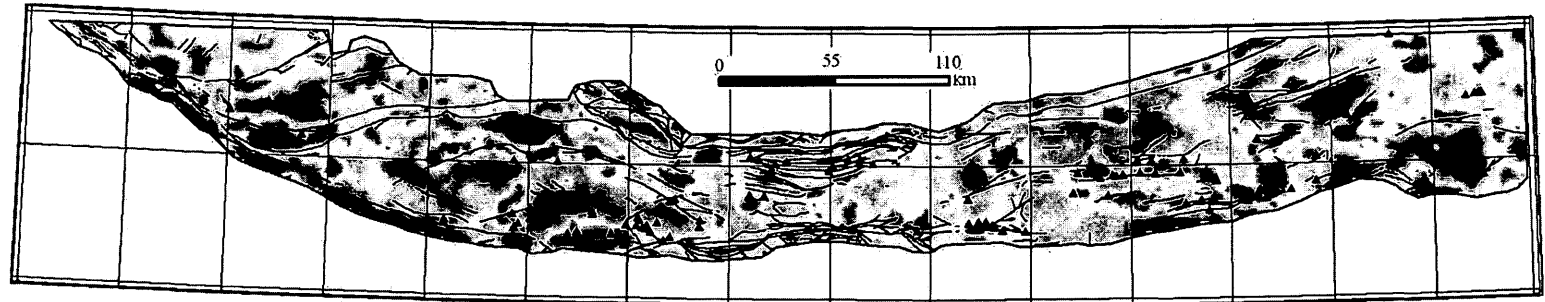
c



PC1: Case 4 ▲ Fe deposits
 High : 7.935 — Faults
 Low : -5.353

d

Fig.4. 3 Score maps of obtained PC1s to delineate spatial distributions of fault systems. a: Case 1; b: Case 2; c: Case 3; d: Case 4.



PC1: Faults ▲ Fe deposits
 ■ High : 5.781 ——— Faults
 ■ Low : -5.651



Fig.4. 4 PC1 scores of singularity indices of 4 selected geochemical signatures (i.e., Au, As, Hg, and Sb) for identification of fault systems. Fault traces and known Fe deposits are shown for reference.

4.4. Summary and discussions

In this chapter, fault systems as an important controlling factor of the Fe mineralization in the study area are investigated through a series of GIS-based spatial analysis methods. In order to enhance the knowledge of fault systems, four geochemical elements associated with fault activities are selected and analyzed. In this study, two issues often reduced exploration efficiency had been concerned. Achieved results can be used to delineate influenced areas of fault systems which are coincident with mineralization favored spaces.

First of all, geochemical concentrations described in forms of proportion are pre-processed by logratio transformation to open the closure system. Through four experiments, experiences beneficial to future applications of logratio transformation are suggested. Secondly, since current study is implemented in a desert area, masses of geochemical anomalies are often masked by ground covers that influence results of geochemical data analysis. In order to enhance weak anomalies hidden within a background with strong variance, singularity index mapping techniques is applied. In comparison with traditionally used geochemical analysis methods, current results are more indicative and informative to describe the influenced areas of fault systems in eastern Tianshan mineral district, China.

In following chapters, other mineralization associated geological features will be

recognized, and then currently achieved faulted areas will be integrated with them to mapping Fe mineral potentials. At the end, all of these features will be investigated jointly to facilitate geological exploration in the study area.

Chapter 5. Identification of felsic igneous rocks

In past decades, mineral exploration in eastern Tianshan mineral district, China has discovered 125 Fe deposits, 87 (or about 70%) of which are spatially and genetically associated with magmatic activities (Table 5.1) (Han and Zhao, 2003; BGEDXP, 2009). A proper understanding of the spatial distribution of igneous rocks is therefore beneficial to Fe mineral exploration in this district. The locations of magmatic igneous rocks have been mapped by traditional geological mapping; however, the ones masked by overburden materials may associate with Fe mineralization have not been investigated sufficiently. In order to enhance knowledge to support future mineral exploration, it is necessary to delineate areas where igneous rocks exist, including areas covered by overburden.

Benefitting from the development of computer sciences and geo-databases, extraction of geo-information from multi-source datasets can satisfy various objectives (e.g., mineral exploration, lithological analysis, age determination, etc.). GIS-based spatial analysis methods provide efficient ways to quantitatively and qualitatively characterize geo-information in spatial and frequency domains (Bonham-Carter, 1994; Darnley, 1995; Pan and Harris, 2000; Carranza, 2008). Geochemical and geophysical signatures are primary indicators of physical and chemical properties of geological

bodies. Geophysical surveys detect the presence of geological bodies in the subsurface. Geochemical data can provide clues about the presence and spatial distribution of geological bodies on/near the surface (Rose et al., 1979). In this chapter, the focus is mainly on geochemical signatures of concealed igneous rocks in the eastern Tianshan district. A comprehensive assessment and prediction of mineral deposits in this area is referred to Cheng (2012).

The study area is a typical arid to semi-arid region in the Gobi desert covered by regolith, tepetate and aeolian sand (Xie and Wang, 2003; Zhuang et al., 2003). Areas above the snowline are snow-covered all year round. Glacier is well developed, the melting of which causes seasonal floods (Wang, 2005b; BGEDXP, 2009). Physical and chemical weathering can result decomposition of exposed rocks. Elements in chemical weathering products occur in the form of solid mineral grains (e.g., quartz and opal), dissolved acid (e.g., silicic acid), silica minerals (e.g., kaolinite), ions (e.g., K^+ and Mg^{2+}), etc (Rose et al., 1979). Among these chemical weathering products, soluble and active materials (e.g., cations and colloids) migrate by surface runoff; whereas insoluble and stable compounds (e.g., quartz and kaolinite) remain kept in situ (Rose et al., 1979). These insoluble and stable compounds constitute the regolith in eastern Tianshan district (Wang et al., 2001). Inherited from the protoliths, geochemical signatures of these compounds in the regolith can be analyzed to infer the covered protoliths (Wang et al., 2001; Brantley and White, 2009).

Table 5. 1 The properties of typical igneous-sedimentary related iron deposits in the eastern Tianshan district, China (modified from BGEDXP, 2009).

| | Deposit Types | Mineralization Time | | Typical Deposit | |
|---------------------|-----------------------------|---------------------|--|--|--|
| | | Total | Time percentage (amount, | Name | Mineralization Process |
| Igneous-related | Magmatic-hydrothermal | 27 | C ₁ (2, 7.4%) C ₂ (10, 37%) P ₁ (15, 55.6%) | Tieling #1, Shuangjingzi | Late Carboniferous granite intruded into Lower-Carboniferous Yamansu volcanic Formation |
| | Marine volcanic | 48 | C ₁ (19, 39.6%) C ₂ (29, 60.4%) | Yamansu, Shaquanzi, Hongyuntan, Bailingshan, Baishanquan, Shuangfengshan | Carboniferous volcanism overlaid by post-igneous hydrothermal alteration. |
| Sedimentary-related | Marine volcanic-sedimentary | 12 | C ₁ (9, 75%) C ₂ (3, 25%) | Kumutag, Lingtietan | Sedimentation of marine volcanics and carbonates overlaid by post-igneous hydrothermal alteration. |

5.1. Identification of felsic igneous rocks with logratio transformed geochemical data

The geochemical data used in identification of felsic igneous rocks consist of major rock-forming oxides (i.e., SiO₂, Al₂O₃, K₂O, Na₂O, CaO, MgO, and Fe₂O₃). Specifically, in the eastern Tianshan district felsic igneous rocks are rich in Ba and Be whereas mafic rocks are rich in Li (BGEDXP, 2009). Three experiments are demonstrated to depict the spatial distribution of felsic igneous rocks by using PCA to 7 log-transformed oxides (i.e., case 1), to 7 air transformed oxides the divider of which is the residual part of the closed system (i.e., $1 - \sum x_i$, $x_i = \text{oxides}$) (i.e., case 2), and to 7 air transformed oxides the divider of which is the sum of weight percent of Ba, Be and Li (i.e., case 3). Among these three experiments, case 1 without opening the closure effect will be treated as a standard to evaluate the improvement of air transformed results. The divider chosen for case 2 is the sum of weight percent of all other compositions (i.e., $1 - \sum x_i$, x_i represents the 7 oxides) which is an intuitive divider without an explicit geological guidance. Consequently, it may cause difficulties to achieve results with explainable geological meanings. The divider used in case 3 is the sum of weight percent of Ba, Be and Li. It is based on previous statements that igneous rocks in eastern Tianshan mineral district is characterized by high concentration of Ba, Be and Li (BEDGXP, 2009). Being the divider in case 3, Ba and Be can enhance geo-information of felsic oxides and depress mafic oxides, while Li

contributes opposite effects. Using the sum of these three as a divider, air transformed data will retain their initial geological meanings.

Table 5. 2 Correlation coefficient matrixes calculated for 7 oxides by logratio transformations using various dividers. Negative values are labeled in bold. **a**: log-transformation; **b**: sum of weight percent of all trace elements (i.e., $1-\sum\text{Oxide}$) as the divider; **c**: sum of weight percent of Ba, Be and Li as the divider.

| a: | SiO ₂ | Na ₂ O | MgO | K ₂ O | Fe ₂ O ₃ | CaO | Al ₂ O ₃ |
|--------------------------------|------------------|-------------------|---------------|------------------|--------------------------------|---------------|--------------------------------|
| SiO ₂ | 1.000 | | | | | | |
| Na ₂ O | 0.312 | 1.000 | | | | | |
| MgO | -0.509 | -0.002 | 1.000 | | | | |
| K ₂ O | 0.280 | 0.167 | -0.510 | 1.000 | | | |
| Fe ₂ O ₃ | -0.237 | 0.149 | 0.737 | -0.511 | 1.000 | | |
| CaO | -0.513 | -0.379 | 0.469 | -0.378 | 0.293 | 1.000 | |
| Al ₂ O ₃ | 0.222 | 0.700 | 0.156 | 0.226 | 0.336 | -0.130 | 1.000 |

| b: | SiO ₂ | Na ₂ O | MgO | K ₂ O | Fe ₂ O ₃ | CaO | Al ₂ O ₃ |
|--------------------------------|------------------|-------------------|---------------|------------------|--------------------------------|-------|--------------------------------|
| SiO ₂ | 1.000 | | | | | | |
| Na ₂ O | 0.779 | 1.000 | | | | | |
| MgO | -0.057 | 0.135 | 1.000 | | | | |
| K ₂ O | 0.655 | 0.561 | -0.313 | 1.000 | | | |
| Fe ₂ O ₃ | 0.271 | 0.397 | 0.726 | -0.130 | 1.000 | | |
| CaO | -0.102 | -0.160 | 0.406 | -0.246 | 0.270 | 1.000 | |
| Al ₂ O ₃ | 0.792 | 0.887 | 0.235 | 0.610 | 0.507 | 0.025 | 1.000 |

| c: | SiO ₂ | Na ₂ O | MgO | K ₂ O | Fe ₂ O ₃ | CaO | Al ₂ O ₃ |
|--------------------------------|------------------|-------------------|---------------|------------------|--------------------------------|-------|--------------------------------|
| SiO ₂ | 1.000 | | | | | | |
| Na ₂ O | 0.732 | 1.000 | | | | | |
| MgO | 0.296 | 0.445 | 1.000 | | | | |
| K ₂ O | 0.477 | 0.373 | -0.109 | 1.000 | | | |
| Fe ₂ O ₃ | 0.435 | 0.541 | 0.827 | -0.107 | 1.000 | | |
| CaO | 0.321 | 0.252 | 0.641 | 0.020 | 0.543 | 1.000 | |
| Al ₂ O ₃ | 0.751 | 0.868 | 0.562 | 0.432 | 0.662 | 0.440 | 1.000 |

Table 5.2 illustrates correlation coefficient matrices calculated for the three pre-processed geochemical data. Confined by the constant sum (i.e., 100%), many correlation coefficients in Table 5.2a are negatively biased; whereas in other two correlation coefficient matrices of alr transformed oxides, negative bias is rectified to different degrees (Tables 5.2b and 5.2c). Based on Kaiser's rule (Kaiser, 1960), PC1s and PC2s of these three cases with eigenvalues greater than 1 can be kept for further analysis (Fig. 5.1). The oxides in compositional data recorded in relative proportion (i.e., weight percent) are commonly used to classify igneous rocks into felsic, intermediate, and mafic/ultramafic. When PCA is applied to the log-transformed geochemical data, the obtained PC with greatest variance (i.e., PC1 in case 1) represents the spatial distribution of different classifications of igneous rocks (Fig. 5.2a and 5.3a). By the alr transformation, opened variables can be considered as the ones characterizing physical existence of geochemical signatures rather than the relative proportion. Compared with the original geochemical data, correlation coefficients of the alr transformed geochemical data shown in Table 5.2 can reflect more realistic relationships among these oxides; moreover, the geo-information of elemental associations (i.e., PC1s in Figs. 5.2b and 5.2c) indicating different ground features (e.g., rocks and desert covers) can be enhanced. Consequently, the greatest variance possessed by new PC1s (i.e., PC1s in case 2 and 3) will no longer denote the classification of igneous rocks but the changes of the ground features (Figs. 5.4b and 5.4c) which were shown by PC2 in case 1 (Fig. 5.4a). Rather than expressed by the

dominating geo-information contained in alr transformed data (i.e., PC1s in case 2 and 3), geochemical signatures classifying igneous rocks (i.e., same as PC1 in case 1 does) are possessed by other PCs (i.e., PC2s in case 2 and 3) (Figs. 5.2b, 5.2c, 5.3b and 5.3c); therefore, based on loadings of these oxides, PC2s of case 2 and 3 can be used to indicate spatial distribution of felsic igneous rocks in current study. Overlaid with geological map, PC2 score map of alr transformed oxides in case 3 performs the best in corresponding with spatial distributions of outcrops of felsic igneous rocks. It can be seen that a divider with explicit geological meanings can enhance the geochemical signatures of numerators in identification of objective geological bodies.

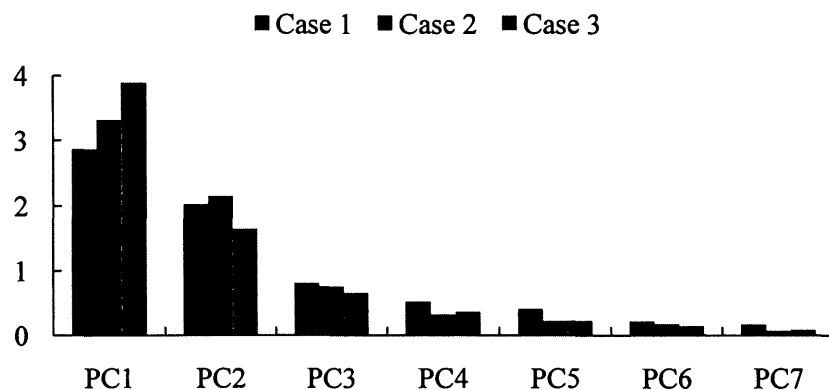
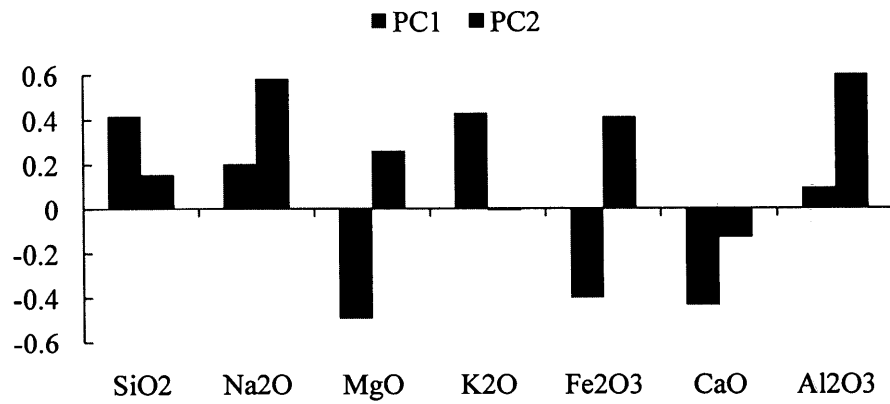
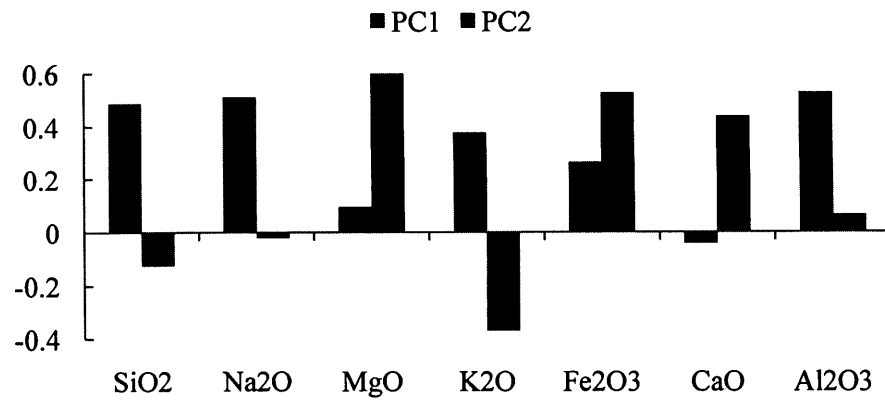


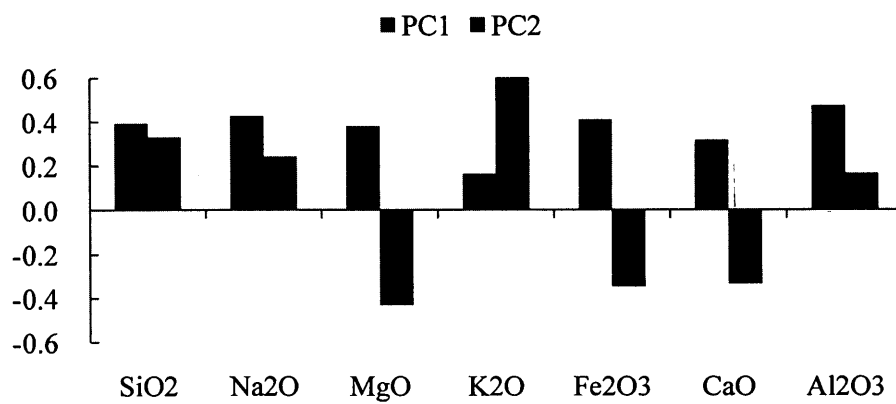
Fig.5. 1 Scree plots of eigenvalues of PCs of the three cases to recognize felsic igneous rocks.



a

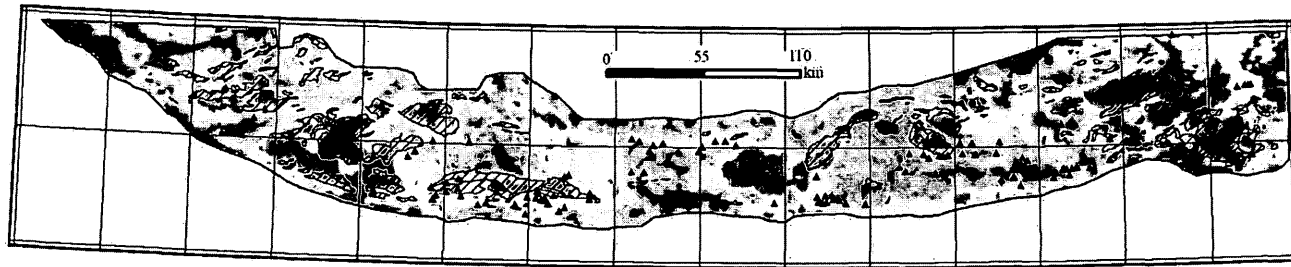


b



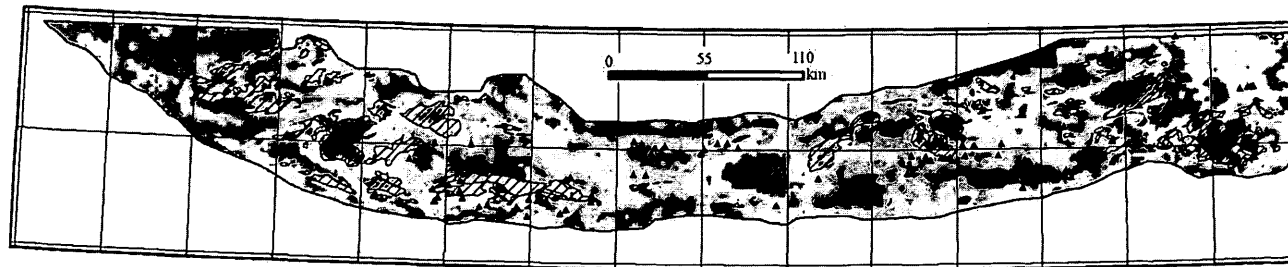
c

Fig.5. 2 Loading of PC1s and PC2s of the three cases to recognize felsic igneous rocks. a: Case 1. b: Case 2. c: Case 3.



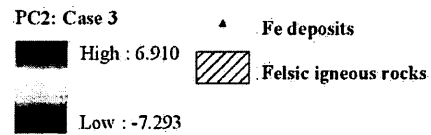
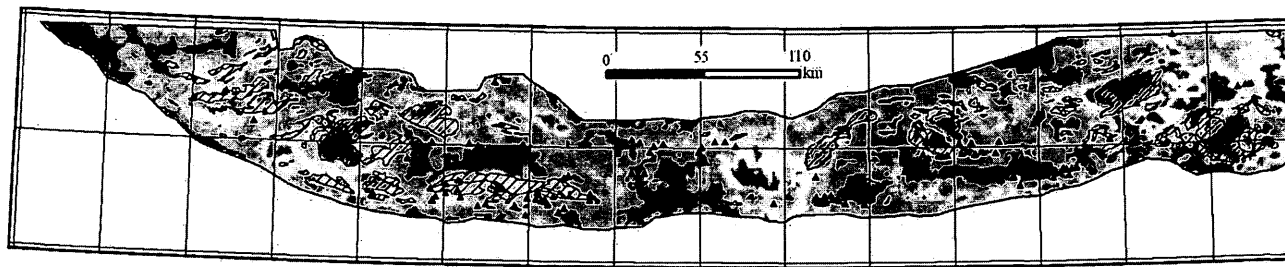
PC1: Case 1
 ▲ Fe deposits
 High : 6.253
 Felsic igneous rocks
 Low : -12.317

a



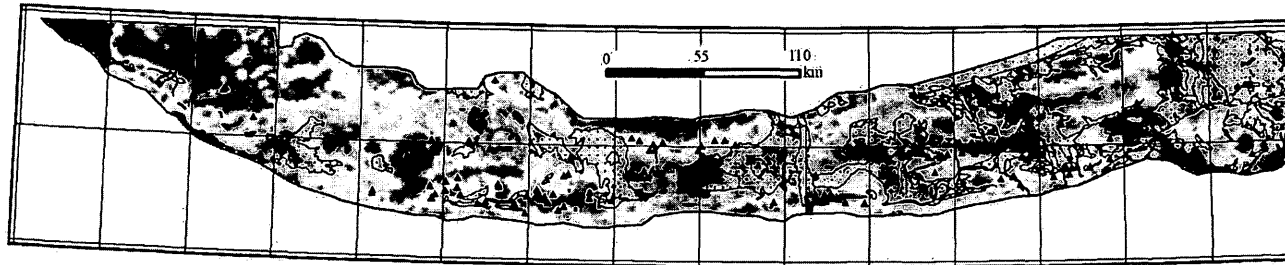
PC2: Case 2
 ▲ Fe deposits
 High : 5.593
 Felsic igneous rocks
 Low : -6.228

b







c

Fig.5. 3 Score maps of obtained PCs to delineate spatial distributions of felsic igneous rocks. a: PC1 of log-transformed geochemical data in case 1. b: PC2 of alr transformed geochemical data in case 2. c: PC2 of alr transformed geochemical data in case 3.

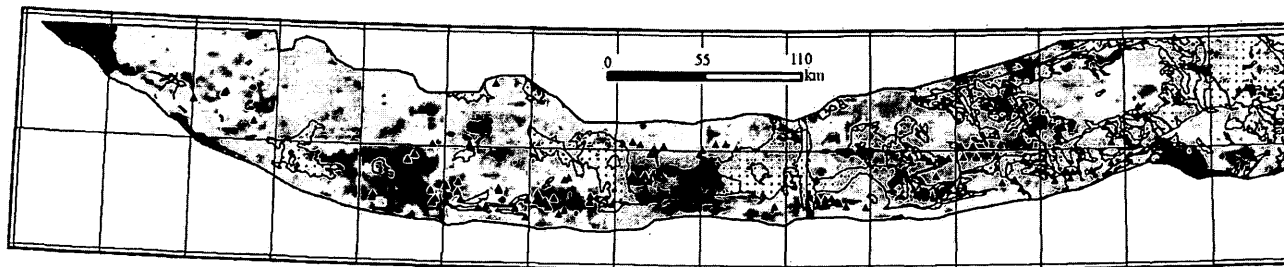


PC2: Case 1




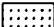
| | | | |
|---|---------------|---|-------------|
|  | High : 3.216 |  | Fe deposits |
|  | Low : -17.273 |  | Desert |



a

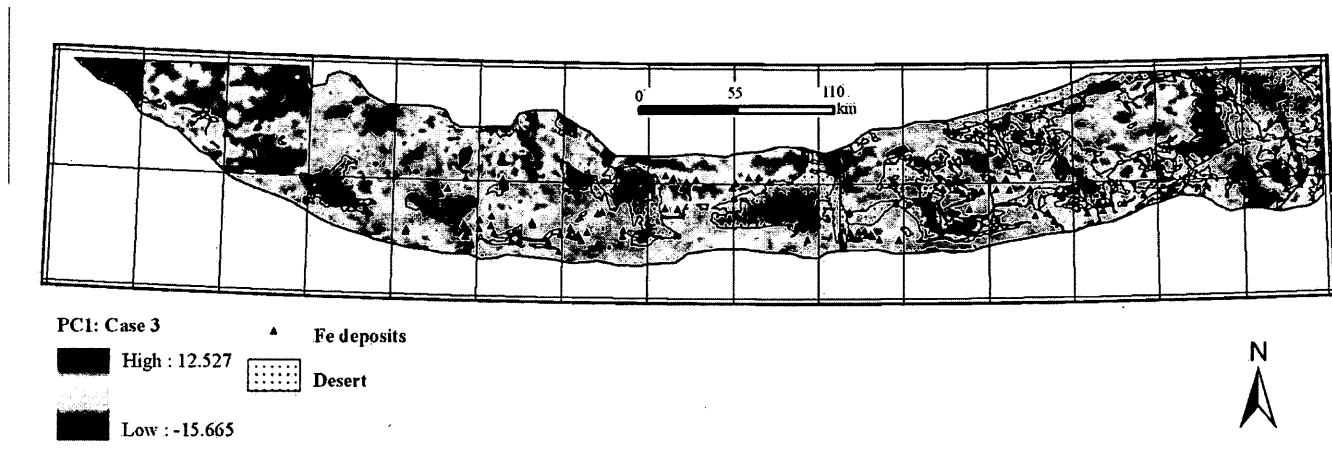


PC1: Case 2

| | | | |
|---|---------------|---|-------------|
|  | High : 8.791 |  | Fe deposits |
|  | Low : -18.135 |  | Desert |



b



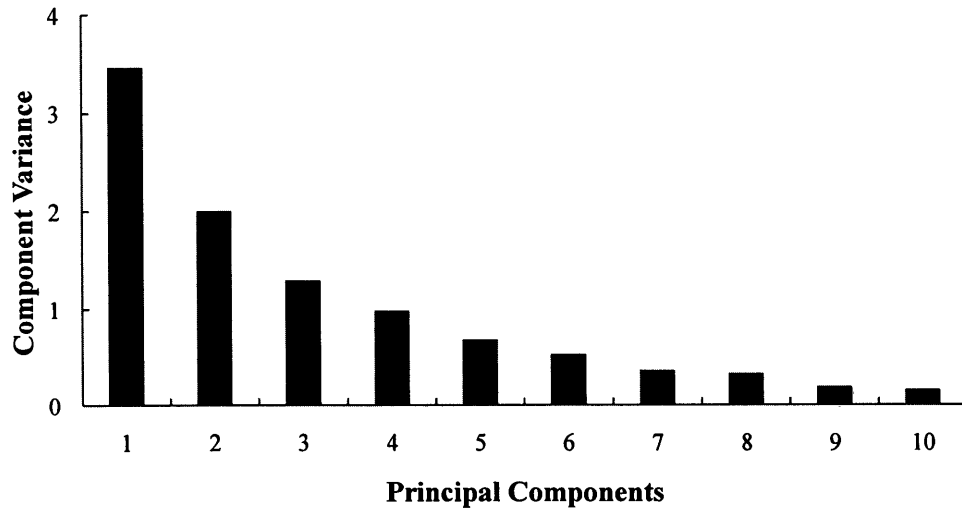
c

Fig.5. 4 Score maps of obtained PCs to indicate changes of rock types. a: PC2 of log-transformed geochemical data in case 1. b: PC1 of alr transformed geochemical data in case 2. c: PC1 of alr transformed geochemical data in case 3.

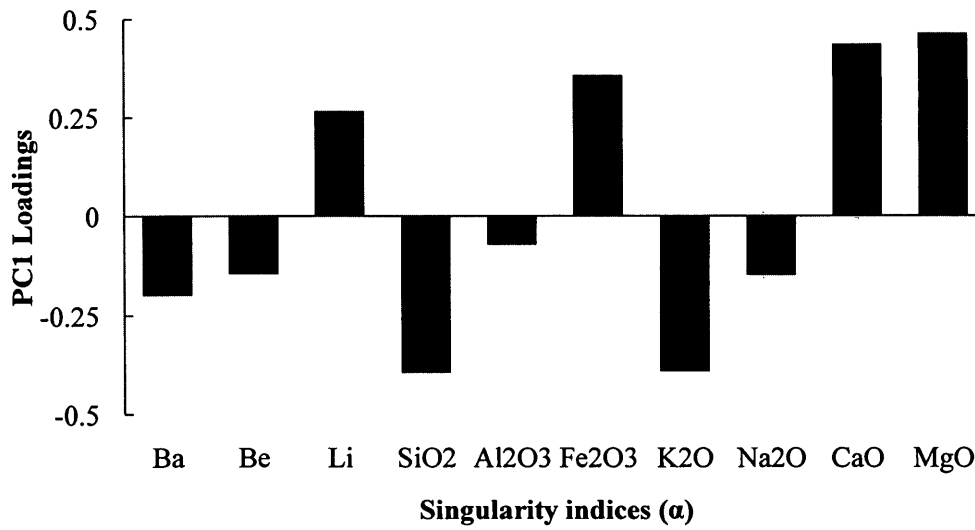
5.2. Identification of felsic igneous rocks with Singularity mapping technique

As main products of magmatism, igneous rocks can be analyzed to investigate magmatic activities (Cheng, 2007). Similar as the tectonism, magmatism is a non-linear geo-process as well. The formation of igneous rocks is frequently accompanied by enormous energy release and material accumulation in narrow spatial-temporal intervals. Local singularity mapping method is consequently satisfied to recognize the spatial distribution of geo-anomalies associated with igneous rocks. Considering both shapes and extents of igneous rocks to be identified, square windows with minimum and maximum window sizes of 2 km and 26 km, respectively, were defined. Many mapped units of igneous rocks in the study area have elliptical shape with an axis longer than 25 km. The defined ε_{max} insures that the estimated singularity indices can properly characterize the geochemical properties of igneous rocks.

Besides the previously introduced 7 oxides (i.e., main component of magmatic rocks), Ba, Be, and Li which are specifically enriched in igneous rocks in eastern Tianshan region are employed to recognize the felsic igneous rocks. The singularity indices calculated for these selected geochemical variables are integrated by PCA. The results are shown in Figs. 5.5 and 6.



a



b

Fig.5. 5 PCA results using singularity indices of geochemical data. **a:** Scree plot of eigenvalues of principal components of singularity indices of geochemical data; **b:** Loadings of geochemical variables on PC1 of singularity indices of geochemical data.

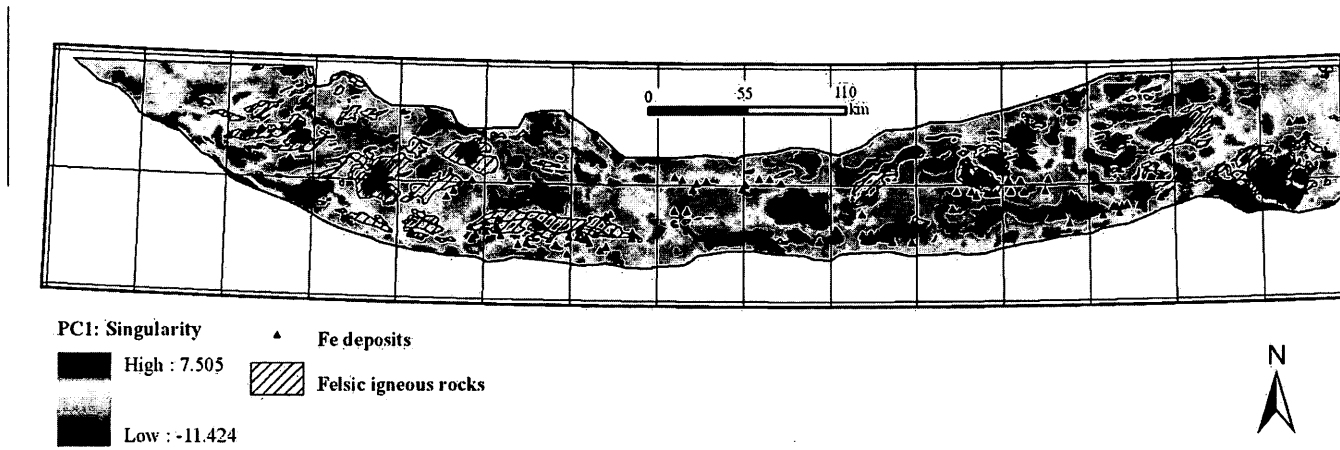


Fig.5. 6 PC1 score maps of singularity indices of geochemical data.

Eigenvalues of the first two PCs greater than 1 support that PC1 and PC2 can be retained for further analysis (Figs. 5.5a); furthermore, loadings of geochemical variables on PC1 suggest that PC1 can be used to indicate presence of felsic intrusive rocks (Fig. 5.5b). Negatively loaded felsic association and positively loaded femic association can be used to infer that the spatial distribution of high PC1 scores (Fig. 5.6) is indicative to felsic intrusions, and the strong coincidence with locations of known felsic igneous rocks in the study area indicates that currently achieved result is geological reasonable and meaningful. More importantly, compare to the result in Fig. 5.3b and 5.3c, the PCA result of singularity indices of selected geochemical signatures in Fig. 5.6 demonstrates a noticeable improvement for recognition of possible igneous rocks especially in the covered areas (Fig. 5.6). The high PC1 scores in the eastern parts of the district (e.g., areas around Jing'erquan and Xingxingxia) illustrate that singularity indices of geochemical data rather than alr-transformed geochemical data can effectively reduce the influence of weathering on geochemical anomalies and allow extraction of geochemical anomalies from high regional elemental background. The high PC1 scores in the western parts of the district illustrate that singularity are advantageous for enhancing weak anomalies within low regional elemental background. Furthermore, the high PC1 scores in the middle parts of the district (Figs. 5.6, 5.3b, and 5.3c) can be interpreted as patterns of exposed and concealed rocks. However, the patterns in the middle parts of the district may be caused by physical drifting of regolith as well. Therefore, the presence of igneous bodies beneath regolith

needs further validation. One way is to compare the results with geophysical data and another way is to validate by drilling. Cheng (2012) explained how singularity index mapping can be used to detect anomalies caused by buried sources in covered areas, and used Fe_2O_3 concentration data for validating the idea. The author also integrated geophysical and geochemical data for the delineation of igneous rocks. It has been proved that singularity indices calculated from geochemical concentrations of oxides are associated with gravity and aeromagnetic anomalies.

5.3. Conclusions

In the study area, most marine volcanic-sedimentary Fe deposits are found in the Yamansu Formation, which is recognized as the ore-hosting strata. Based on the spatial distribution of felsic igneous outcrops and Fe deposits, the area is divided from the middle into eastern and western parts. In the western half, Fe deposits are primarily found within the contact zones of felsic igneous rocks with the Yamansu Formation. This indicates that the felsic igneous rocks provided heat and ore-forming materials for the formation of Fe deposits and/or hydrothermal alteration. Future mineral exploration in the western part can focus on skarn rocks within the contact zones of felsic igneous rocks with Yamansu Formation carbonate rocks. In contrast, Fe deposits in the eastern half are associated with mafic extrusive rocks of the Yamansu Formation. This indicates that the formation of Fe deposits experienced the processes of volcanic extrusion, magma migration, ore-forming material

sedimentation, and mineralization. The scattered distributions of felsic igneous rocks in the eastern part could have enriched the Fe mineralization as in the western part. Therefore, intersections of mafic extrusive rocks of Yamansu Formation with felsic igneous rocks are interesting targets for future exploration of Fe deposit in the eastern part.

Geochemical exploration in overburden areas has become a major challenge in recent decades. In the Gobi desert region, geo-anomalies related to mineralization in eastern Tianshan district are masked by overburden to a great extent. In this paper, principal components analysis was applied separately to alr-transformed stream sediment geochemical data and to singularity indices of stream sediment geochemical data. The scores of interpretable principal components indicate well the spatial distribution of exposed igneous rocks and, to some extent, those with concealed by desert overburden. Finally, the results show that singularity indices of geochemical data are more advantageous than ilr-transformed geochemical data for mapping of areas likely underlain by igneous rocks beneath overburden.

Chapter 6. Identification of the Yamansu Formation

In eastern Tianshan district, the most primary ore-hosting unit is the Lower Carboniferous Yamansu Formation which is mainly distributed within the extent of the Yamansu volcanic basin (Wang et al., 2006). Lithologically, the Yamansu Formation is composed of complex sediment series including submarine felsic-mafic lava, volcanoclastic rocks, terrigenous clastics, and carbonate rocks, etc. (Ding, 1990; Hou et al., 2006; Xiao et al., 2004). Among various rock types, the mafic extrusive rocks are believed to provide ore sources for Fe mineralization (Jiang et al., 2002). Although Fe ore types are diverse (e.g., volcanic-sedimentary, hydrothermal, and contact skarn deposits, etc.), most of them distributed around ancient volcanic edifices are stratigraphically controlled. Moreover, due to the Paleozoic collision between the Junggar plate (in the north) and Tarim plate (in the south), the volcanic edifices produced by the tectonism are linearly distributed in an EW direction in eastern Tianshan mineral district. As a result, the long axes of the extrusive rocks are in accordance with the trending orientation of major faults. Previous literatures revealed that the stratiform, stratiform-like, and lens ores with same attitudes as their hosts are mainly embraced by carbonate-rich fine-grained volcanoclastics or skarns (Ding, 1990; Han et al., 2002). By hydrothermal alteration, the banded structure of ore bodies consisting of ore minerals (e.g., magnetite), gangue minerals (e.g., garnet, chlorite,

actinolite, epidote, calcite and quartz, etc.) and sulfide minerals (e.g., pyrite and chalcopyrite) can be widely observed (BGEDXP, 2009; Deng et al., 2006; Han et al., 2002; Lu et al., 1996). Preliminary results of geochemical exploration indicate that the Yamansu Formation is rich in Cu, Pb, Zn, Au, Ag, Bi, Mo, W, As, Hg, and Sb (BGEDXP, 2009). Among these elements, Au, Ag, Cu, Pb, and Zn correspond to the main metallic mineralization in the Yamansu Formation. Bi, Mo, and W (i.e., the group 6 elements) correspond to the felsic igneous rocks associated mineralization. As, Hg and Sb (i.e., the semimetal and mineralizer elements) formerly used to indicate the fault systems can be employed to illustrate fault controlled volcanic strata (BGEDXP, 2009).

6.1. Identification of the Yamansu Formation with logratio transformed geochemical data

Similar to the identification of fault systems in chapter 4, 11 trace elements (i.e., Cu, Pb, Zn, Au, Ag, Bi, Mo, W, As, Hg, and Sb) are selected to recognize the Yamansu Formation. Two experiments demonstrated in this chapter to delineate the spatial distribution of the Yamansu Formation are applications of PCA to the log-transformed selected geochemical signatures (i.e., case 1) and to the alr transformed selected geochemical signatures (i.e., case 2). As introduced in the section 4.2, the major oxide SiO_2 is chemically stable and distributed continuously across the space, the weight percent of which is used as the divider of alr transformation for these elements.

Table 6. 1 Correlation coefficient matrix calculated for **a**: 11 log-transformed trace elements and **b**: 11 air transformed trace elements using the weight percent of SiO₂ as the divider. Negative values (in Table 6.1a) and the increased correlation coefficients (in Table 6.1b) are labeled in red.

| a: | Sb | Bi | As | W | Mo | Zn | Pb | Hg | Cu | Au | Ag |
|-----------|-----------|-----------|-----------|----------|-----------|-----------|-----------|-----------|-----------|-----------|-----------|
| Sb | 1.000 | | | | | | | | | | |
| Bi | 0.112 | 1.000 | | | | | | | | | |
| As | 0.716 | 0.198 | 1.000 | | | | | | | | |
| W | 0.202 | 0.586 | 0.287 | 1.000 | | | | | | | |
| Mo | 0.274 | -0.048 | 0.342 | 0.047 | 1.000 | | | | | | |
| Zn | 0.361 | 0.040 | 0.442 | 0.144 | 0.240 | 1.000 | | | | | |
| Pb | 0.104 | 0.316 | -0.003 | 0.234 | 0.102 | -0.032 | 1.000 | | | | |
| Hg | 0.463 | -0.065 | 0.341 | -0.002 | 0.247 | 0.186 | 0.013 | 1.000 | | | |
| Cu | 0.184 | 0.005 | 0.310 | 0.034 | 0.222 | 0.636 | -0.096 | 0.173 | 1.000 | | |
| Au | 0.354 | 0.176 | 0.485 | 0.162 | 0.234 | 0.205 | 0.028 | 0.186 | 0.291 | 1.000 | |
| Ag | 0.338 | -0.071 | 0.361 | -0.085 | 0.386 | 0.251 | 0.120 | 0.265 | 0.208 | 0.236 | 1.000 |

| b: | Sb | Bi | As | W | Mo | Zn | Pb | Hg | Cu | Au | Ag |
|-----------|-----------|-----------|-----------|----------|-----------|-----------|-----------|-----------|-----------|-----------|-----------|
| Sb | 1.000 | | | | | | | | | | |
| Bi | 0.222 | 1.000 | | | | | | | | | |
| As | 0.712 | 0.266 | 1.000 | | | | | | | | |
| W | 0.407 | 0.564 | 0.394 | 1.000 | | | | | | | |
| Mo | 0.441 | 0.259 | 0.579 | 0.356 | 1.000 | | | | | | |
| Zn | 0.438 | 0.126 | 0.545 | 0.273 | 0.564 | 1.000 | | | | | |
| Pb | 0.299 | 0.400 | 0.244 | 0.365 | 0.275 | 0.256 | 1.000 | | | | |
| Hg | 0.414 | 0.085 | 0.354 | 0.170 | 0.353 | 0.246 | 0.244 | 1.000 | | | |
| Cu | 0.385 | 0.078 | 0.548 | 0.184 | 0.573 | 0.774 | 0.131 | 0.283 | 1.000 | | |
| Au | 0.343 | 0.202 | 0.532 | 0.183 | 0.386 | 0.252 | 0.125 | 0.237 | 0.365 | 1.000 | |
| Ag | 0.381 | 0.180 | 0.460 | 0.251 | 0.510 | 0.521 | 0.381 | 0.196 | 0.473 | 0.262 | 1.000 |

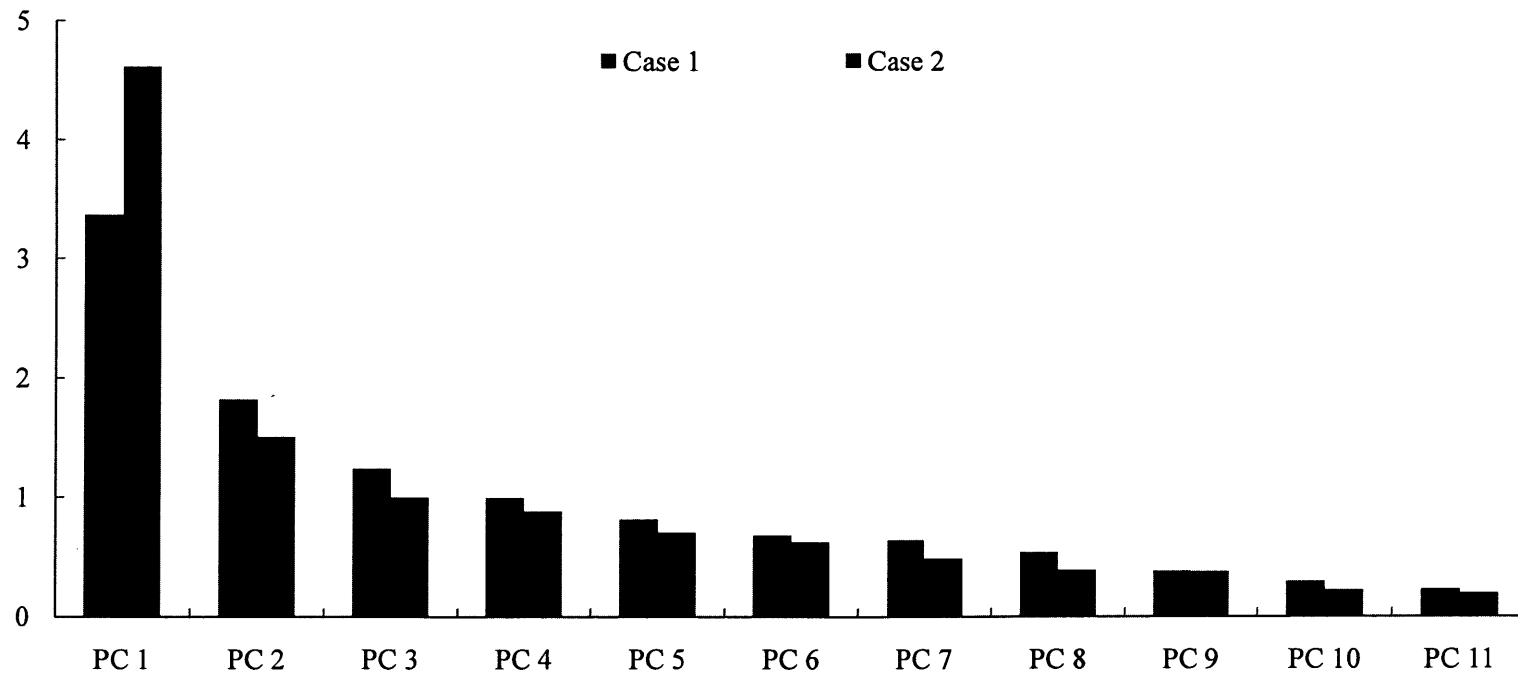


Fig.6. 1 Scree plots of eigenvalues of PC1s of the two cases to recognize the Yamansu Formation.

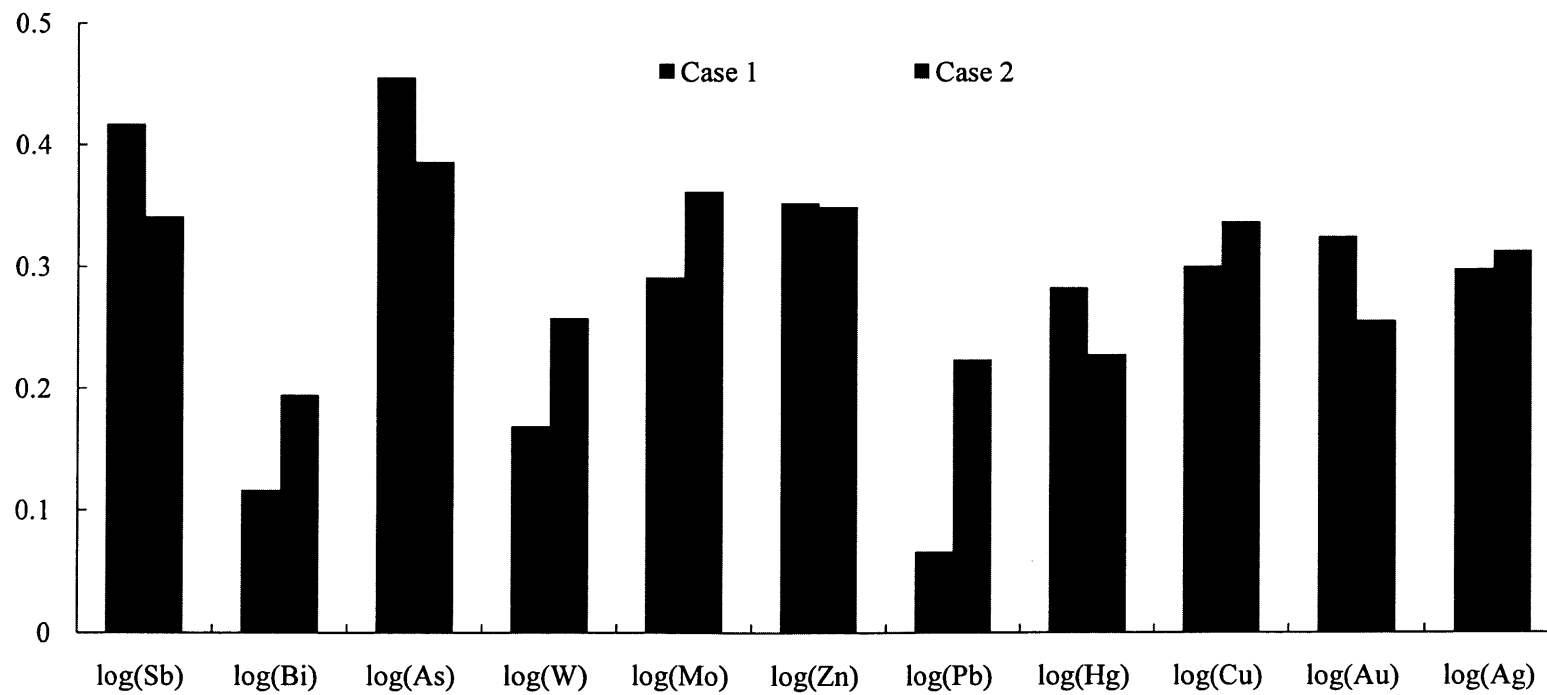


Fig.6. 2 Loading of PC1s of the two cases to recognize the Yamansu Formation.

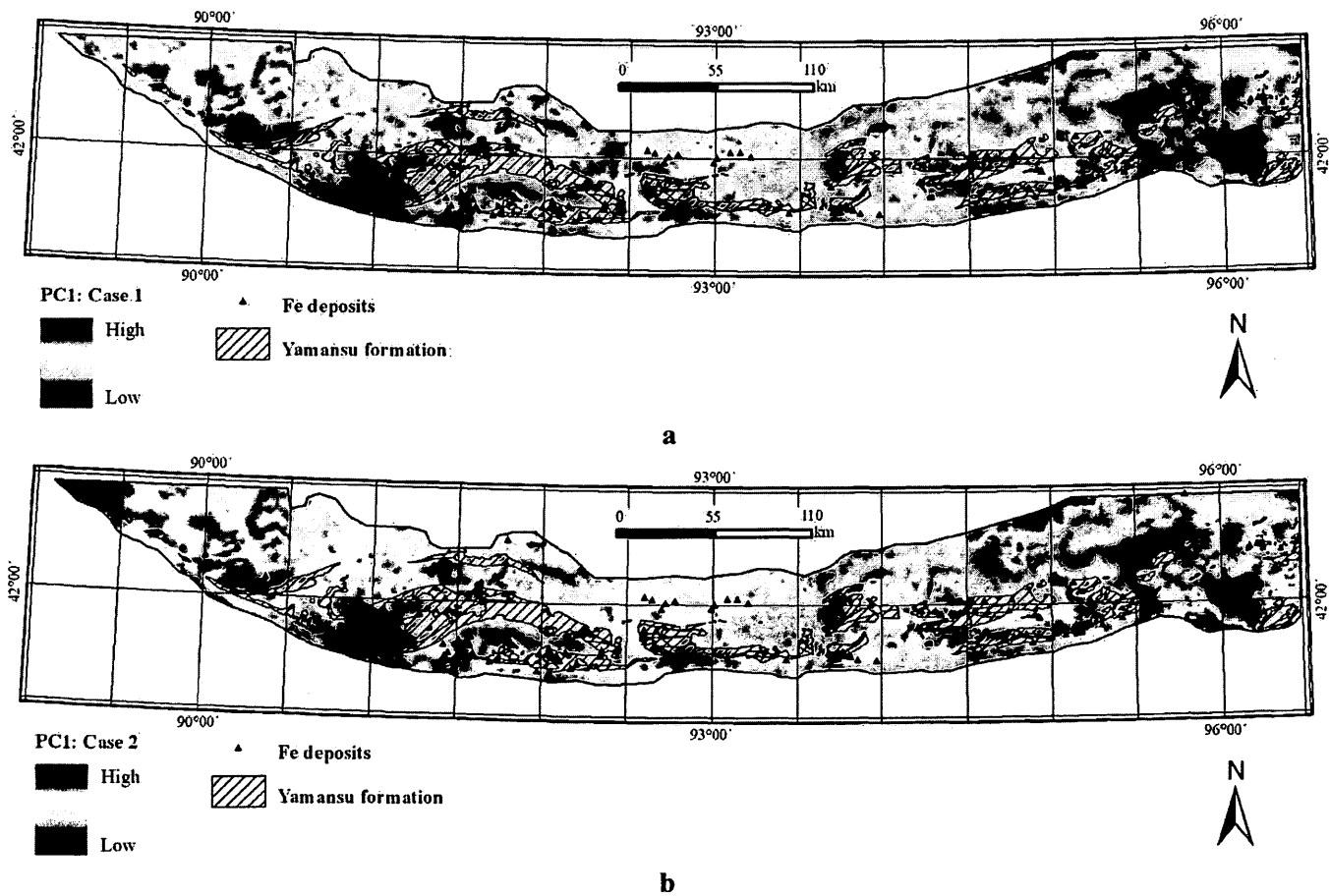


Fig.6. 3 Score maps of obtained PC1s to delineate spatial distributions of the Yamansu Formation. a: Case 1. b: Case 2. Outcrops of the Yamansu Formation and known Fe deposits are shown for reference.

The correlation coefficient matrices demonstrated in Table 6.1 imply that the bias to negative correlation between pairs of variables has been greatly rectified by log-ratio transformation that there is no more negative values shown in the correlation coefficient matrix of 11 alr transformed selected geochemical signatures. Moreover, most of the correlation coefficients have been improved by alr transformation. It means that the closure effect existed among the geochemical data has been solved, although trace elements may not be affected by the closure effect as much as the oxides. The greater eigenvalue of the first PC in case 2 than in case 1 (Fig. 6.1) implies that the PC1 of alr transformed geochemical signatures possesses greater variance of the geochemical data. Considering the geo-information contained in PC1 and other PCs as signal and noise, PC1 of the case 2 with higher signal to noise ratio (SNR) may reflect the reality more precisely than of the case 1. Positive loadings of all the trace elements on PC1s of both cases (Fig. 6.2) satisfy geochemical signatures of the Yamansu Formation. It is suggested that the two PC1s can indicate presence the igneous strata. High values of both PC1 score maps showing similar patterns are coincident to the spatial distribution of the Yamansu Formation (Fig. 6.3). The fact implies that using SiO_2 (i.e., the major oxide with stable spatial distributions across the space) as the divider in alr transformation does not significantly affect the geochemical property of elements. Therefore, the alr transformed geochemical signatures are superior in possessing the geological meanings of the original data and eliminating the closure effect.

6.2. Identification of the Yamansu Formation with singularity mapping technique

Based on the metallogeny of volcanic sedimentary Fe deposit in eastern Tianshan mineral district, the formation of Fe deposit is mainly associated with the Yamansu Formation and the Late Carboniferous felsic intrusions. The mafic and felsic members are believed as the main ore resources and carrier of heat and materials in support of metasomatism for Fe mineralization, respectively (BGEDXP, 2009). The contact between these two lithological units may probably be beneficial to the formation of Fe deposits. Therefore, delineating spatial distributions of geochemical signatures of the Yamansu Formation and the variations of lithology will be beneficial to mineral exploration in the study area. As introduced in former sections, the Yamansu Formation is generally a volcanic strata produced by the Early Carboniferous volcanism. Similar to mineralization, the volcanic eruption accompanied with enormous releases of energy and accumulation of materials is a non-linear geo-process. The location of volcanic edifices presents fractal geometry in space. Confined by the volcanic eruption center, the spatial distribution of the volcanic strata which are located around the volcanic edifices can be investigated with fractal and multifractal modeling technique. Similar as the description of geochemical signatures of felsic igneous rocks in chapter 5, singularity index mapping technique is currently applied to the 11 elements (i.e., Cu, Pb, Zn, Au, Ag, Bi, Mo, W, As, Hg, and Sb) to demonstrate their geochemical behaviors (i.e.,

accumulation and depletion) in the study area. Derived singularity indices of these elements are further integrated by PCA to characterize the enrichment of the element association which indicates geochemical signatures of the Yamansu Formation.

By singularity mapping technique, accumulation of element in space is characterized by $\alpha < 2$ whereas depletion of element is by $\alpha > 2$. Stability in content of an element in a given area is characterized by $\alpha = 2$. In order to recognize the Yamansu Formation related geochemical behaviors of element association, singularity indices of the 11 geochemical distributions are integrated by PCA. Singularity indices of all elements possessing same signs in PC1 (Table 6.2) suggests that PC1 can be used to indicate the geochemical signatures of element association related to the Yamansu Formation. In addition, since all elements contribute positively in PC1, low scores can be used to represent positive geochemical anomalies of the element association (i.e., accumulation) (Fig. 6.4). The spatial distribution of the low PC1 scores indicating the enrichment of element association can therefore be used to characterize the present of the Yamansu Formation. Overlying with geological occurrences, patterns with low PC1 scores (i.e., positive anomalies) are well coincident with the outcrops of the Yamansu Formation and most of known Fe deposits. It satisfies the fact that Fe deposits in eastern Tianshan mineral district are mainly hosted by the Yamansu Formation. Compared with the PC1 scores of all transformed geochemical signatures illustrated in the previous sections (Fig. 6.3b), currently derived PC1 score map based on singularity indices shows a better

performance in identifying the spatial distribution of the Yamansu Formation. The patterns well coincident with the outcropped Yamansu Formation demonstrate that singularity mapping technique can enhance weak geochemical anomalies hidden in both the strong (i.e., Xiaorequanzi volcanic basin in the western tail of the study area) and the weak background (i.e., desert cover in the eastern tail of the study area). Referring to the geological map shown in Fig. 2.1b, geochemical anomalies of the element association located in desert areas are enhanced to supports the Fe exploration in covered areas. Therefore, the singularity-based PCA result indicating spatial distribution of the Carboniferous Yamansu volcanic Formation will be used jointly with other two controlling factors (i.e., fault systems and felsic intrusions) in future data integration procedure.

Table 6. 2 PCA results of singularity indices of 11 selected geochemical signatures for recognition of the Yamansu Formation.

| Component variance: | PC1 | PC2 | PC3 | PC4 | PC5 | PC6 | PC7 | PC8 | PC9 | PC10 | PC11 |
|--|------|------|------|------|------|------|------|------|------|------|------|
| | 3.66 | 1.49 | 1.07 | 1.00 | 0.85 | 0.74 | 0.66 | 0.49 | 0.47 | 0.30 | 0.27 |
| Loadings of singularity indices of geochemical signatures on PC1 | Au | Ag | Cu | Pb | Zn | Bi | Mo | W | As | Hg | Sb |
| | 0.22 | 0.28 | 0.29 | 0.23 | 0.33 | 0.25 | 0.37 | 0.33 | 0.42 | 0.16 | 0.36 |

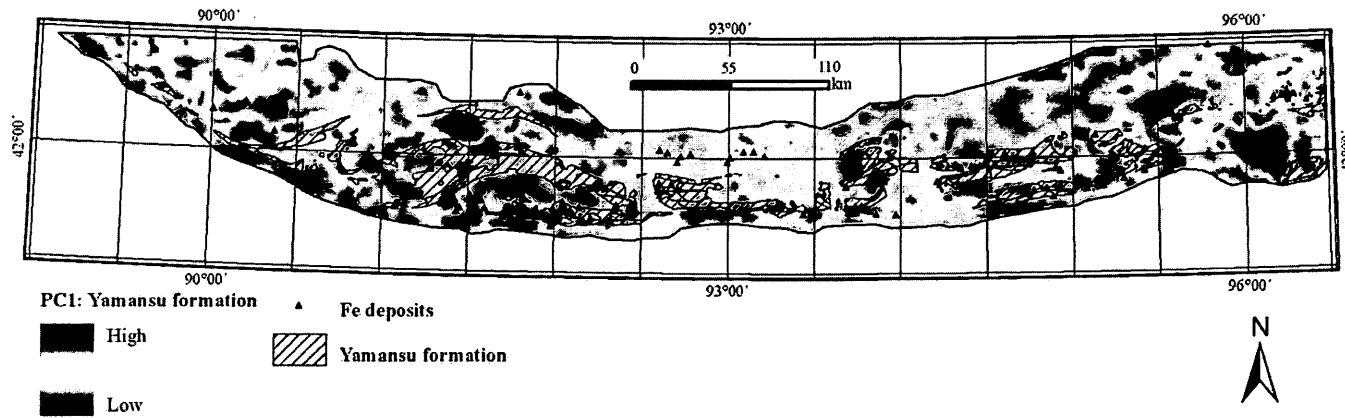


Fig.6. 4 PC1 scores of singularity indices of 11 selected geochemical signatures for identification of the Yamansu Formation. Outcrops of the Yamansu Formation and known Fe deposits are shown for reference.

6.3. Discussions

Trace elements commonly used to characterize mineralization associated geochemical signatures are currently used to characterize geological features. In this chapter, following the recognition of the mineralization associated fault systems and felsic igneous rocks, the spatial distribution of the Yamansu Formation is delineated by applying PCA to alr transformed elements (associated with the Yamansu Formation) and to singularity indices of these elements.

Comparing these two delineations, the singularity index-based PC1 more efficient in identifying geo-information in eastern Tianshan mineral district (i.e., a cover area); whereas, the alr transformation-based result can not indicate the distribution, appropriately, due to the cover effects. Therefore, the PC1 by integrating singularity indices of the 7 elements is chosen to represent presence of the Yamansu Formation. In the following chapters, current result will be integrated with other mineralization associated geological features to mapping the mineralization favored areas supported by tectonism, magmatism and metamorphism.

Chapter 7. Recognition of Fe mineralization

Former mineral exploration indicates that mineralization no matter types (e.g., hydrothermal, sedimentary, etc.) and conditions of occurrences (e.g., buried or exposed) is always accompanied with geochemical anomalies (Jiang et al., 2006). These anomalies may exist around the ore bodies shown as geochemical halos. As the distance from the mineralization centers increasing, their strength decreases until reaches the background. In practice, geochemical anomalies can be recorded in rocks, soil, water, gas, and even vegetation, detection of which is advanced to locate mineralization centers (Jiang, 2006). Among various media, sample collected from soil, rocks and stream sediments are commonly applied because of their superiority in relatively stable, less affected, and easier to preserve. In recent decades, geochemical survey are routinely used in almost all mineral exploration programs, with the assist of which, mechanism of relative enrichment of economic elements in various positions of an interested area can be determined to satisfy human needs (Rose et al., 1979).

Geochemical exploration in eastern Tianshan mineral district, China was first launched in 1985. Delineated anomalous areas (about 7,738 km²) by previous researches are mainly distributed in the Yamansu and Xiaorequanzi volcanic basins. Confined by the exploration technology, equipment, and resolution of geochemical data, only 28 out of 135 Fe deposits in the study area were located within the anomalous area, although the threshold to separate geochemical anomalies and background was not strict at all (BGEDXP, 2009). Apparently, the efficiency of

previous geochemical exploration cannot satisfy to map mineral potentials in the study area. In this study, geochemical data with higher resolution and advanced data processing methods are available to assist the geochemical exploration. The data processing procedure with better performance in delineating potential areas of Fe mineralization will be demonstrated in the following sections in this chapter.

7.1. Geochemical signatures of Fe mineralization mapping

7.1.1. Geochemical signatures of Fe

Fe concentration in currently used stream sediment geochemical data is recorded in form of Fe_2O_3 . In eastern Tianshan mineral district, the spatial distribution of Fe_2O_3 concentration is nonuniform (Fig. 7.1) (BGEDXP, 2009). The most prominent geochemical anomalies of Fe_2O_3 concentration are located in the Xiaorequanzi volcanic basin that corresponds to the Fe enrichment in the Xiaorequanzi volcanic Formation; however, there were not so many Fe deposits discovered in this area. In addition, the Fe mineralization is eminent in the Aqishan-Bailingshan area, the Kanggurtag-Tuwu area, the east district of the Kumtag sand ridge, the Yamansu volcanic basin, and the Shaquanzi area as well. Typical volcanic sedimentary Fe deposits located in these areas include the Kumtag, the Chilongfeng, the Tieling, the Yufeng, the Bailingshan, the Hongyuntan, and the Yamansu deposits, etc. As introduced in previous chapters, Fe mineralization in the study area is mainly associated with intermediate-mafic volcanic rocks, spatial distribution of which is generally confined by the EW trending fault systems. These mineralization areas are consequently extending along EW direction (BGEDXP, 2009; Li et al., 2002; Mao et

al., 2005; Yang et al., 1996).

In addition to the Fe mineralization in eastern Tianshan mineral district, intermediate-mafic volcanic rocks composed of Fe rich minerals (e.g., olivine, pyroxene, and hornblende) are another main source of Fe_2O_3 (Han et al., 2002; Ma et al., 1993; Wang et al., 2006). Broadly distributed intermediate-mafic volcanic rocks in the study area can result high values in Fe_2O_3 concentration and high geochemical background. It might be the reason why only a small number of Fe deposits were discovered in anomalous areas of Fe_2O_3 coincident with the Xiaorequanzi volcanic basin. On the contrary, the east tail of the study area (i.e., the Jing'erquan subarea) is mainly covered by desert, where the insufficiency of Fe-rich minerals in the sandy coverage causes low Fe_2O_3 concentration or low geochemical background. However, remarkable Fe mineralization is still performed in this area. These two situations imply that delineating of Fe potential areas by analyzing the spatial distribution of Fe_2O_3 concentration is unreliable. The strategy of geochemical exploration in this area should be based on eliminating the influence of both Fe-rich igneous rocks and sandy coverage.

7.1.2. Fe anomalies mapping

As described above, employment of geochemical data for characterizing anomalies associated with mineralization in eastern Tianshan mineral district, China requires advanced spatial analysis methods, because geochemical data used to analyze Fe concentration is recorded in Fe_2O_3 . This form of iron concentration can reflect the

spatial distribution of both Fe deposits and Fe-rich geological bodies (e.g., intermediate-mafic igneous rocks) in the study area. Furthermore, influenced by the desert, geochemical anomalies associated with Fe mineralization in covered areas are weak. These two situations are frequently termed as high and low geochemical background, respectively. However, the mineralization is a typical non-linear process accompanied with enormous energy release and material accumulation. Consequently, the concentration of Fe_2O_3 in Fe deposits is overwhelmingly greater than those in Fe-rich igneous rocks. In addition, geochemical properties of the Fe mineralization are extraordinarily distinguished from desert coverage, although the Fe mineralization only occurs within a narrow space. Therefore, recognition of the differences between Fe mineralization and its surroundings is beneficial to the Fe potential mapping. The singularity mapping technique applied in former chapters to identify spatial distributions of mineralization associated geological bodies (i.e., fault systems, felsic intrusions, and the Yamansu Formation) is currently used to describe the spatial variations of Fe_2O_3 concentration. By this method, geochemical anomalies associated with Fe mineralization can be identified from both high and low background.

Fig. 7.2 illustrates the spatial distribution of singularity indices of Fe_2O_3 concentration calculated by window-based method with sizes ranging from 2 km to 26 km. Based on the definition of singularity index, areas with α less than 2 (i.e., low values) represent accumulation of Fe_2O_3 (i.e., positive anomalies) while areas with α greater than 2 (i.e., high values) represent depletion of Fe_2O_3 (i.e., negative anomalies). As

the primary advantage of singularity index mapping technique, geochemical anomalies can be separated from both strong and weak background efficiently. Specifically, positive anomalies of Fe_2O_3 at exposed area (e.g., the Xiaorequanzi volcanic basin, the Aqishan-Bailingshan area, and the Yamansu volcanic basin) demonstrate the separation of Fe mineralization associated anomalies from the ones with Fe-rich igneous rocks. Anomalous areas indicated by the spatial distribution of singularity indices of Fe_2O_3 have been greatly reduced, especially in the Xiaorequanzi volcanic basin (Fig. 7.2). Meanwhile, positive anomalies at covered area (e.g., the Jing'erquan area) have been notably enhanced which demonstrates the separation of weak Fe anomalies blurred by sandy cover.

7.2. Geochemical signatures of Fe mineralization associated elements mapping

Element measured for detecting ore bodies is termed as indicator element, such as Fe for Fe ores or Cu for Cu ores. However, the indicator element being sought, in a majority of situations, may be difficult to detect, or yielding features which are unreliable and difficult to interpret (Ross et al., 1979). Elements with similar physical-chemical properties have a tendency to aggregate together by various geo-processes (Jiang et al., 2006). These elements are so-called element association. Rather than a single element, anomalies of element association are commonly employed to investigate related geological bodies due to their priority of being stable and reliable to interpret corresponding geological processes (BGEDXP, 2009).

Therefore, knowledge to the spatial distribution of element associations means significantly to mineral potential mapping.

7.2.1. Geochemical signatures of element association

In this research, using Fe_2O_3 as the indicator for mapping of Fe potentials encounters many problems. The most important issue is that the Fe anomalies are indicative to both Fe deposits and Fe-rich rocks. In order to locate potential areas of Fe mineralization, variations in Fe_2O_3 concentration has been derived by the singularity mapping technique. However, the spatial distribution of singularity indices of Fe_2O_3 is still doubtful, because the relative enrichment of Fe_2O_3 (i.e., positive singularity) within the mafic igneous rocks may not probably related with Fe mineralization. Therefore, it is necessary to consult with elements which are specifically enriched in Fe ores other than igneous rocks. In the following sections, more reliable result to depict potential areas of Fe mineralization will be obtained by investigating geochemical signatures element association related to Fe mineralization.

Published literatures (BGEDXP, 2009; Han et al., 2002; Qin et al, 2003; Wang et al., 2006) indicate that the Fe mineralization can be sorted into four sub-categories according to ore element assemblages: Fe deposits, Fe-Mn deposits, Fe-V-Ti deposits, and Fe-Cu-Zn deposits. From a geochemical perspective, the geochemical anomalies of element associations are more reliable than of a single element to assist in Fe mineral exploration; mapping of the spatial distributions of these geochemical signatures is therefore necessary to depict target areas. In currently study, the element

association consisting of Fe_2O_3 , Mn, V, Ti, Co, Ni, Cu, and Zn which are specifically enriched in Fe ore bodies will be used to investigate the geochemical signatures related to Fe mineralization.

Applying PCA to these elements, achieved results suggest that PC1 satisfies characterization of the geochemical signatures of the element association (Fig. 7.3). The low PC1 scores can be used to delineate geochemical anomalies associated with Fe mineralization (Fig. 7.3c). In addition, the variance and the loadings on PC1 also illustrate the strong coexistence of the 8 selected geochemical signatures. By comparing the spatial distribution of Fe_2O_3 concentration (Fig. 7.1) and the geochemical signatures of element association (Fig. 7.3c), the coexistence can also be observed from these two similar patterns. Although patterns with high values are similarly distributed in these two maps, the spatial distribution of geochemical signatures of element association with stronger geological guidance is more reliable to depict mineralization associated geochemical anomalies than the Fe_2O_3 (Fig. 7.1).

7.2.2. Anomaly mapping

From the perspective of non-linear theory, mineralization as a singular geo-process exhibit fractal/multifractal properties (Cheng, 2007, 2012; Zhao et al., 2012). Consequently, fractal or multifractal analysis of element association related to mineralization might be more reasonable to characterize mineralization. The multifractal-based singularity mapping technique is currently used. Similar to

identification of the fault systems, felsic igneous rocks, and the Yamansu Formation, deriving geo-information of Fe mineralization from geochemical signatures of the element association requires a combining usage of the singularity mapping technique and PCA. By this model, singularity indices of each element can be estimated, and then PCA is applied to delineate the spatial distribution of the element association.

From the results of PCA, PC1 with highest eigenvalue possesses the greatest variance of the geochemical data sets and all elements are positively loaded, loadings of which suggested that the PC1 satisfies characterization of the geochemical signatures of element association related to Fe mineralization (Fig. 7.4). Based on properties of singularity index (i.e., $\alpha < 2$ represents positive anomalies and $\alpha > 2$ represents negative anomalies), low values in PC1 scores are coincident with Fe anomalies. Comparing the two PC1 score maps (Figs. 7.3c and 7.4c), the latter is eligible to detect both strong and weak anomalies from background from either exposed or covered areas. It indicates that based on singularity mapping technique, the precision in depicting spatial variations of geochemical signatures of Fe mineralization has been improved.

In order to compare these depicted Fe mineralization (Figs. 7.1-7.4), the Student's *t*-value in the context of weights of evidence (WofE) is applied to evaluate the statistical significance of spatial relationship between known Fe deposits and evidence layers. Patterns with highest spatial association with known Fe deposits are defined as

the target areas of Fe mineralization for each map. In this chapter, evidence layers derived in the previous sections include the spatial distribution of Fe concentration (Fig. 7.1), singularity indices of Fe concentration (Fig. 7.2), PC1 scores of geochemical signatures of element association (Fig. 7.3c), and PC1 scores of singularity indices of geochemical signatures of element association (Fig. 7.4c). By the Student's *t*-value, their efficiency in indicating Fe mineral occurrences can be achieved and compared (Figs. 7.5 and 7.6), and some useful information can be derived from the statistics (Table 7.1). For the spatial distribution of Fe₂O₃ concentration, although covering the most known deposits, the targets occupying nearly half of the study area may not be an efficient prediction to Fe deposits (Fig. 7.6a). The similar problem is possessed by the PC1 scores of geochemical signatures of element association as well (Fig. 7.6c). On the contrary, targets delineated by spatial distributions of both singularity indices of Fe₂O₃ concentration (Fig. 7.6b) and the element association (Fig. 7.6d) circle more than half number of the known Fe deposits by covering less than a quarter of the study area that provide more efficient references for mineral exploration. By eliminating influences of both strong and weak geochemical background, anomalous areas depicted by the singularity index method are more likely to be related with Fe mineralization rather than mixed with Fe-rich igneous rocks (Figs. 7.6b and 7.6d). Moreover, target areas derived based on the geochemical signatures of element association can provide more reliable indication in mapping mineral potentials (Fig. 7.6d), because the element association, in a majority

of situations, performs better than a single element in describing geochemical signatures related to mineralization (Figs. 7.6b).

7.3 Discussions

In this chapter, the singularity index mapping technique is currently applied to depict spatial variations of Fe mineralization associated geochemical signatures. With the assist of the advanced technology, influences of both Fe-rich rocks and sandy coverage can be eliminated appropriately. In addition, the spatial distribution of geochemical signatures related to Fe mineralization has been depicted using both single element and element associations. From the perspective of exploration geochemistry, the element association providing more reliable geo-information regarding mineralization is commonly employed to assist mineral potential mapping. The Student's *t*-value is applied to further depict target areas of Fe mineralization. By comparing the efficiency of all evidence layers (Fig. 7.6), the PC1 scores of singularity indices of element association with more confidence in indicating geo-information of Fe mineralization and with higher efficiency in depicting target areas will be used in following chapters.

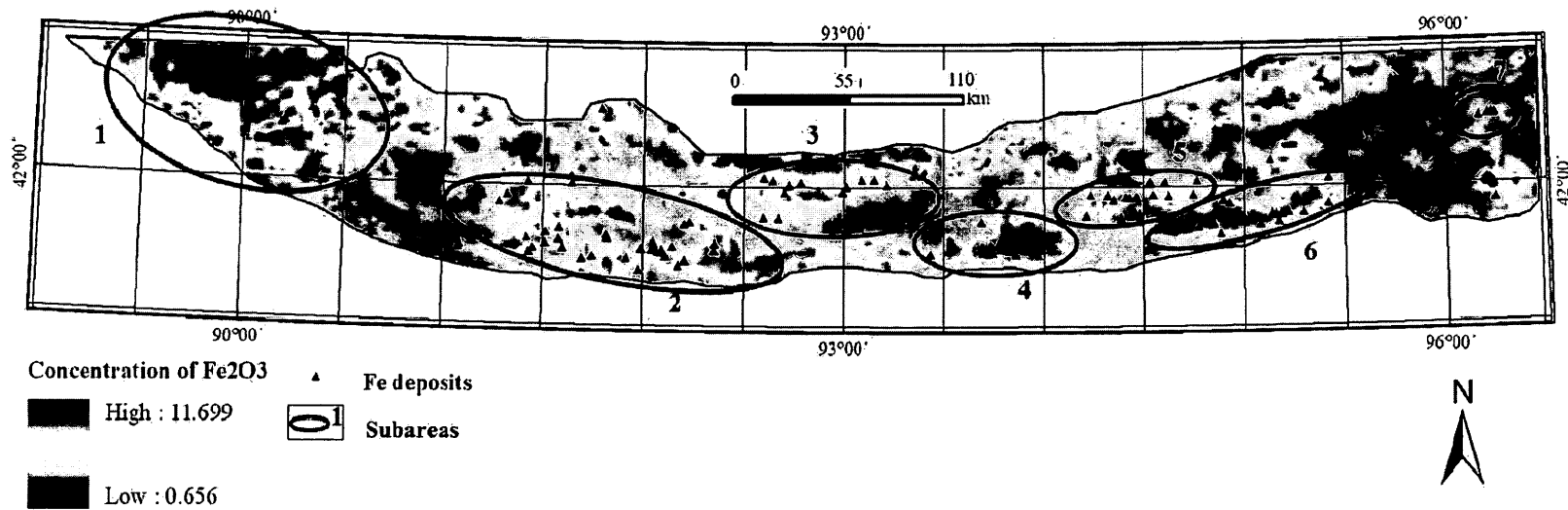


Fig.7. 1 Spatial distributions of Fe₂O₃ concentration in eastern Tianshan mineral district. High values are corresponding to high Fe concentration. 7 subareas are circled in red color. From the west to the east, they are (1) the Xiaorequanzi volcanic basin, (2) the Aqishan-Bailingshan subarea, (3) the Kanggurtag-Tuwu subarea, (4) the east district of the Kumtag sand ridge, (5) the Yamansu volcanic basin, (6) the Shaquanzi subarea, and (7) the Jing'erquan subarea.

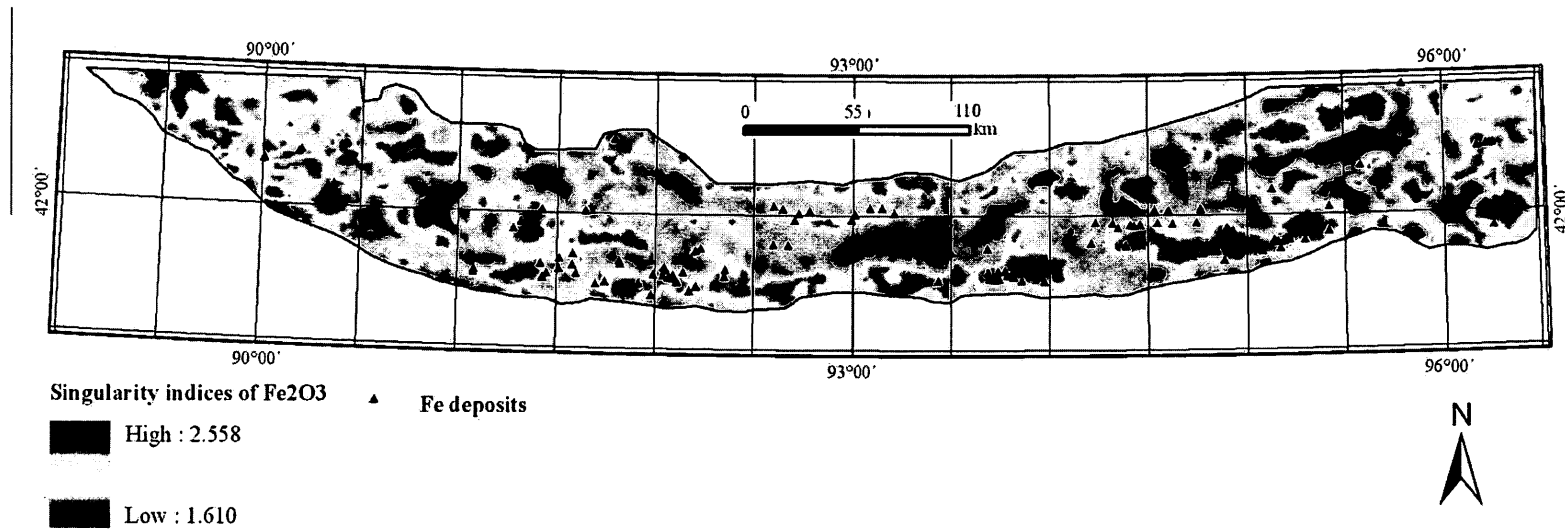
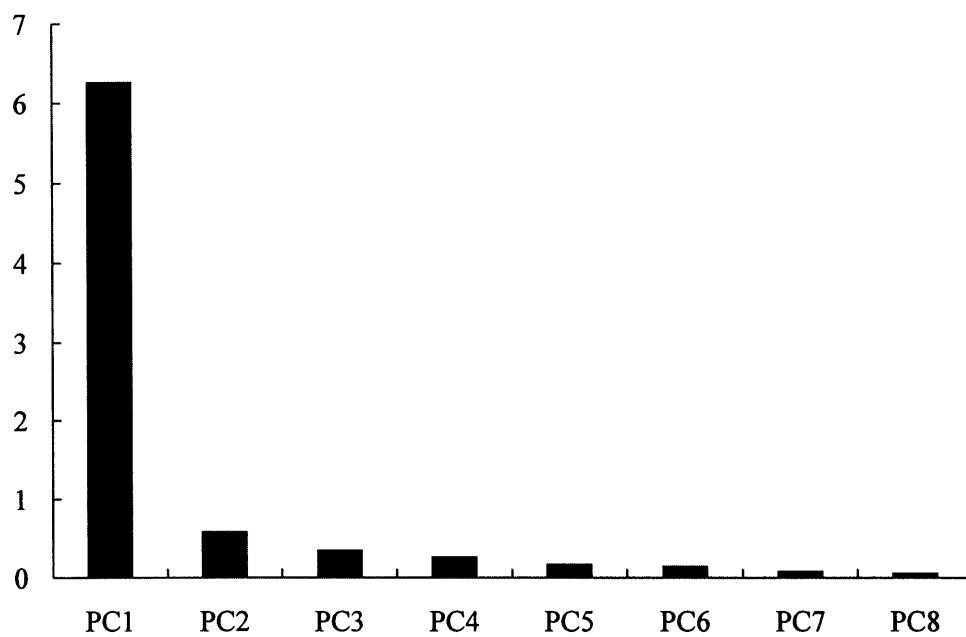
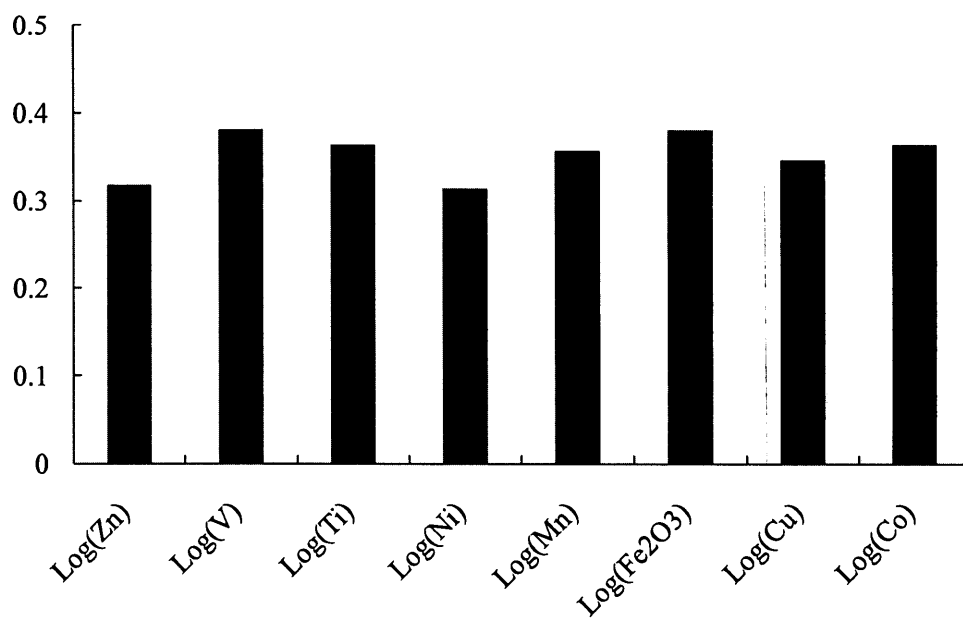


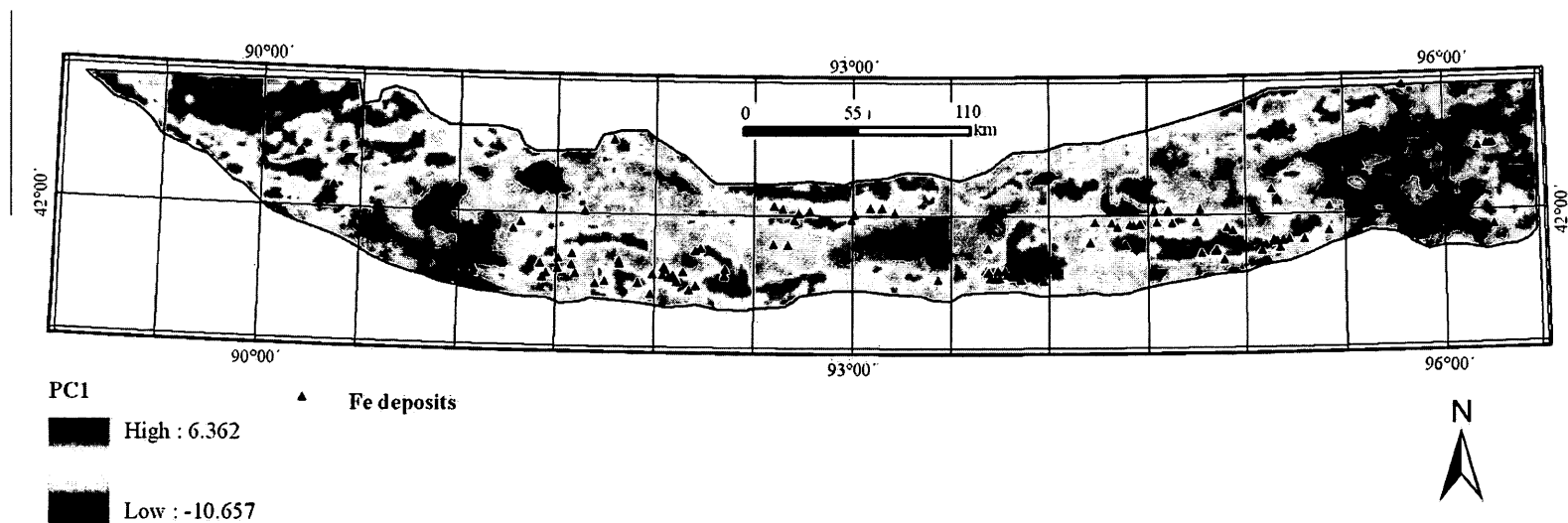
Fig.7. 2 Spatial distribution of singularity indices of Fe₂O₃ concentration describing geochemical behaviors caused by Fe accumulation. Black triangles indicate the location of known Fe deposits and occurrences.



a

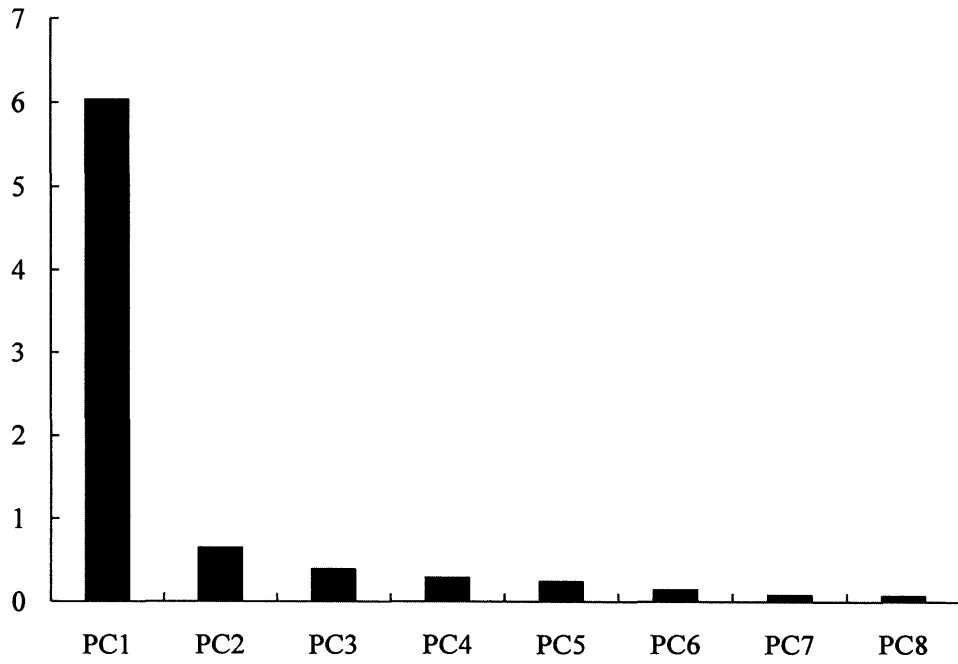


b

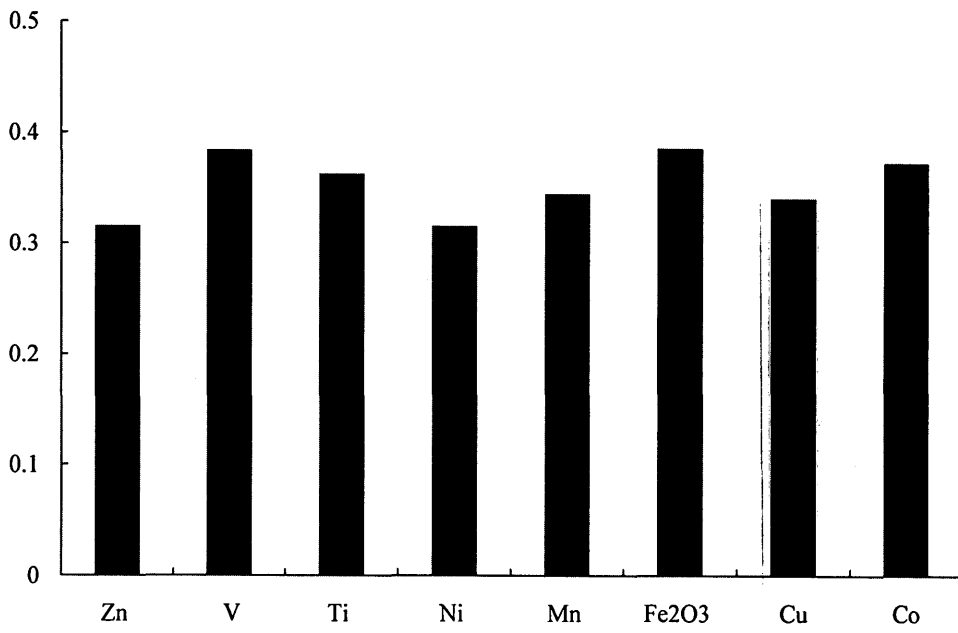


c

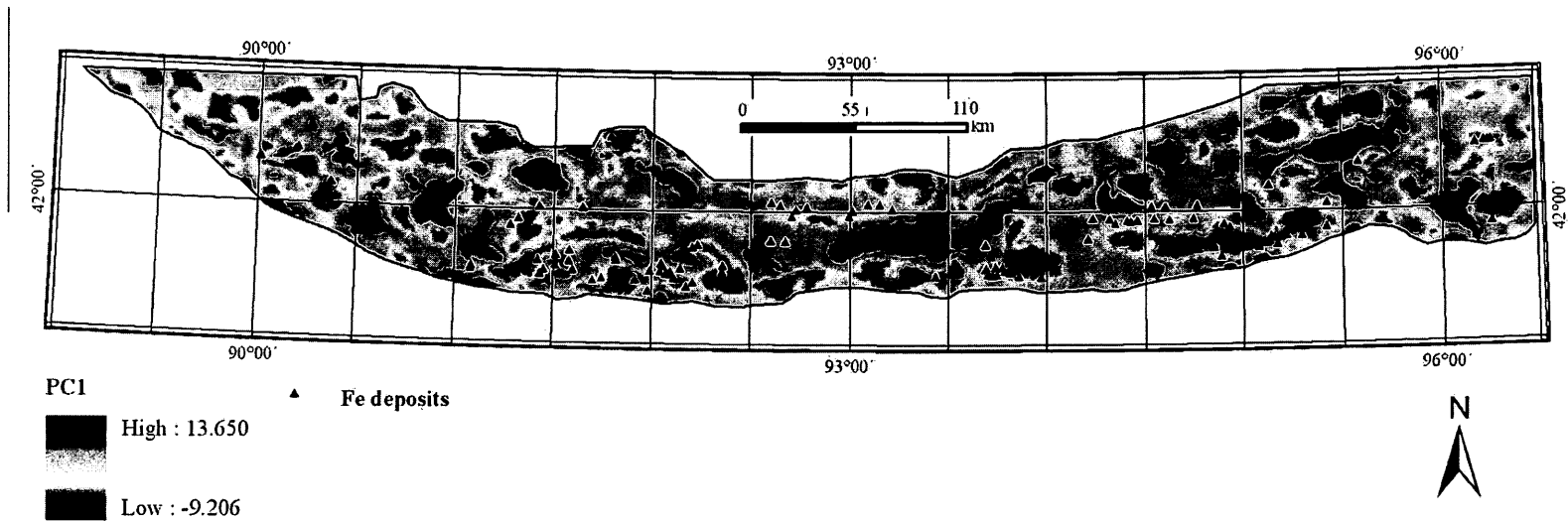
Fig.7. 3 PCA results for identifying geochemical signatures of element association related to Fe mineralization. a. Scree plots of eigenvalues of PCs; b. Loading of 8 selected geochemical signatures on PC1; c. Score map of obtained PC1 to delineate spatial distribution of geochemical signatures of element association. Known Fe deposits are shown for reference.



a



b



c

Fig.7. 4 PCA results for identifying singularity indices of geochemical signatures of element association related to Fe mineralization. a. Scree plots of eigenvalues of PCs; b. Loadings of singularity indices of 8 selected geochemical signatures on PC1; c. PC1 scores of singularity indices of geochemical signatures of element association. Known Fe deposits are shown for reference.

Table 7. 1 Statistical results showing the comparison of the efficiency in delineating the potential areas of Fe mineralization based on the spatial distribution of Fe₂O₃ concentration (Fig. 7.1), singularity indices of Fe₂O₃ concentration (Fig. 7.2), PC1 scores of geochemical signatures of element association (Fig. 7.3c) and PC1 scores of singularity indices of geochemical signatures of element association (Fig. 7.4c).

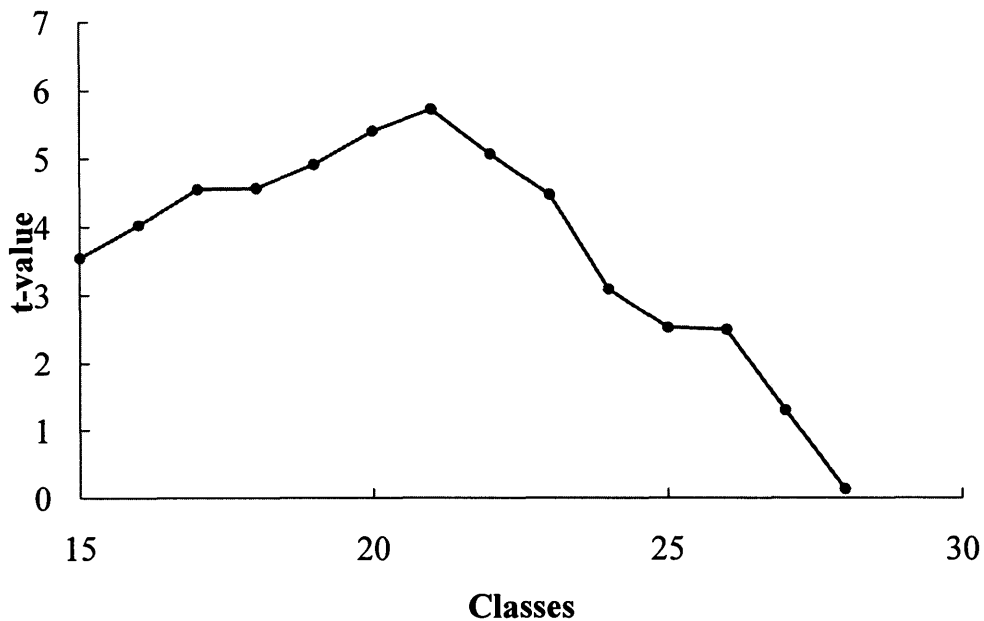
| | Anomalous area (in km ²) (percentage accounting for the whole study area) | Numbers of the known Fe deposits overlapped (percentage accounting for the total number of Fe deposits) | $Efficiency = \frac{\#deposits\%}{AnomalousArea\%}$ |
|---|--|---|---|
| Spatial distribution of Fe ₂ O ₃ concentration (in Fig. 7.1) | 15, 136 (43.16%) | 80 (73.39%) | $\frac{73.39\%}{43.16\%} = 1.700$ |
| Spatial distribution of singularity indices of Fe ₂ O ₃ concentration (in Fig. 7.2) | 7,928 (22.60%) | 59 (54.13%) | $\frac{54.13\%}{22.60\%} = 2.395$ |
| PC1 score of geochemical signatures of element association (in Fig. 7.3c) | 14,608 (41.65%) | 79 (72.48%) | $\frac{72.48\%}{41.65\%} = 1.740$ |
| PC1 score of singularity indices of geochemical signatures of element association (in Fig. 7.4c) | 11,728 (33.44%) | 65 (59.63%) | $\frac{59.63\%}{33.44\%} = 1.783$ |



a



b

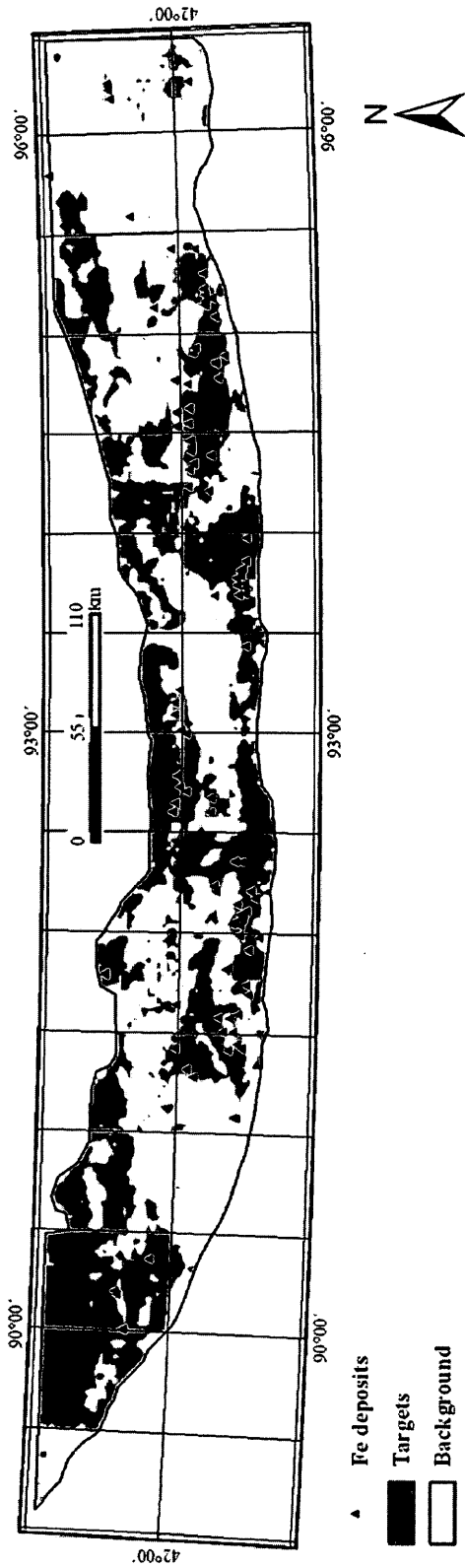


c

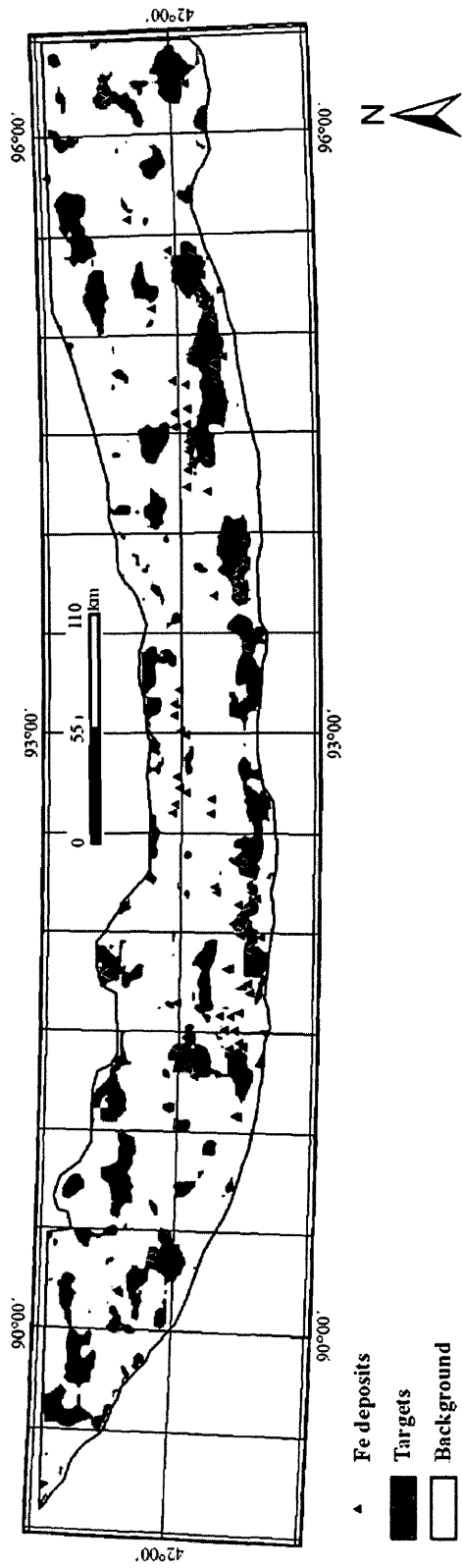


d

Fig.7. 5 Student's *t*-values calculated for measuring spatial relationship between known Fe deposits and **a.** the spatial distribution of Fe_2O_3 concentration demonstrated in Fig. 7.1; **b.** the spatial distribution of singularity indices of Fe_2O_3 concentration demonstrated in Fig. 7.2; **c.** PC1 of geochemical signatures of element association demonstrated in Fig. 7.3c; and **d.** PC1 of singularity indices of geochemical signatures of element association demonstrated in Fig. 7.4c.

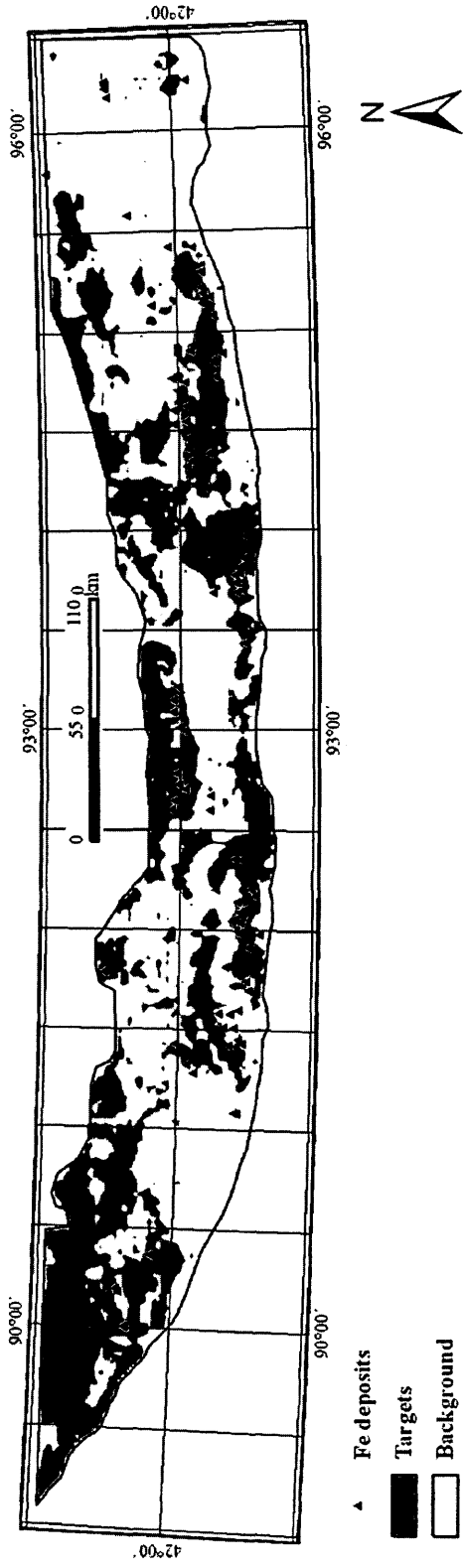


a

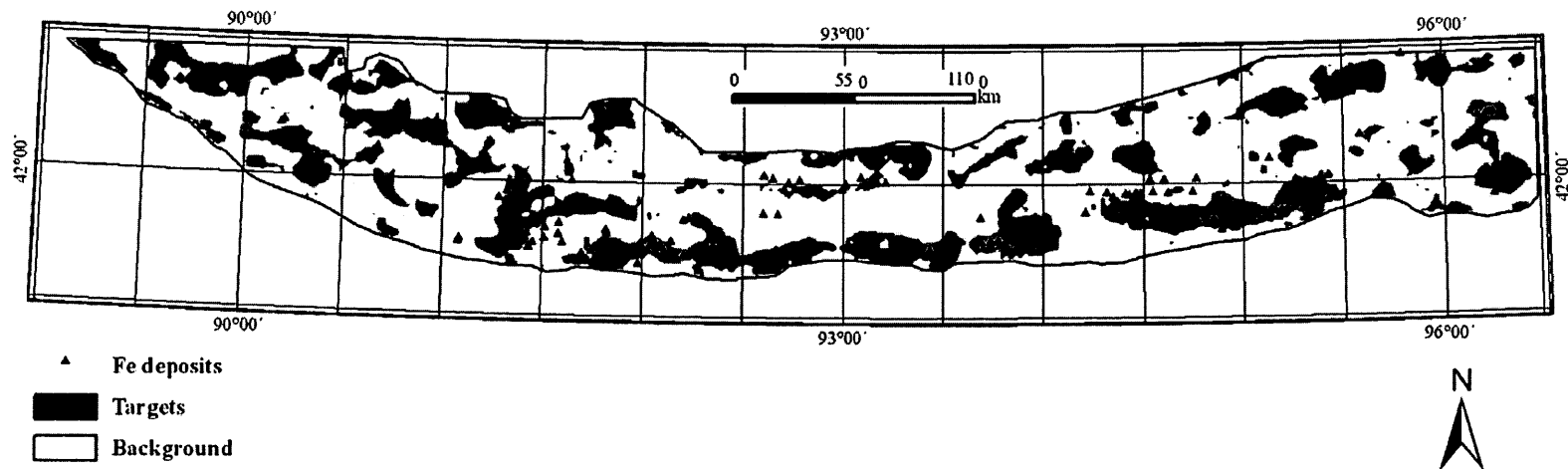


▲ Fe deposits
 ■ Targets
 □ Background

b



c



d

Fig.7. 6 Optimum targets with highest probability of being underlain by known Fe deposits. The grey patterns in **a.** are derived based on thresholds of the 13th class of the spatial distribution of Fe concentration demonstrated in Fig. 7.1; in **b.** are based on the 10th class of spatial distribution of singularity indices of Fe concentration demonstrated in Fig. 7.2; in **c.** are based on the 21st class of PC1 scores demonstrated in Fig. 7.3c; and in **d.** are based on the 10th class of PC1 scores demonstrated in Fig. 7.4c, respectively. The thresholds are determined by the Student's *t*-values illustrated in Fig. 7.5.

Chapter 8. Geo-information integration for mineral potential mapping by SWPCA model

From a geological perspective, mineral deposits are the end products dominated by complex geo-processes and the formation of which are temporally, spatially and mechanically confined by various geological bodies associated with these geo-processes. As introduced previously, most of the volcanic sedimentary Fe deposits are located within the extent of Jueluotag rift and dominated by regional tectonic-magmatic activities (Han and Zhao, 2003; Hou et al., 2006; Zhou et al., 2001). Specifically, the volcanic Fe deposits were formed along with the eruption and following sedimentation of the Yamansu volcanic rocks, especially the intermediate-mafic rocks. Genetically, the volcanic eruption was triggered by plate collision between the Junggar plate and the Tarim plate occurred from the Ordovician. As a result, the spatial distributions of volcanic edifices, volcanic rocks and even Fe mineralization belts are highly associated with the latticed fault systems (BGEDXP, 2009), which are generally distributed along EW direction. Influenced by subsequent felsic magmatic emplacement in the Late Carboniferous, previously formed Fe ore bodies within the Yamansu volcanic strata were altered and enriched by hydrothermal fluids. Contact zones of the Yamansu Formation and felsic intrusions have long been

considered as exploration targets.

As a Gobi Desert area, general mineral exploration in eastern Tianshan mineral district is seriously limited by ground coverage mainly consisting of aeolian sand, tepetate, and regolith. Advanced techniques for mineral exploration are desired to delineate potential areas of Fe mineralization. With the development in techniques and database construction, there is a great improvement in geo-information identification approaches (e.g., regression analysis, characteristic analysis, principal component analysis, weights of evidence, etc.) from multi-source and multi-scale geo-datasets (Wang and Cheng, 2008). These advances encourage the characterization of geo-anomalies associated with mineralization (Bonham-Carter, 1994; Ranjbar and Honarmand, 2004).

Being an efficient image processing method, principal component analysis (PCA) is frequently employed in earth sciences (Cheng et al., 2011). One of the primary objectives of using PCA is to achieve comprehensive geo-information (i.e., geo-anomaly) from multisource datasets. The identified geo-information can be used to support concerns regarding to geological decision making by geological interpreters. In order to enhance the efficiency of PCA, several extensions of PCA were proposed by former researches (e.g., robust PCA, weighted PCA, kernel PCA, etc.) (Jolliffe, 2002; Zhao et al., 2007). In Cheng (2006), three extended PCA algorithms consisting of spatially weighted PCA (SWPCA) and high-order PCA based

on correlation coefficient matrix, and spatial autocorrelation and cross-correlation matrix-based PCA were proposed to enhance interpretation of objective geo-information. Many inspirational applications of SWPCA have been published in past decade. Wang and Cheng (2008) used buffer distances of outcropping intrusive rocks as the spatially weighting factor to enhance the spatial distributions of intrusions. In Cheng et al. (2011), SWPCA was applied to integrate felsic intrusions related stream sedimentary geochemical data, and the results by using various weighting factors were compared. After that, spatially weighting factors associated with other geological issues were attempted as well (Xiao et al., 2012). Based on formerly recognized ore controlling factors (i.e., fault systems, felsic intrusions, and the Yamansu Formation) in eastern Tianshan mineral district, China, SWPCA method is currently applied as a hybrid geo-information integration method to delineate spatial distributions of Fe mineralization-associated geochemical signatures, results of which are compared with of ordinary PCA. An improved delineation, SWPCA involving more geological significances can enhance the mineral potential mapping that will benefit the future Fe exploration in the study area.

8.1. SWPCA model and definition of weighting factor

In this chapter, SWPCA is applied to stream sediment geochemical data for delineating geo-information associated with Fe mineralization in eastern Tianshan district, China. Based on mechanism of these Fe deposits recognized by former

researches, a general process of SWPCA modeling in this area consists of input variable selection and spatially weighting factor definition.

The Fe mineralization in eastern Tianshan district is generally controlled by three factors as fault systems, the Yamansu volcanic strata and hydrothermal alteration associated with felsic intrusions. Because most of the Fe deposits are located within extents of the Yamansu Formation and were altered by hydrothermal fluids differentiated from felsic intrusions, a spatially weighting factor which intends to highlight objective Fe mineralization favored spaces is defined as follow: (1) since contact zones between the Yamansu Formation and felsic igneous intrusions are optimal places for the Fe mineralization, the first step is to outline intersections of these two geo-bodies; (2) Euclidean distances from the intersections are created to determine a decay function of weighting factor (i.e., the further the location away from the intersection, the lower the weight is assigned to the location); (3) areas out of the Yamansu Formation which do not possess great Fe mineralization potentials are spatially weighted as 0 and expelled from the calculation of correlation coefficient matrix. Therefore, in current SWPCA model (Fig. 8.1), the Euclidian buffers of the intersections between the Yamansu Formation and felsic intrusions, which are confined within the extent of the Yamansu Formation are used as the weighting factor (Fig. 8.2); spatial distributions of felsic igneous rocks, fault systems, the Yamansu Formation, and geochemical signatures of element association related to Fe mineralization derived in previous chapters (i.e., chapters 4, 5, 6 and 7) are assigned

to be the input variables. By this SWPCA model, Fe mineralization favored areas associated with different controlling factors can be delineated.

As discussed in previous chapters, PC1 scores of singularity indices of geochemical signatures performed better in depicting spatial distributions of corresponding geological bodies than the ones without applying singularity index mapping technique. Therefore, the singularity index-based patterns (Figs. 4.4, 5.6, 6.4, and 7.4c) are currently applied as input variables in this SWPCA model (Fig. 8.1) to represent spatial distributions of fault systems, felsic intrusions, the Yamansu Formation, and the element association, respectively.

8.2. Mapping of Fe mineralization by SWPCA

Based on achieved geo-information, SWPCA is currently used to map the potentials of Fe mineralization in eastern Tianshan mineral district, China. The PCA and SWPCA results are shown in Figs. 8.3 and 8.4. As discussed above, the weighting factor to highlight objective Fe mineralization favored spaces is participated in calculation of the correlation coefficient matrix, and then differences between ordinary PCA and SWPCA eigenvector matrixes can be investigated to evaluate the improvement. Geometrically, rotation of eigenvectors of each PC_i will be performed on corresponding $SWPC_i$. Consequently, $SWPC_1$ will no longer possess the greatest variance of the entire geochemical datasets and eigenvalue of $SWPC_1$ will be less than of the PC_1 (Fig. 3.1). Variance held by other eigenvectors will increase or

decrease according to their rotation directions. Comparison of the relative importance of all PCs and SWPCs demonstrates the effect of rotation in eigenvector matrixes, although the variation is not changed significantly (Fig. 8.3a). Eigenvalues of both PC1 and SWPC1 are greater than 1 imply that they can be retained for further interpretation.

All input variables are positively loaded on PC1 and SWPC1 implies that they both are suitable to describe combining effect of the controlling factors on the Fe mineralization in the study area (Fig. 8.3b). The loading of the Yamansu Formation is increased in SWPC1 that well demonstrate the effect of the weighting factor to highlight geo-information of Fe mineralization within the volcanic strata. Meanwhile, the raised contribution of fault systems on SWPC1 implies their spatial restriction to the Yamansu volcanic strata. Because all input variables are positively loaded in both PC1 and SWPC1, based on the properties of singularity indices (i.e., low value represents enrichment and high value represents depletion), locations with lower scores in both PC1 and SWPC1 represent the Fe mineralization in the Yamansu Formation (Fig. 8.4). Since the Fe mineralization is the main geo-information dominating the most variance of the input variables, with greatest eigenvalues information in both PC1 and SWPC1 indicative to Fe mineralization are shown as extremely similar patterns. However, the influence of the Yamansu Formation to the Fe mineralization is emphasized by SWPCA (Fig. 8.3b); meanwhile SWPC1 with greater contributions of the Yamansu Formation and fault systems and less

contribution of felsic igneous rocks is more mechanically significant than ordinary PC1. At the end, locations with lower PC1 (Fig. 8.4a) and SWPC1 scores (Fig. 8.4b) coincident with the Yamansu Formation but not corresponding with known Fe deposits can be inferred as target areas for exploration of volcanic sedimentary Fe deposits.

8.3. Discussions

In this chapter, previously achieved geo-information of Fe mineralization related controlling factors (i.e., fault systems, felsic intrusions, and the Yamansu Formation) and element association are integrated by both PCA and SWPCA methods. Different from former PCA applications by which the input variables were direct and explicit, the input variables used in this chapter are based on interpretation of controlling factors from secondary geo-information (i.e., geochemical anomalies related to each controlling factor). Compared with the location information of various geological bodies from geological maps, spatial distributions of corresponding geological bodies characterized by geochemical signatures are more flexible to represent spatial variations of geochemical properties (e.g., composition, geochemical influence on mineralization, etc.).

By employing a spatially weighting factor, SWPCA provides more reliable results than PCA. Since derived favorable locations of mineralization by SWPC1 are not significantly improved, it indicates that more practices should be considered in future

work. This case study can be introduced to other data sets and study areas where different weighting factors can be tested to achieve more prominent geo-information integration results in support of mineral exploration. Furthermore, geo-information integration for the mineral potential mapping by means of weighted sum may not be efficient in some cases due to the limitations introduced in chapter 1 (i.e., data quality and method limitation); therefore, an advanced geo-information analysis methods is applied to the Fe mineral exploration in next chapter.

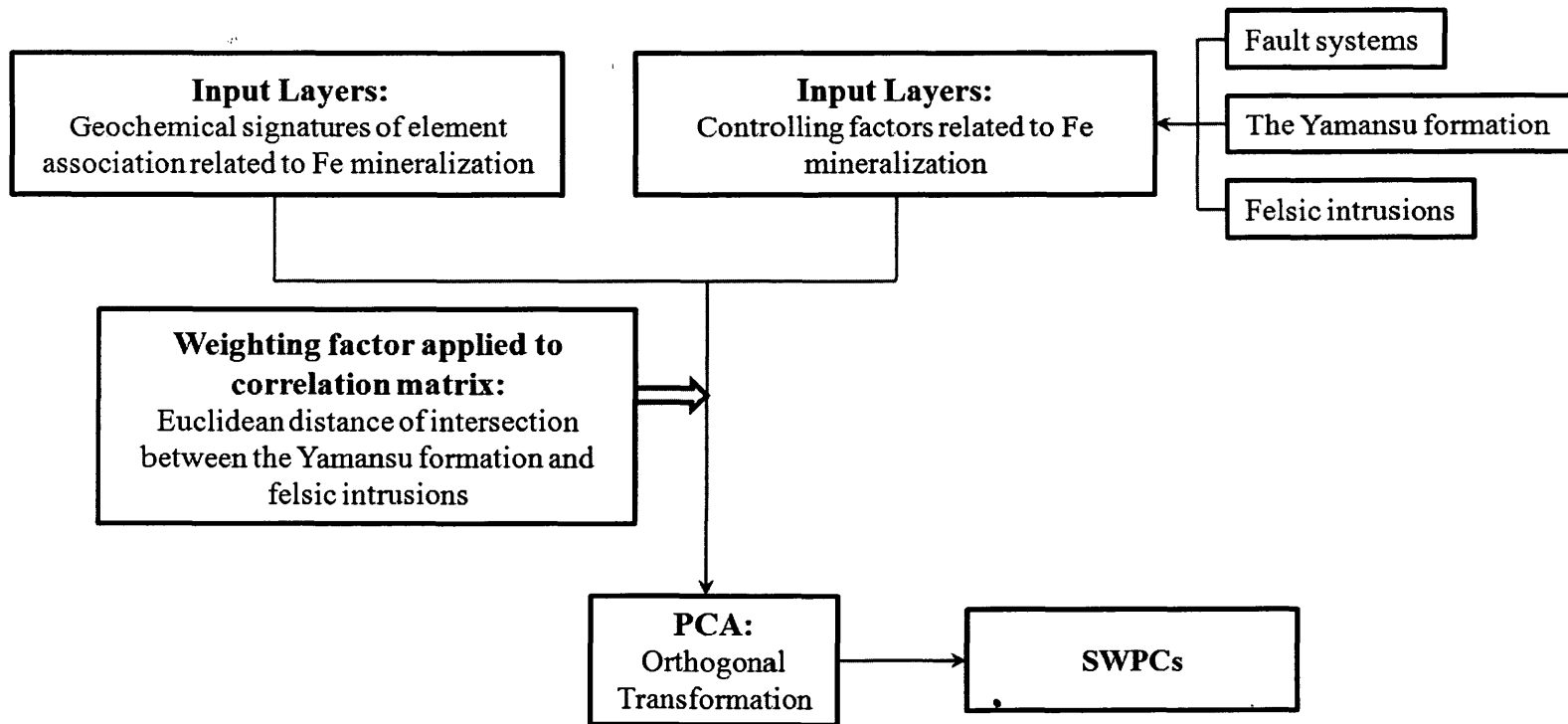


Fig.8. 1 SWPCA model. In the SWPCA model, controlling factors (i.e., fault systems, the Yamansu Formation and felsic intrusions) and geochemical signatures of the element association derived in the previous chapters are currently used as input variables. Weighting factor is defined in Fig. 8.2.

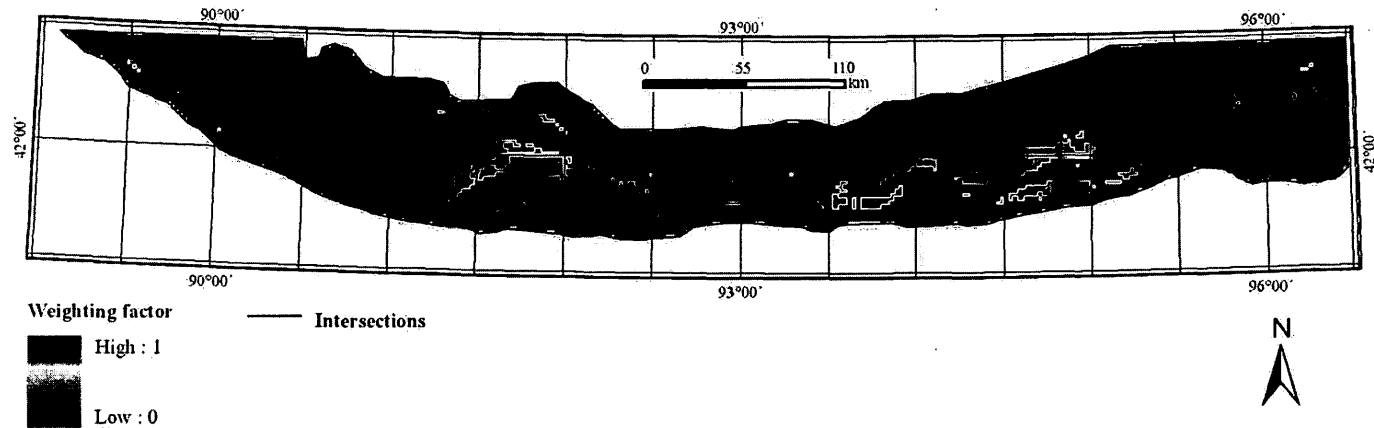
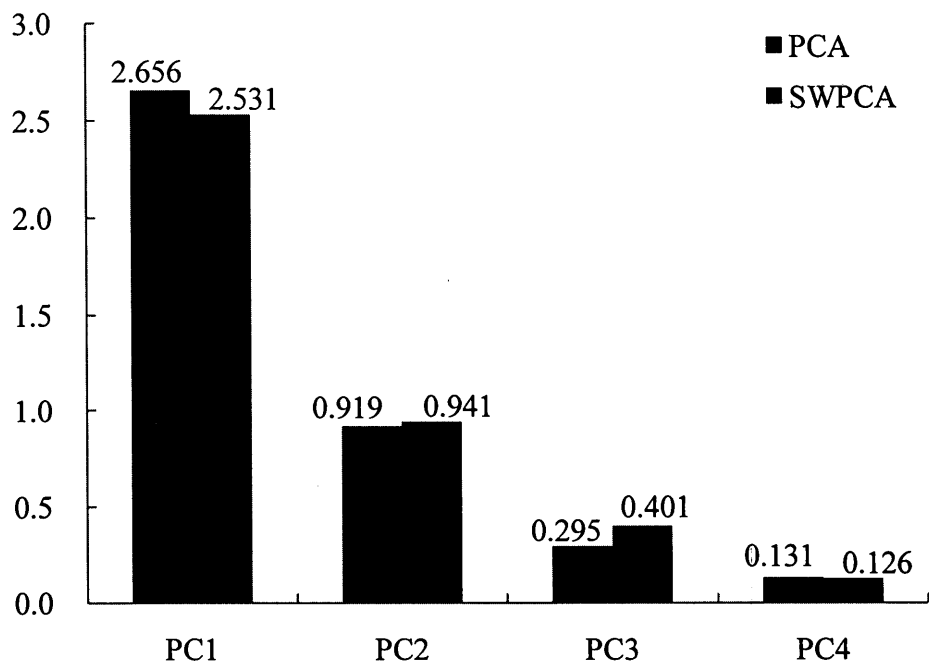
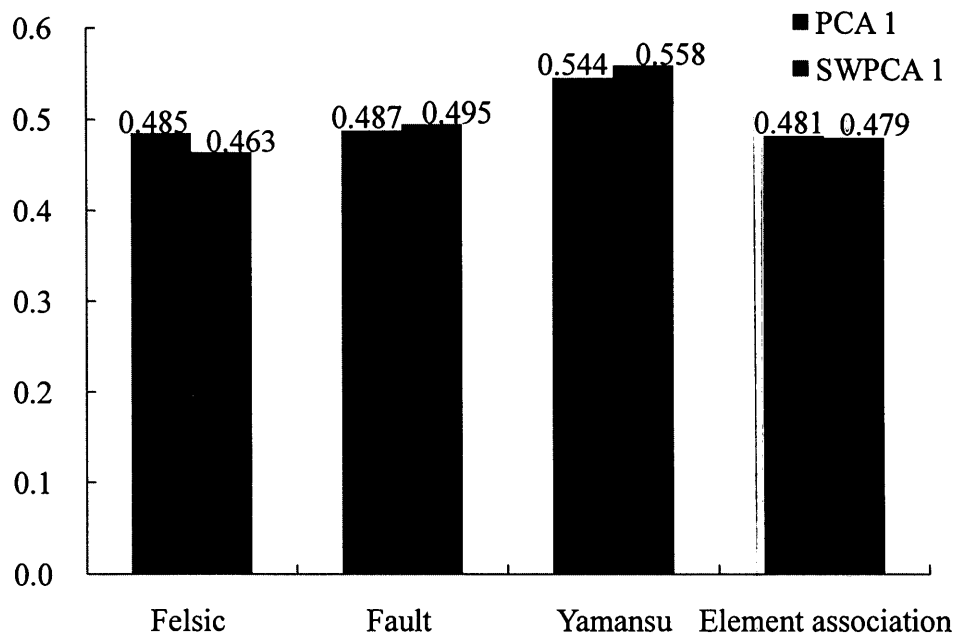


Fig.8. 2 Spatial distribution of the spatially weighting factor. The Euclidian distance of pixels from the intersections between the Yamansu Formation and felsic intrusions is currently used as the weighting factor in SWPCA model. The farther the pixel away from the intersection, the lower weighting value is assigned to the pixel. The pixels located out of the extent of the Yamansu Formation are weighting 0. Intersections between the Yamansu Formation and felsic intrusions are displayed for reference.

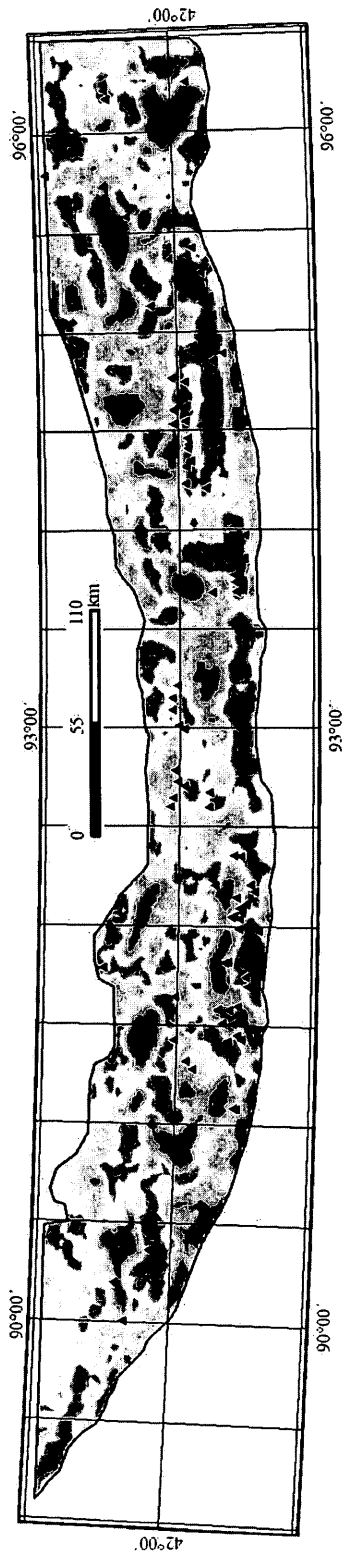


a



b

Fig.8. 3 Comparison of the statistics of PCA and SWPCA results. a: Scree plots of eigenvalues of PCs and SWPCs. b: Loadings of input variables on PC1 and SWPC1.

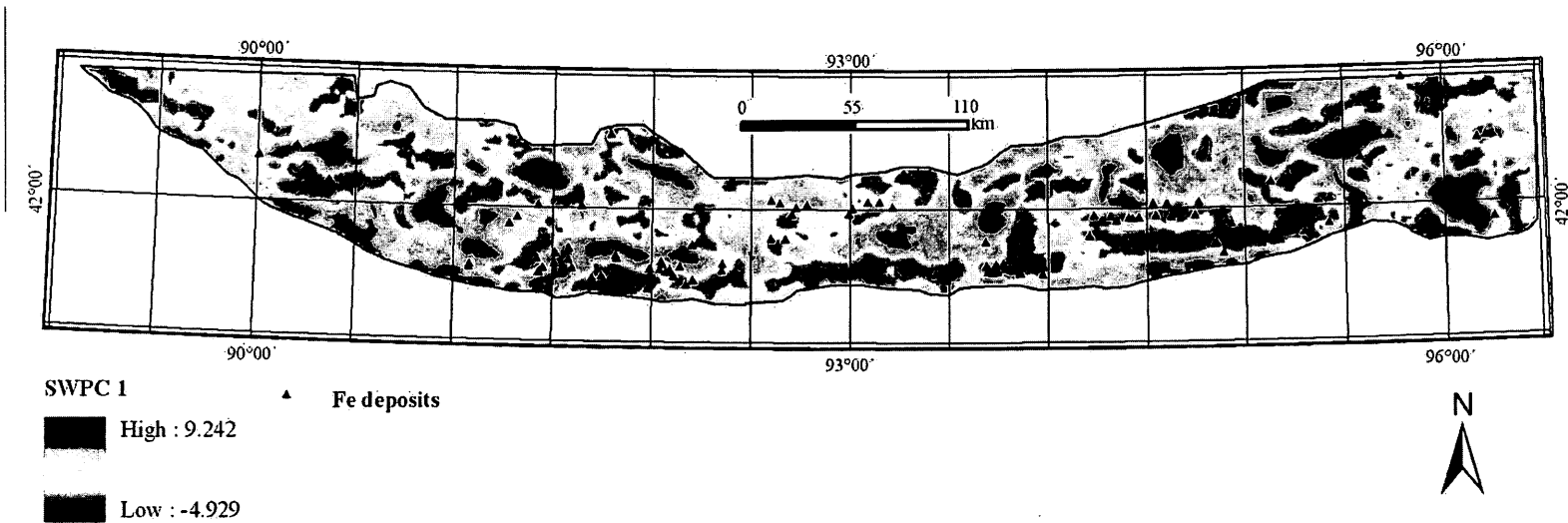


PC 1 ▲ Fe deposits

High : 9.221

Low : -4.922

a



b

Fig.8. 4 Spatial distribution of interactions of fault systems, felsic igneous rocks, the Yamansu Formation and geochemical signatures of element association indicating favorable locations for Fe mineralization by a. PC1 scores and b. SWPC1 scores. Known Fe deposits are shown for reference.

Chapter 9. Identification of spatially non-stationary relationships between Fe mineralization and its controlling factors

Ore deposits are characterized by accumulation of ore-forming elements and/or minerals in favorable geological environment, the formation of which is dominated by diverse geological issues so-called controlling factors (e.g., fault systems, magmatism, strata, lithologic units, regional geochemical field and petrophacies, etc.) (Guilbert and Park, 1986; Wang et al., 2011, 2012). Normally, metallogenesis is influenced by cooperation of multiple controlling factors; however, for an individual deposit, the mineralization might be caused by only one or few controlling factors. The superimposed effect of various controlling factors confines the properties of ore deposits, which is frequently anisotropic over an entire space (Cheng, 2007; Yuan et al., 1979). In eastern Tianshan mineral district, the Carboniferous volcanic rocks are the main hosts of Fe deposits broadly distributed within volcanic basins; nevertheless Fe mineralization can only take place at limited locations due to the changing influence of controlling factors on mineralization. Thus, relationships between Fe mineralization and diverse controlling factors are varying over space. The spatial variation is termed as spatial non-stationarity (Brunsdon et al., 1996; Fotheringham et al., 1996, 1998). It is currently used to describe the spatially varying and

heterogeneous relationships existed among the Fe mineralization and its controlling factors. The spatially non-stationary relationships may considerably influence the prediction and evaluation for Fe mineral resources. Therefore, depiction of the spatial non-stationarity of the relationships between Fe mineralization and its controlling factors is necessary for enhancing the efficiency of Fe exploration at different locations.

Regression analysis is a popular method to discern relationships between a single dependent variable and one or more independent variables (Fotheringham et al., 1998; Ryan, 2009). By modeling the spatial relationships, regression analysis allows to predict occurrences of events (e.g., ore deposits) and to investigate the explanatory factors (e.g., igneous rocks, strata, geochemical background, etc.) (Fotheringham and Brunson, 1999). Based on scales of observation, regression analysis involves global and local regressions. Relationships between variables can be examined accordingly by global and local statistics (Fotheringham et al., 2002). A global model (e.g., ordinary least square, OLS) calibrates a dependent geo-variable with linear combination of a series of independent geo-variables, the algorithm of which is readily available and widely employed in spatial analysis of geochemical data (Rollinson, 1993). Relationships between each pair of geo-variables for the entire study area can be estimated and described by a constant regression coefficient. In other words, one regression model characterizes all situations across the space. However, it may not be able to correctly depict the relationships between variables in

reality, especially when the relationships exhibit spatial non-stationarity (Fotheringham et al., 2002).

Geographically weighted regression (GWR) allows the relationships among geo-variables to be estimated locally by using a spatially weighted least square regression to a small number of samples fallen in a given area (Fotheringham et al., 2002). In comparison with OLS model, GWR can describe more localized and detailed variations in relationships rather than a general trend by global models (de Smith et al., 2007). Therefore, GWR can be seen as disaggregation of OLS model. By their natures, global regression models investigate similarity of relationships between variables in space; whereas, local regression models concern differences of the relationships at different locations (Fotheringham et al., 2002).

Former practices of GWR mainly concerned to social science, like relationship between car ownership and household incomes (Brunsdon et al., 1996), relationship between spatial distribution of long-term illness and unemployment (Fotheringham et al., 1998; Brunsdon et al., 1998), and relationship between school performance and local education environment (Fotheringham et al., 2001). After these applications, GWR has been gradually introduced to natural science. Páez et al. (2002) used GWR to examine relationship between heat island and land use. Su et al. (2012) used GWR to analyze relationship between agricultural landscape patterns and urbanization. Tu and Xia (2008) applied GWR to estimate relationship between land use and water

quality. Considering the spatial non-stationary property exists universally in geosciences, it might be a meaningful attempt to characterize interactions or relationships of mineralization associated geological issues by GWR in spatial scenario.

In general, the formation of volcanic sedimentary Fe deposits in eastern Tianshan mineral district is genetically and spatially controlled by three geological processes consisting of fault activities started from Ordovician, the volcanic eruption during the Early Carboniferous and hydrothermal alteration of ore bodies accompanied with the emplacement of felsic igneous rocks in the Late Carboniferous (Ding, 1990; Lu et al., 1995). In previous chapters (i.e., chapters 4, 5, 6, and 7), combination of singularity index mapping technique and PCA has been employed to characterize Fe mineralization associated tectono-magnetism in eastern Tianshan mineral district (i.e., fault activities, the emplacement of felsic igneous rocks, and the formation of Yamansu volcanic strata). In this chapter, GWR is utilized to inspect the spatially non-stationary relationships between Fe mineralization and these geological activities or processes.

9.1. Regression analysis

9.1.1. OLS model

To enhance knowledge of spatial non-stationary relationships between Fe

mineralization and tectono-magmatism in eastern Tianshan mineral district, China, regression analysis methods including OLS and GWR are employed to evaluate the global (i.e., general trend) and local relationships, respectively. In OLS model, geochemical anomalies related to Fe mineralization are assigned to be the dependent variable, while geochemical anomalies of fault systems, felsic igneous rocks and the Yamansu Formation are assigned to be independent variables. By OLS model, the regression can be:

$$PC_{association_i} = a_0 + a_1 \times PC_{faults} + a_2 \times PC_{felsic} + a_3 \times PC_{Yamansu} + \varepsilon_i \quad (9-1)$$

where, the dependent variable $PC_{association}$ is the PC1 scores of singularity indices of element association (Fig. 7.4c) at location i ; independent variables PC_{faults} , PC_{felsic} and $PC_{Yamansu}$ represent PC1 scores of singularity indices of geochemical signatures of fault systems (Fig. 4.4), felsic igneous rocks (Fig. 5.6) and the Yamansu Formation (Fig. 6.4), respectively. Influences of independent variables to the dependent variable can be described by their corresponding regression coefficients a_1 , a_2 , and a_3 . a_0 and ε_i are the intercept and the residuals at location i of regression model.

Before the application of regression analysis, several important characteristics of the four variables (Table 9.1) are listed to facilitate interpretation of the relationships. For the PC1 of singularity indices of element association related to Fe mineralization, high values represent depletion of element association, while low values well coincident with distribution of Fe deposits represent accumulation of element

association. Therefore, it currently used as indicator of Fe mineralization. In addition, low values of all three independent variables are associated with Fe mineralization. By OLS, relationships between Fe mineralization and the tectono-magmatism are expressed as:

$$Fe_2O_3 = 0.000059 - 0.528 \times PC_{faults} + 0.782 \times PC_{felsic} + 0.619 \times PC_{Yamansu} + \varepsilon_i \quad (9-2)$$

Examining correlation coefficients derived from the global model, positive contributions of felsic intrusions and the Yamansu Formation and negative contribution of fault systems to the estimation of Fe accumulation suggest that the Fe accumulation is mainly associated with the Yamansu Formation and relatively mafic rock types (i.e., mafic igneous rocks and skarns) rather than fault systems. The estimation of the regression coefficients is somehow missing the expectation on Table 9.1. Theoretically, relationships between Fe mineralization and these three controlling factors are positive; however, the estimation of OLS is based on a global trend and controlling effects of fault systems to Fe mineralization can only occur within limited areas. Consequently, the negative estimation indicates that the influence of fault systems on Fe accumulation in the entire study area is indirect. Furthermore, estimated regression coefficients are stationary that is often invalid for exploring relationships between geo-processes and mineralization at specific locations. Therefore, a localized regression model, GWR is employed in this research work to estimate the non-stationary relationships between variables in different areas.

9.1.2. GWR model

By the GWR model, equation (9.1) can be updated by introducing spatial information:

$$PC_{association_i} = a_0(u_i, v_i) + a_1(u_i, v_i) \times PC_{faults} + a_2(u_i, v_i) \times PC_{felsic} + a_3(u_i, v_i) \times PC_{Yamansu} + \varepsilon_i \quad (9-3)$$

where, (u_i, v_i) indicates the location of point i in the study area, and $a_1(u_i, v_i)$, $a_2(u_i, v_i)$, and $a_3(u_i, v_i)$ are the localized regression coefficients of PC_{faults} , PC_{felsic} and $PC_{Yamansu}$, respectively, at location i . By the nature of localized model, regression coefficients estimated by GWR can describe spatial variations of relationships between Fe mineralization and its controlling factors across the space (Fig. 9.1) rather than constant estimation generated by OLS model.

According to estimated spatial non-stationary relationships (Figs. 9.1a, 9.1c, 9.1e), two issues should be noticed. First of all, most of known Fe deposits are located in the areas with high regression coefficients of the three controlling factors. It proves that the Fe accumulation is positively and highly associated with corresponding tectono-magmatism in eastern Tianshan mineral district, China. Secondly, comparing spatial locations of known Fe deposits and spatial distributions of regression coefficients, Fe occurrences can be discovered in areas with low regression coefficients of individual controlling factors as well. It satisfies the fact that influences of these controlling factors on Fe accumulation are spatially non-stationary and Fe mineralization can only occur in areas with optimum interactions of these

controlling factors. Based on properties of singularity indices, the GWR results imply that the Fe accumulation is dominated by enrichment of element associations related to relatively mafic rocks (e.g., volcanic rocks and skarns), fault systems and the Yamansu Formation. Furthermore, controlling effects of these geo-processes (i.e., fault activities, hydrothermal alteration by felsic igneous rocks, and bimodal volcanic eruption of the Yamansu Formation) are varied across the space, and spatial distributions of these effects can be delineated, quantitatively and qualitatively.

If interpretation of spatial non-stationary relationships are limited to the previously defined Fe mineralization target areas (Fig. 7.6d), more explicit explanation for the controlling effects of tectono-magnetism on Fe mineralization can be achieved (Figs. 9.1b, 9.1d, and 9.1f). Negative coefficients of PC_{fault} (Fig. 9.1b) indicate that fault systems may not directly influence Fe mineralization in many areas. It is in accordance with geological background of the study area that fault activities caused volcanism which led to eruption, migration and sedimentation of ore-bearing fluids in lower basins; meanwhile, positive coefficients of PC_{fault} demonstrate direct controlling effects of fault systems on Fe mineralization (e.g., vein type Fe deposits). Positive coefficients of $PC_{igneous}$ at most of the target areas (Fig. 9.1d) imply that relative mafic rocks around felsic intrusions (i.e., skarns) highly associated with Fe mineralization. It is coincident with the metallogeny of Fe deposits that most of the Fe ores are altered by hydrothermal fluids differentiated from granitoid intrusions. Extensively distributed positive and negative coefficients of $PC_{Yamansu}$ imply that the

Yamansu Formation may not dominate the spatial distribution of Fe mineralization at all locations. It is in accordance with the lithological properties of the Yamansu Formation (i.e. bimodal volcanic strata) that mafic volcanic rocks may have great potential in hosting Fe deposits, but the felsic volcanic rocks may not.

9.2. Improvement of GWR to OLS

Two commonly used diagnostic parameters to evaluate improvement of GWR to OLS are the coefficient of determination R^2 value and corrected Akaike Information Criterion value (AIC_c) (Akaike, 1974, 1987). R^2 ranging from 0 to 1 is to verify the correctness (i.e., goodness of fit) of a regression model, and regression with higher R^2 value will produce more credible results (Ryan, 2009). AIC_c is to evaluate information distances between the modeled distribution and the true distribution, and regression with a smaller AIC_c value indicates better parameter estimation and reflectance of reality (Chalton and Fotheringham, 2009; Fotheringham et al., 2002). The GWR model with a much higher maximum R^2 value than the OLS model indicates that the GWR results are more credible (Table 9.2). Using the R^2 value of OLS model as a threshold, the binary map of R^2 values of GWR model implies that GWR model severs a better performance than OLS model at most locations, especially the areas with known Fe deposits (Fig. 9.2). Two AIC_c values indicate that results of GWR model possess shorter information distance between parameter estimation and reality than the results of OLS model (Table 9.2).

Comparing the two models with spatial distribution of PC1 scores of singularity indices of geochemical signatures of element association related to Fe mineralization (Fig. 7.4c), residuals of OLS model (Fig. 9.3a) showing obvious spatial clustering distribution indicate imperfect prediction of dependent variable (Fig. 9.3b); whereas residuals derived from GWR (Fig. 9.4a) with more random spatial distribution across the space indicate a better performance in predicting the dependent variable (Fig. 9.4b). Moreover, given by $PC_{\text{association}_i} - PC_{\text{association}_i}^*$ (i.e., real value – predicted value), the spatial distribution of residuals of GWR model may provide some useful clues for Fe exploration in eastern Tianshan mineral district. Based on the values, residuals are sorted into two categories. First of all, $PC_{\text{association}_i} = PC_{\text{association}_i}^*$ corresponding with an equal estimation (i.e., residual = 0) indicates that the three independent variables can fully describe the Fe mineralization. It can be inferred that the Fe mineralization is completely dominated by the three factors discussed in this paper. Secondly, $PC_{\text{association}_i} \neq PC_{\text{association}_i}^*$ corresponds an unequal estimation (i.e., residual $\neq 0$). Specifically, $PC_{\text{association}_i} < PC_{\text{association}_i}^*$ and $PC_{\text{association}_i} > PC_{\text{association}_i}^*$ represent over-estimation (i.e., residual < 0) and under-estimation (i.e., residual > 0), respectively. It can be inferred that the Fe mineralization might be dominated by other geo-processes besides the three controlling factors discussed above. More local controlling factors (e.g., ground coverage, aeolian sand, buried depth of geological bodies, and measurement error of stream sediment samples) should be taken into consideration of Fe exploration in the unequally estimated areas. In other words, the

over-estimation and under-estimation reflect the decreased and increased association between Fe accumulation and tectono-magnetism, respectively. In addition to achieve the relationships between Fe mineralization and its controlling factors, further detailed studies focusing on interpretation of residuals may assist to understand local metallogeny of Fe mineralization.

9.3. Suggestions on Fe mineral exploration in eastern Tianshan mineral district

Investigating the relationships between Fe mineralization and its controlling factors can benefit understandings of metallogeny of Fe deposits. The spatial non-stationarity existed among various geological variables (i.e., geo-processes) can be further used as a guide for Fe mineral exploration at different locations in the study area. In this dissertation, seven subareas which are sorted based on the spatial distribution of known Fe deposits in Fig. 7.1 are discussed here. The subareas from the west to the east are (1) the Xiaorequanzi volcanic basin, (2) the Aqishan-Bailingshan subarea, (3) the Kanggurtag-Tuwu subarea, (4) the east district of the Kumtag sand ridge, (5) the Yamansu mineralization district, (6) the Shaquanzi subarea, and (7) the Jing'erquan subarea.

(1) The Xiaorequanzi volcanic basin. The host rock of known Fe deposits in this subarea is the Carboniferous strata, especially the Xiaorequanzi Formation which is mainly composed of mafic-felsic volcanic rocks. In this subarea, patterns with high values describe high correlation between Xiaorequanzi volcanic strata and Fe anomalies (Fig. 9.1e). The known deposits are also located around the felsic

intrusions, and patterns with high coefficients are presented within the extent of felsic intrusions (Fig. 9.1c). It implies that the felsic igneous rocks in this subarea containing Fe-rich materials provided not only thermodynamic conditions but also ore-forming materials for Fe mineralization in nearby areas. Therefore, the focus of Fe mineral exploration in this subarea is suggested to the Fe mineralization in the Carboniferous strata which are located around felsic intrusions.

(2) The Aqishan-Bailingshan subarea. Most of the known Fe deposits in this subarea are mainly hosted by the Yamansu Formation which is validated by the high-middle coefficients of $PC1_{(Yamansu)}$ in the Yamansu Formation (Fig. 9.1e). The high coefficients of $PC1_{(Felsic)}$ in some of the felsic igneous rocks (Fig. 9.1c) illustrate Fe enriches in felsic intrusions as well. It corresponds to the known deposits located within the felsic intrusions and near the boundary between the intrusions and the Yamansu Formation. Meanwhile, the known deposits are mainly scattered along the fault systems, where high coefficients of fault systems are shown as well. Consequently, interior and exterior contact zones of the felsic intrusions and the Yamansu Formation, especially the places are highly fractured are defined as targets of Fe mineral exploration in this subarea.

(3) The Kanggurtag-Tuwu subarea. Fig. 7.4c shows that the known deposits in this subarea are in accordance with the geochemical anomalies of element association and are strictly limited within the extent of the Carboniferous strata. High-middle coefficients within the Carboniferous strata in Fig. 9.1e indicate the enrichment of element association related to Fe mineralization. Therefore the mineral exploration in this subarea may focus on the Yamansu Formation under the guidance of spatial

distribution of geochemical anomalies of element association related to Fe mineralization (Fig. 7.4c).

(4) The east district of the Kumtag sand ridge. The known deposits are mainly hosted by the Carboniferous strata. The Formation of Fe deposits may relate to the intermediate and mafic volcanism in the Carboniferous period, since high coefficients are distributed around the known deposits (Fig. 9.1e). In addition, middle to high coefficient of fault systems is displayed in this area as well. All of these facts are in accordance with close spatial relationship between known Fe deposits and fault systems. The hydrothermal influence of felsic igneous rocks on Fe mineralization is described by middle coefficients of felsic igneous rocks. Mineral exploration in this area might be based on consideration of all the three controlling factors.

(5) The Yamansu mineralization district. Most of the known deposits in this district are located in the Yamansu volcanic rocks and/or around the felsic intrusions, which are also occupied by distinct geochemical anomalies of element association related to Fe mineralization (Fig. 7.4c). As shown in Fig. 9.1e, the middle-high coefficients within the extent of the Yamansu Formation indicate that the Fe ore bodies were formed during the mafic extrusion (the Yamansu Formation). These ore bodies were further hydrothermally enriched by the intrusion of felsic magma, since middle-high values are shown in Yamansu volcanic basin (Fig. 9.1c). The depiction of Fe geochemical anomalies around the exterior contact zones between the felsic rocks and the Yamansu Formation may be efficient to Fe mineral exploration in this subarea.

(6) The Shaquanzi subarea. Noticeable Fe geochemical anomalies are in accordance

with known Fe deposits in this area (Fig. 7.4c). The high coefficients of both felsic igneous rocks (Fig. 9.1c) and the Yamansu Formation (Fig. 9.1e) imply that the intermediate-mafic extrusion in the Yamansu Formation is the main controlling factor to the formation of Fe ores which were further hydrothermally altered by felsic igneous rocks.

(7) The Jing'erquan subarea. Only a few of deposits have been discovered in this aeolian sand covered area. In Fig. 9.1e, high coefficients within and around the Yamansu Formation implies enrichment of Fe in the volcanic strata. Fig. 5.6 shows great potential of felsic intrusions which might be seriously covered by the aeolian sand. However, the middle-low coefficients around the known deposits in this subarea may imply hydrothermal transformation conducted by felsic intrusions (Fig. 9.1c). It can be inferred that there might still have great potentials of Fe mineralization in the Yamansu Formation, especially the layers covered by the desert.

9.4. Discussions

From a statistical perspective, relationships between variables estimated by a traditional global regression model are constant over space. In other words, global model can only present integral trends across the space. PCs can be seen as a series of global regressions, and constant contributions of geochemical variables in PCs are the regression coefficients. However, the straightforward linear regression, either PCA or OLS may have limitations to appropriately characterize the cause-and-effect relationships between geological events at different locations if the relationships are

spatially non-stationary (e.g., mineralization and its associated issues). As a complement to global regression models, GWR model is applied in current research to study the mechanism of Fe mineralization. The parameter estimates can depict more realistic spatial relationships between Fe mineralization and its controlling factors at different locations with higher confidence.

Compared with global regression models (e.g., OLS and PCA), GWR shows its advantages to characterize localized spatial relationships between geological issues, and provides an alternative way to demonstrate variations of the relationships over a geographical space. GWR is suitable approach to analyze non-linear geo-processes (e.g., analysis of ore-genesis theory, prediction of floods, etc.) whose causative factors are anisotropic. Current research applied both global and local regression models to identify the spatial relationships between marine volcanic-sedimentary Fe mineralization and its controlling factors. Suggestions to support future mineral exploration based on GWR analysis at seven subareas are proposed.

In this chapter, the application of GWR to investigate non-stationary relationships between mineralization and its associated geo-processes is a new trial of this method in geological field. According to the discussion above, the result is reasonable and meaningful in support of the Fe mineral exploration in eastern Tianshan region, China. However, due to the resolution limit of currently used geological and stream sediment geochemical datasets, only general and regional controlling factors of the Fe mineralization (i.e., the Yamansu Formation, intermediate-mafic extrusions and felsic

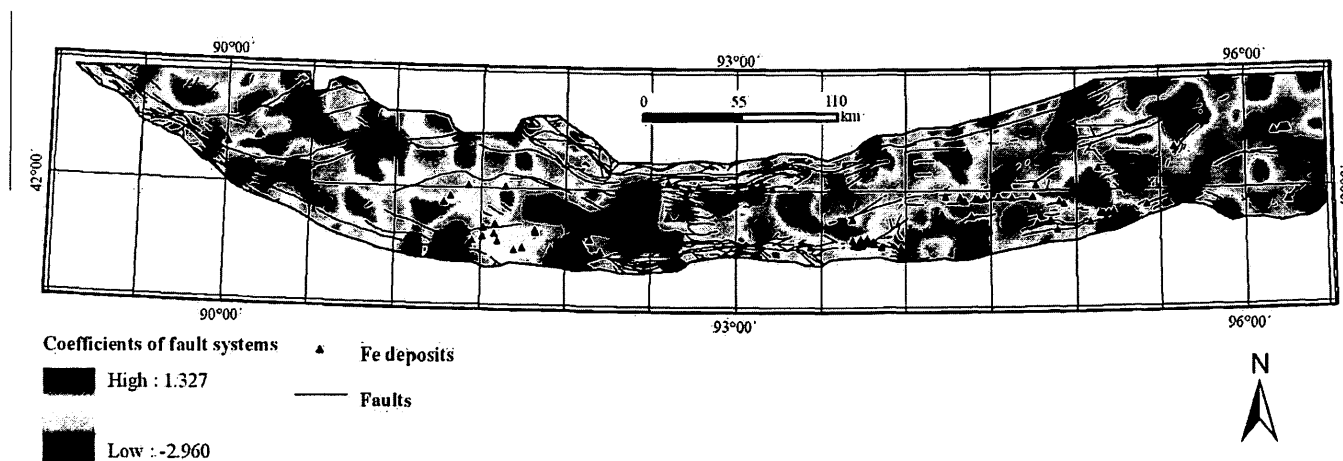
intrusions) are chosen. For individual deposit, other factors (e.g., oxidation, denudation, tectonism and geochemical/geophysical anomalies) might specifically contribute to the formation of Fe ores. Therefore, in order to further facilitate the analysis, more detailed controlling factors identified from other sources of geo-datasets will be considered in our future researches.

Table 9. 1 Depiction of four geo-variables employed in regression analysis.

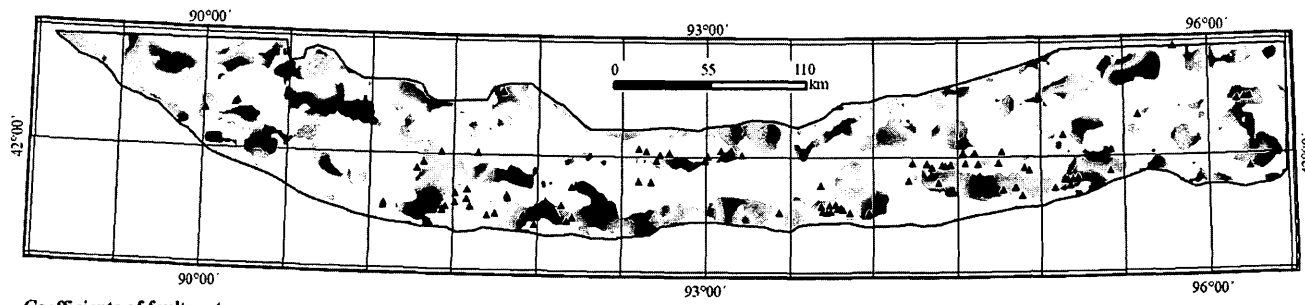
| | Dependent variable | Independent variables | | |
|---|---|-------------------------------------|--|---|
| | PC1 of element association (Fig. 7.4c) | PC1 of fault systems (Fig. 4.4) | PC1 of felsic igneous rocks (Fig. 5.6) | PC1 of the Yamansu Formation (Fig. 6.4) |
| Low value | Accumulation of Fe concentration | Accumulation of element association | Accumulation of mafic element association | Accumulation of element association |
| High value | Depletion of Fe concentration | Depletion of element association | Accumulation of felsic element association | Depletion of element association |
| Value range associated with Fe mineralization | Low | Low | Low | Low |

Table 9. 2 Diagnostic parameters calculated by OLS and GWR models.

| | OLS | GWR |
|---------|-----------|----------------------|
| R^2 | 0.576 | 0.9433 (Max = 0.980) |
| AIC_c | 33132.188 | 17642.501 |



a

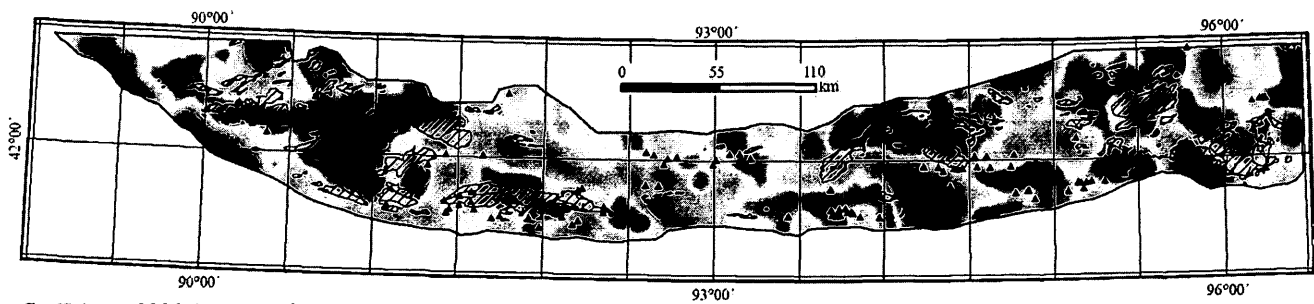


Coefficients of fault systems ▲ Fe deposits

■ High : 1.327

■ Low : -2.960

b



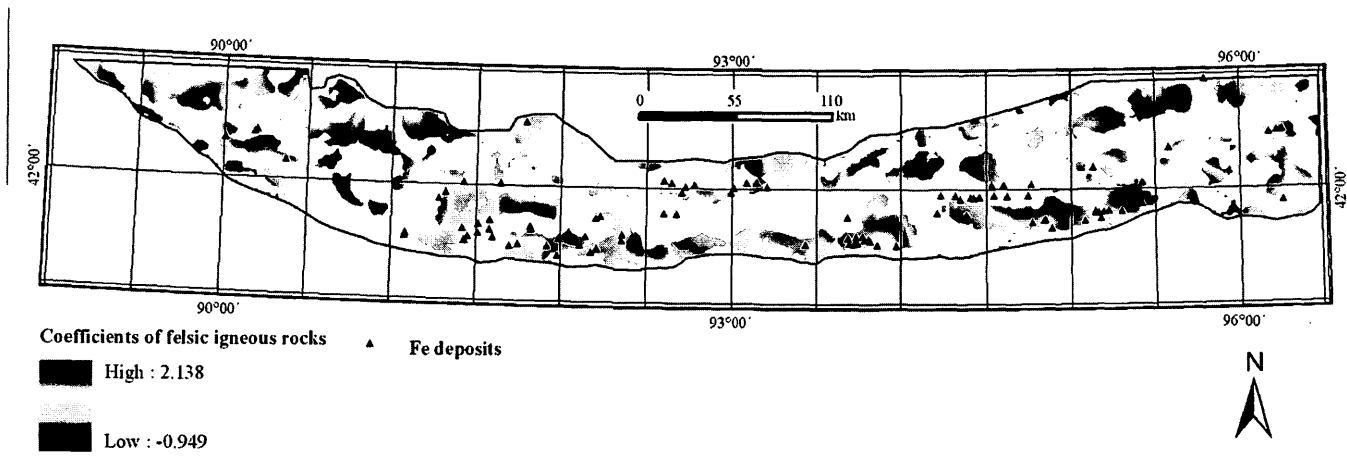
Coefficients of felsic igneous rocks ▲ Fe deposits

■ High : 2.138

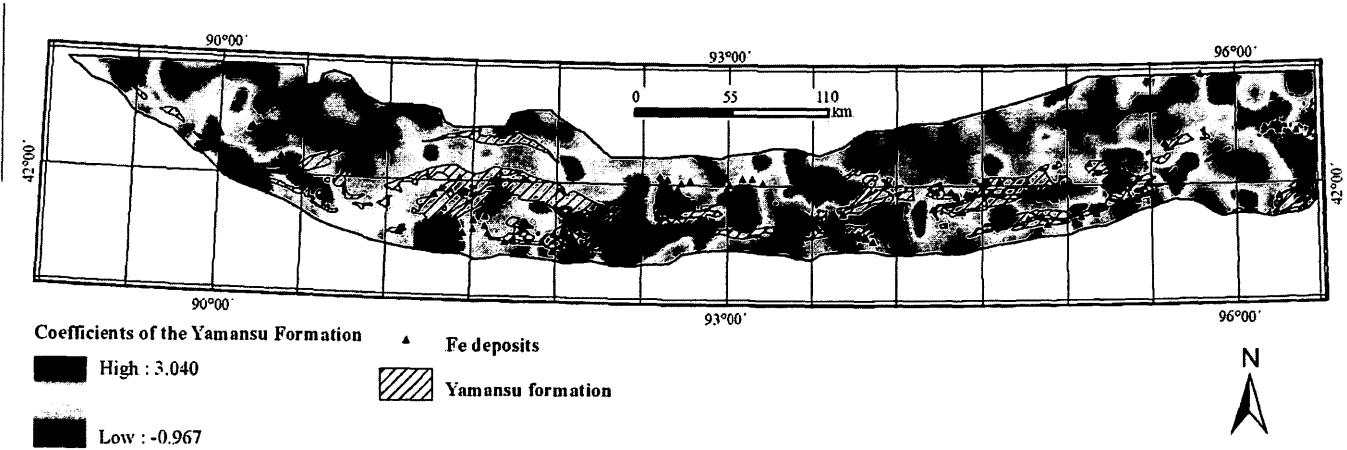
■ Low : -0.949

▨ Felsic igneous rocks

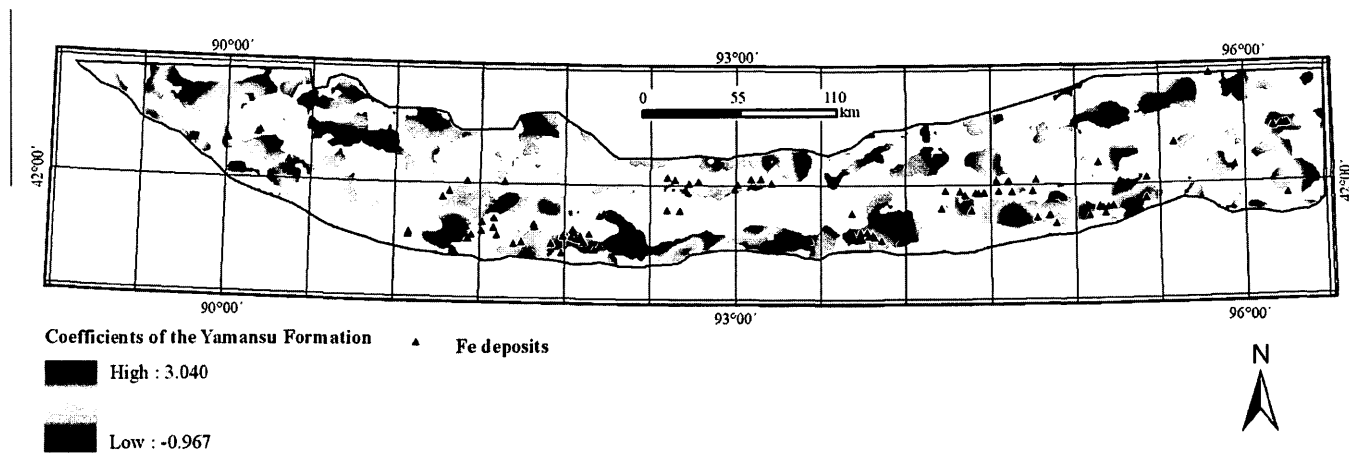
c



d

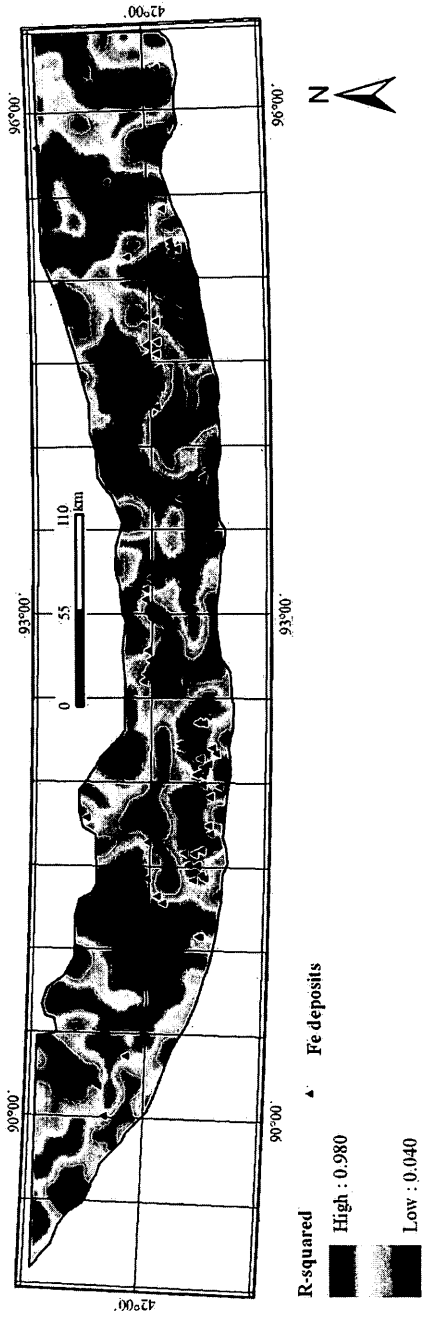


e

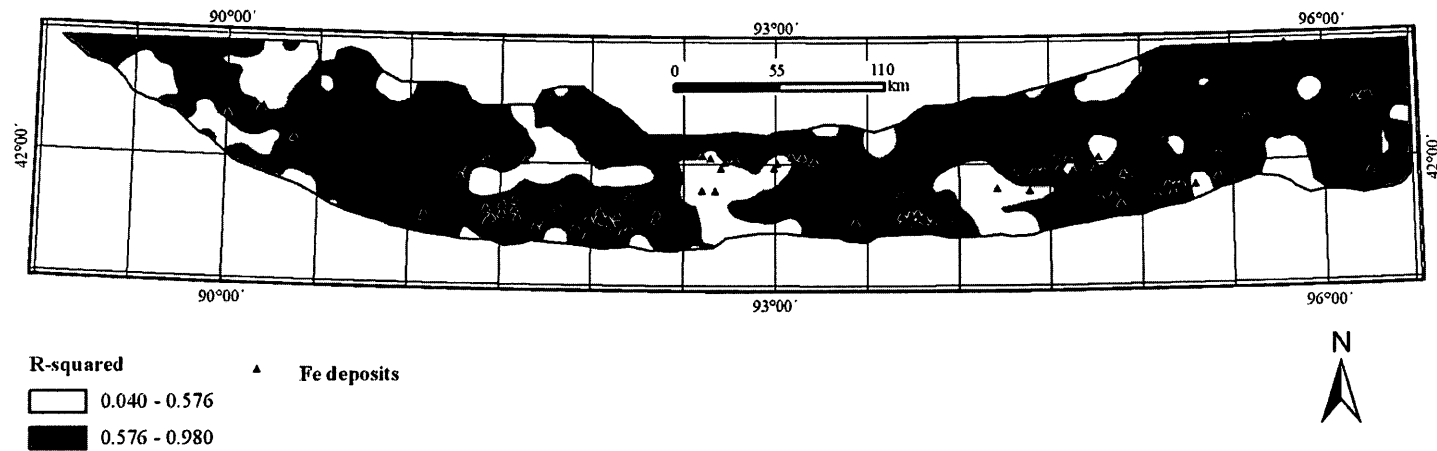


f

Fig.9. 1 Regression coefficients estimated by GWR model. a, c, and e represent spatial distributions of non-stationary relationships between accumulation of element association and fault systems, felsic igneous rocks and the Yamansu Formation, respectively; b, d, and f represent the relationships limited to the target areas of Fe mineralization.

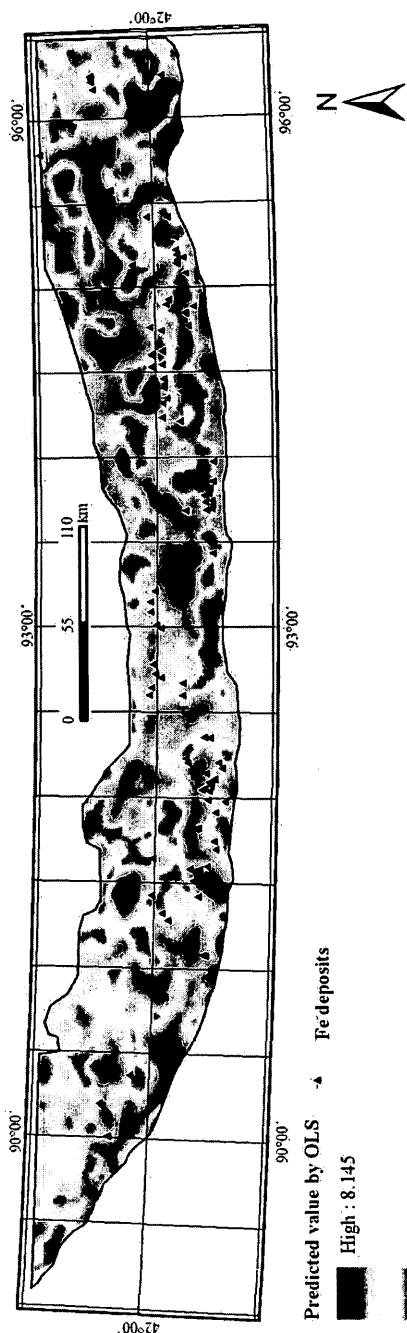


a



b

Fig.9. 2 R^2 values estimated by GWR model. **a**: Non-stationary distribution of R^2 value calculated by GWR model; **b**: A binary map of R^2 distribution defined by using the R^2 value of OLS model (i.e., $R^2 = 0.576$) as the threshold.

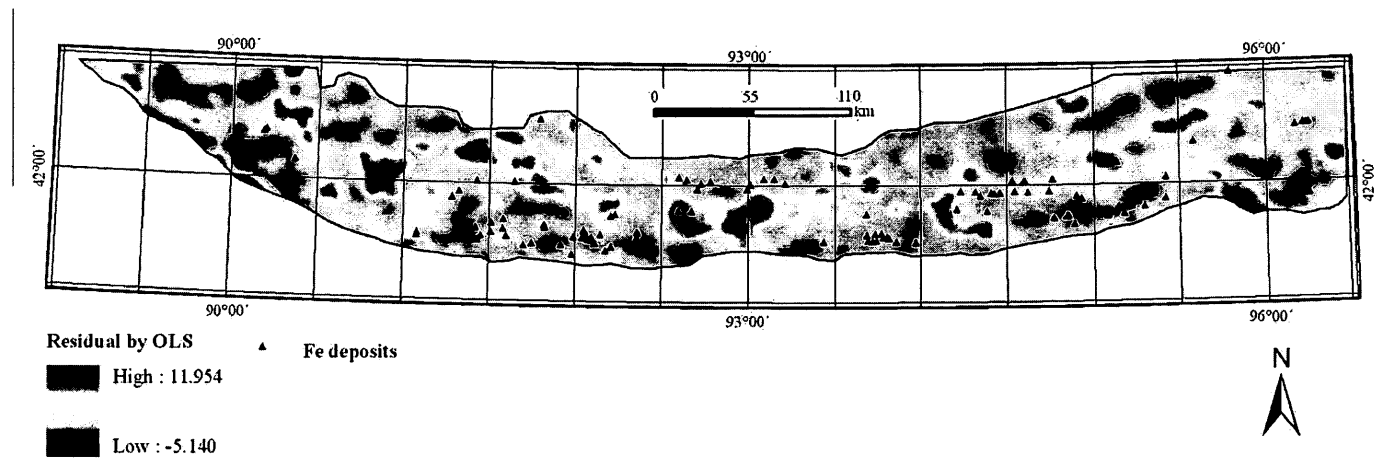


Predicted value by OLS → Fe deposits

High : 8.145

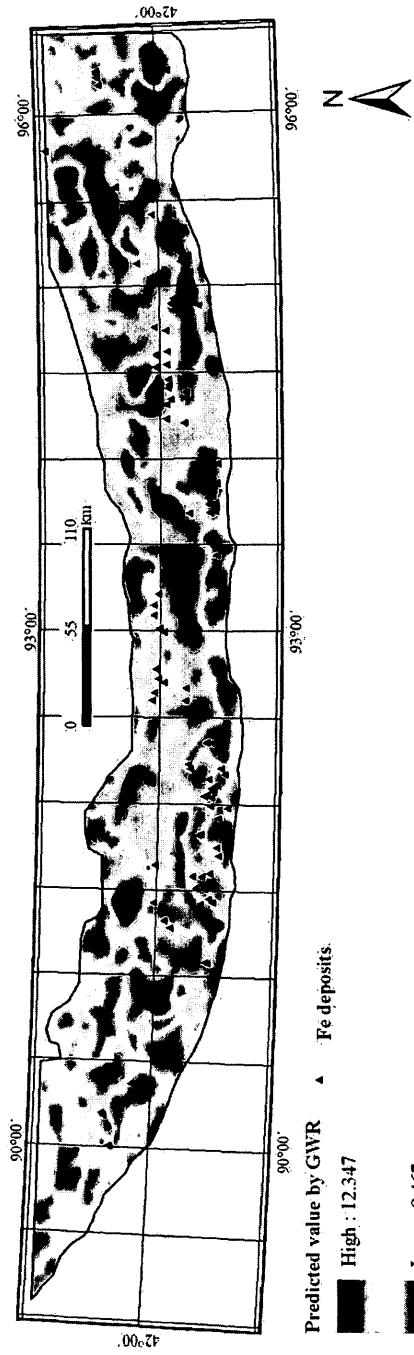
Low : -7.654

a

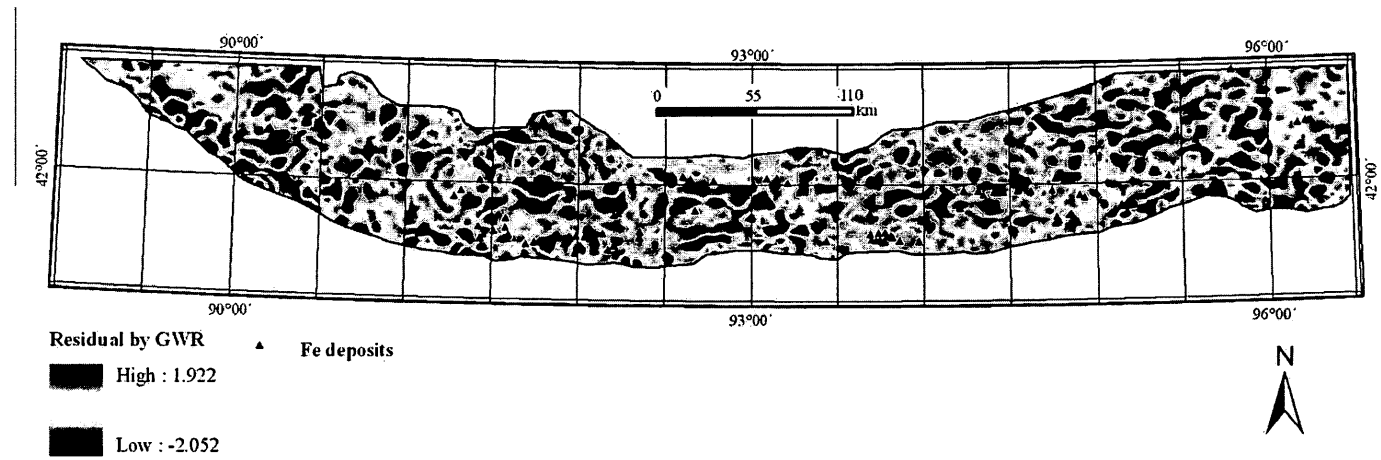


b

Fig.9. 3 Several other results of OLS. a: Predicted spatial distribution of $PC_{association\ i}$ by OLS model; b: The spatial distribution of residuals by OLS model.



a



b

Fig.9. 4 Several other results of GWR. a: Predicted spatial distribution of singularity indices of Fe_2O_3 concentration by GWR model; b: The spatial distribution of residuals by GWR model.

Chapter 10. Summary and conclusions

The study area located in eastern Tianshan mineral district, China is a Gobi desert area. Impeded by the sandy coverage, geo-anomalies associated with the marine volcanic sedimentary Fe mineralization and its dominating geo-processes are often weak or even missing and traditional mineral exploration approaches may not be efficient in detecting them. Therefore, advanced techniques which are more efficient in separating weak geo-anomalies from background are necessary to be applied to assist mineral exploration in this region. Moreover, Fe deposits and their associated geological bodies may be buried at depth, recognition of which may rely on more indirect geo-information with consideration of relationships between Fe mineralization and its controlling factors. By their singular natures, relationships between Fe mineralization and controlling geo-processes present spatial non-stationarity which is commonly existed in various types of deposits. Routine statistics (e.g., ordinary least square) may not be efficient in estimating the relationships properly, confined by which knowledge regarding to the spatially non-stationary relationships were not sufficiently concerned in former mineral exploration. To improve the efficiency of Fe mineral exploration in eastern Tianshan mineral district statistics which are able to characterize complex spatial heterogeneity are necessary to enhance the prediction of mineral potentials.

In order to solve the problems encountered by previous mineral exploration researches, objectives to overcome each of the difficulties can be addressed in this dissertation. First of all, current study intends to achieve better knowledge regarding to the controlling factors of volcanic sedimentary Fe mineralization in eastern Tianshan mineral district. Instead of using location information provided by geological maps which may be unreliable in some desert covered areas, geochemical signatures of elements association related to controlling factors of Fe mineralization (i.e., fault systems, felsic igneous rocks, and the Yamansu Formation) are characterized by various GIS-based spatial analysis methods. Specifically, the singularity index mapping technique inspecting geo-information in both spatial and frequency domain is attempted to separate geochemical anomalies from background, especially in the desert covered areas. After that, Principal component analysis is further used in integrating the geochemical anomalies to identify geo-information of Fe mineralization associated controlling factors, results of which (i.e., element associations) can indicate spatial distributions of these mineralization associated geological bodies or geological activities. Second of all, current study intends to provide a more reliable and improved geo-information integration for Fe mineral potential mapping. In order to delineate mineral potential maps for following sequences of mineral exploration, SWPCA with more geological guidance is tried to integrate these identified controlling factors, interactions of which to Fe mineralization can then be derived. Thirdly, current study intends to provide a new

geo-information to enhance the knowledge of spatially non-stationary relationships between Fe mineralization and its controlling factors. As the first time been introduced to mineral exploration, a GWR method is applied to investigate spatial non-stationary relationships between Fe mineralization and its controlling factors that provides important suggestions regarding to the strategy making of Fe mineral exploration in eastern Tianshan mineral district.

Through all studies in this dissertation, some valuable experiences are received. First of all, in the aspect of geo-information extraction, the singularity index mapping technique is successfully used to identify geochemical anomalies from both weak and strong backgrounds in the study area, especially in the desert covered area; therefore, the interference of overburden can be removed. It is the first time that this method has been applied in identify spatial distributions of geological bodies other than mineralization in an overburden area. This method is suggested to be attempted in study areas with other types of coverage (e.g., grassland, forest, frozen soil, etc.). Identified geochemical signatures by singularity index mapping technique are further integrated by PCA. The whole process used to be employed to delineate geochemical anomalies related to mineralization in previous studies is currently extended to characterize geochemical anomalies produced by other geological bodies or processes (i.e., faults, magmatic rocks and strata). Furthermore, rather than the location information of controlling factors derived from geological maps, identified geo-information by the whole process is more reliable to describe spatial variations in

geochemical signatures caused by the presence of different geological bodies. Second of all, a hybrid geo-information integration method, spatially weighted principal component analysis (SWPCA) demonstrates a technically improved application of principal component analysis (PCA) for mapping mineral potentials, results of which with emphases on geological significance are more informative to following sequences of Fe mineral exploration. The SWPCA method is firstly applied in research in eastern Tianshan mineral district and the weighting factor proposed in this dissertation is strictly following the geological model. Abundant experiments of SWPCA with different weighting factors are suggested to be conducted in other study areas to derive geo-information of interested geological issues. Thirdly, spatially non-stationary relationships between the Fe mineralization and controlling factors are investigated. As a broadly existed characteristic of geological issues, spatially varied interactions of various geological activities did not attract many concerns in previous geological studies. Using the applications in social science for the reference, geographically weighted regression (GWR) which is firstly introduced to assist mineral exploration provides inspiring estimations on spatial relationships between geo-processes. The case study demonstrated in this dissertation is an innovational application of GIS-based spatial analysis, which extends the application of GWR to geological issues. GIS-based mineral exploration proposed in this dissertation serves not only producing maps of mineral potentials but also providing strategies for following sequences of mineral exploration. Therefore, the entire GIS-based data

processing procedure demonstrated in this dissertation can be established as a valuable mineral exploration model dealing with the geological issues not only in the study area but also in other mineral district with various types of coverage.

In this dissertation, there are still some insufficiencies. In the aspect of datasets, only geochemical data are employed, whereas gravity, aeromagnetic and remote sensing data efficient in identifying both exposed and covered geological bodies are not involved. Consequently, based on the exploration model proposed in this dissertation, more exploratory geo-datasets are necessary to be considered for a comprehensive investigation of the Fe mineralization in this area. In the aspect of delineation to the mineral potentials, the SWPCA result does not show a significant improvement in comparison with the PCA result; however, it still encourages the further attempts to achieve more noticeable improvements with informative geological guidance by determining new spatially weighting factors or input variables. Moreover, this dissertation demonstrates a few methods (e.g., Student's *t*-test, and *R*-squared value, and *AIC* value) of uncertainty assessment. In this research, uncertainty may be resulted from but not limited to (1) imprecision in the data collection and measurement; (2) misuse of element assemblage in characterization of different geological bodies; (3) misuse of window sizes for the calculation of singularity indices in recognition of geological bodies; and (4) imprecision in construction of regression model. Errors caused by the first situation will be intrinsically delivered to the following data processing approaches, which may only be solved by employing

data sets with higher precision. The information integration results and regression results are estimated by the Student's *t*-test and R^2 and *AIC* values, respectively. However, the uncertainty caused by the latter three situations can be probably reduced by enhancing the knowledge of geological model. The future work could be suggested to focus on systematic uncertainty assessment and improving the statistical results of the entire exploration model.

Field work regarding to this research had been carried out in summers 2010 and 2011. During the field trips typical deposits such as the Yamansu, Hongyuntan, Bailingshan, Tieling deposits had been visited in summer 2010. Data processing results (i.e., identification of felsic igneous rocks in tongue-shape rock) had been validated in July, 2011. However, recognition results of other geological bodies, geo-information integration results, GWR results, and even the target areas delineated in current research should be further validated in future work.

References

- Abdi, H., Williams, L.J., 2010. Principal component analysis. *Wiley Interdisciplinary Reviews: Computational Statistics* 2, 433-459.
- Agterberg, F., Bonham-Carter, G., Wright, D., 1990. Statistical pattern integration for mineral exploration. In: Gaal, G., Merriam, D.F., (eds.), 1990. *Computer applications in resource estimation prediction and assessment for metals and petroleum*, Pergamon Press, Oxford, p. 1-21.
- Aitchison, J., 1982. The statistical analysis of compositional data. *Journal of the Royal Statistical Society: Series B (Methodological)* 44, 139-177.
- Aitchison, J., 1983. Principal component analysis of compositional data. *Biometrika* 70, 57-65.
- Aitchison, J., 1986. *The statistical analysis of compositional data*, first ed. Chapman and Hall, London.
- Aitchison, J., Egozcue, J., 2005. Compositional data analysis: where are we and where should we be heading? *Mathematical Geology* 37, 829-850.
- Ali, K., Cheng, Q., Chen, Z., 2007. Multifractal power spectrum and singularity analysis for modelling stream sediment geochemical distribution patterns to identify anomalies related to gold mineralization in Yunnan Province, South China. *Geochemistry: Exploration, Environment, Analysis* 7, 293-301.
- Allen, M., Windley, B., Zhang, C., 1992. Palaeozoic collisional tectonics and magmatism of the Chinese Tien Shan, central Asia. *Tectonophysics* 220, 89-115.
- Bai, J., Porwal, A., Hart, C., Ford, A., Yu, L., 2010. Mapping geochemical singularity using multifractal analysis: Application to anomaly definition on stream sediments data from Funin Sheet, Yunnan, China. *Journal of Geochemical Exploration* 104, 1-11.
- Barton, M.D., Johnson, D.A., 2000. Alternative brine sources for Fe-oxide (-Cu-Au) systems: implications for hydrothermal alteration and metals. In: Porter, T.M., (ed), *Hydrothermal Iron Oxide Copper-Gold & Related Deposits: A Global Perspective*, Australian Mineral Foundation, Adelaide, pp. 43-60.
- BGEDXP, 2009. Report of mineralization exploration in Eastern Tianshan, unpublished report (in Chinese). Bureau of Geological Exploration & Development of Xinjiang Province (BGEDXP).

Bogoch, R., Shirav, M., Beyth, M., Halicz, L., Geochemistry of ephemeral stream sediments in the Precambrian mountainous arid terrain of southern Israel. *Journal of Geochemical Exploration* 46, 349-364.

Bonham-Carter, G.F., 1994. *Geographic information systems for geoscientists: modeling with GIS*, Computer Methods in the Geosciences, first ed. Pergamon, New York. 398 pp.

Bonham-Carter, G.F., Agterberg, F.P., Wright, D.F., 1989. Weights of evidence modeling: a new approach to mapping mineral potential. In: Bonham-Carter, G.F., Agterberg, F.P. (Eds.), *Statistical Applications in the Earth Sciences*. Geological Survey of Canada, Ottawa, Ontario, pp. 171-183.

Brantley, S.L., White, A.F., 2009. Approaches to modeling weathered regolith. *Reviews in Mineralogy and Geochemistry* 70, 435-484.

Brunsdon, C., Fotheringham, A.S., Charlton, M., 1998. Geographically weighted regression-modelling spatial non-stationarity. *The Statistician* 47, 431-443.

Brunsdon, C., Fotheringham, A.S., Charlton, M., 1999. Some notes on parametric significance tests for geographically weighted regression. *Journal of Regional Science* 39, 497-524.

Brunsdon, C., Fotheringham, A.S., Charlton, M., 2002. Geographically weighted summary statistics – a framework for localised exploratory data analysis. *Computers, Environment and Urban Systems* 26, 501-524.

Brunsdon, C., Fotheringham, A.S., Charlton, M.E., 1996. Geographically weighted regression: a method for exploring spatial nonstationarity. *Geogr. Anal.* 28, 281-298.

Brunsdon, C., McClatchey, J., Unwin, D.J., 2001. Spatial variations in the average rainfall-altitude relationship in Great Britain: an approach using geographically weighted regression. *International Journal of Climatology* 21, 455-466.

Buccianti, A., Mateu-Figueras, G., Pawlowsky-Glahn, V., 2006. *Compositional data analysis in the Geosciences: From theory to practice*. Geological Society, London, Special publication 264, pp212.

Carranza, E. J. M., Mangaoang, J. C., Hale, M., 1999. Application of mineral exploration models and GIS to generate mineral potential maps as input for optimum land-use planning in the Philippines. *Natural Resources Research* 8, 165-173.

Carranza, E.J.M., 2008. *Geochemical Anomaly and Mineral Prospectivity Mapping in GIS*. Handbook of Exploration and Environmental Geochemistry, vol. 11. Elsevier, Amsterdam.

Carranza, E.J.M., 2011. *Analysis and mapping of geochemical anomalies using*

logratio-transformed stream sediment data with censored values. *Journal of Geochemical Exploration* 110, 167-185.

Chayes, F., Trochimczyk, J., 1978. An effect of closure on the structure of principal components. *Mathematical Geology* 10, 323-333.

Cheng, Q., 1999a. Spatial and scaling modeling for geochemical anomaly separation. *Journal of Geochemical Exploration* 65, 175-194.

Cheng, Q., 1999b. Multifractality and spatial statistics. *Computers and Geosciences* 25, 949-961.

Cheng, Q., 2000. *GeoDAS phase I: User's Guide & Exercise Manual*. Unpublished notes, York University, 298pp.

Cheng, Q., 2002. New versions of principal component analysis for image enhancement and classification. *Geoscience and remote sensing symposium, IGARSS '02*. In: *Proceedings of the IEEE International*, June 24-28 2002, vol. 6, pp. 3372-3374.

Cheng, Q., 2006. Spatial and spatially weighted principal component analysis for images processing. *Geoscience and remote sensing symposium, IGARSS '06*. In: *Proceedings of the IEEE International*, July 31-August 4 2006, pp. 972-975.

Cheng, Q., 2007. Mapping singularities with stream sediment geochemical data for prediction of undiscovered mineral deposits in Gejiu, Yunnan Province, China. *Ore Geology Reviews* 32, 314-324.

Cheng, Q., 2012. Singularity theory and methods for mapping geochemical anomalies caused by buried sources and for predicting undiscovered mineral deposits in covered areas. *Journal of Geochemical Exploration* 122, 55-70

Cheng, Q., Agterberg, F.P., 2009. Singularity analysis of ore-mineral and toxic trace elements in stream sediments. *Computers & Geosciences* 35, 234-244.

Cheng, Q., Agterberg, F.P., Ballantyne, S.B., 1994. The separation of geochemical anomalies from background by fractal methods. *Journal of Geochemical Exploration* 51, 109-130.

Cheng, Q., Bonham-Carter, G., Wang, W., Zhang, S., Li, W., Xia, Q., 2011. A spatially weighted principal component analysis for multi-element geochemical data for mapping locations of felsic intrusions in the Gejiu mineral district of Yunnan, China. *Computers & Geosciences* 37, 662-669.

Cheng, Q., Zhao, P., 2011. Singularity theories and methods for characterizing mineralization processes and mapping geo-anomalies for mineral deposit prediction. *Geoscience Frontiers* 2, 67-79.

Cheng, Q., 2012. Singularity theory and methods for mapping geochemical anomalies caused by buried sources and for predicting undiscovered mineral deposits in covered areas. *Journal of Geochemical Exploration* 122, 55-70.

Christophersen, N., Hooper, R.P., 1992. Multivariate analysis of stream water chemical data: The use of principal components analysis for the end-member mixing problem. *Water Resources Research* 28, 99-107.

Chung, C.F., Agterberg, F.P., 1980. Regression models for estimating mineral resources from geological map data: *Mathematical Geology* 12, 473-488.

Chung, C.G., Moon, W.M., 1990. Combinatin rules of spatial geoscience data for mineral exploration. *Geoinformatics* 2, 159-169.

Curewitz, D., Karson, J.A., 1997. Structural settings of hydrothermal outflow: fracture permeability maintained by fault propagation and interaction. *Journal of Volcanology and Geothermal Research* 79, 149-168.

Darnley, A.G., 1995. International geochemical mapping - A review. *Journal of Geochemical Exploration* 55, 5-10.

Davenport, P.H., 1990. A comparison of regional geochemical data from lakes and streams in northern Labrador; implications for mixed-media geochemical mapping. *Journal of Geochemical Exploration* 39, 117-151.

de Smith, M., Goodchild, M., Longley, P., 2007. *Geospatial analysis: a comprehensive guide to principles, techniques and software tools*, second ed. Matador, Leicester.

Ding, T., 1990. The geological characteristics of stratabound iron deposits in the Yamansu formation in Xinjiang. *Regional Geology of China* 1990, 269-272 (in Chinese with English abstract).

Drew, L., Grunsky, E., Sutphin, D., Woodruff, L., 2010. Multivariate analysis of the geochemistry and mineralogy of soils along two continental-scale transects in North America. *Science of the Total Environment* 409, 218-277.

Edwards, R. and Atkinson, K., 1986. *Ore Deposit Geology and its influence on mineral exploration*. first ed. Chapman and Hall, London, 466 pp.

Egozcue, J., Pawlowsky-Glahn, V., 2006. *Simplicial geometry for compositional data. Compositional Data Analysis in the Geosciences: From Theory to Practice*. Geological Society, London, Special Publications 264, 145-160.

Egozcue, J., Pawlowsky-Glahn, V., Mateu-Figueras, G., Barceló-Vidal, C., 2003. Isometric logratio transformations for compositional data analysis. *Mathematical Geology* 35, 279-300.

- Ellis, A.J., 1968. Natural hydrothermal systems and experimental hot-water/rock interaction: reactions with NaCl solutions and trace metal extraction. *Geochimica et Cosmochimica Acta* 32, 1356-1363.
- Everett, C.E., Wilkinson, J.J., Rye, D.M., 1999. Fracture-controlled fluid flow in the Lower Palaeozoic basement rocks of Ireland: implications for the genesis of Irish-type Zn-Pb deposits. In: McCaffrey, K.J.W., Lonergan, L., Wilkinson, J.J., (eds.), *Fractures, fluid flow and mineralization*. Geological Society, London, Special Publications 155, 247-276.
- Feng, Y., Zhu, B., Yang, J., Zhang, K., 2002. Tectonics and Evolution of the eastern Tianshan mountains - A brief introduction to "Tectonic map (1:500, 000) of the eastern Tianshan mountains of Xinjiang". *Xinjiang Geology* 20, 309-314.
- Filzmoser, P., Hron, K., Reimann, C., 2009. Univariate statistical analysis of environmental (compositional) data: Problems and possibilities. *Science of the Total Environment* 407, 6100-6108.
- Filzmoser, P., Hron, K., Reimann, C., 2012. Interpretation of multivariate outliers for compositional data. *Computers & Geosciences* 39, 77-85.
- Fotheringham, A.S., Brunson, C., 1999. Local forms of spatial analysis. *Geogr. Anal.* 31, 340-358.
- Fotheringham, A.S., Brunson, C., Charlton, M., 2002. *Geographically weighted regression: the analysis of spatially varying relationships*. 1st ed. Wiley, Chichester.
- Fotheringham, A.S., Charlton, M., Brunson C., 2001. Spatial variations in school performance: a local analysis using geographically weighted regression. *Geographical & Environmental Modelling* 5, 43-66.
- Fotheringham, A.S., Charlton, M., Brunson, C., 1996. The geography of parameter space: an investigation of spatial non-stationarity. *Int. J. Geogr. Inf. Syst.* 10, 605-627.
- Fotheringham, A.S., Charlton, M., Brunson, C., 1998. Geographically weighted regression: a natural evolution of the expansion method for spatial data analysis. *Environ. Plann. A* 30, 1905-1927.
- Gao, J., Li, S., 2011. Detecting spatially non-stationary and scale-dependent relationships between urban landscape fragmentation and related factors using Geographically Weighted Regression. *Applied Geography* 31, 292-302.
- Guilbert, J.M., Park, C.F., 1986. *The geology of ore deposits*. 4th ed. W. H. Freeman and Company, New York.
- Haldar, S.K., 2012. *Mineral Exploration: Principles and Applications*. first ed. Elsevier. Oxford.

Han, C., Mao, J., Yang, J., Wang, Z., Cui, B., 2002. Types of Late Palaeozoic endogenous metal deposits and related geodynamical evolution in the East Tianshan. *Acta Geologica Sinica* 76, 222-233 (in Chinese with English abstract).

Han, C., Zhao, G., 2003. Major types and characteristics of Late Paleozoic ore deposit, East Tianshan, Northwest China. *International Geology Review* 45, 798-813.

Hao, L., Lu, J., Li, L., Mo, G., Yan, G., Shi, Y., Zhao, Y., 2007. Method of using regional geochemical data in geological mapping in shallow overburden areas. *Geology in China* 34, 710-715 (in Chinese with English abstract).

Harris, J. R., Sanborn-Barrie, M., 2006. Mineral potential mapping: examples from the Red Lake greenstone belt, northwest Ontario. In: *GIS for the Earth Sciences*, Geological Association of Canada, Special Paper 44, 1-22.

Harris, J.R., 1989. Data integration for gold exploration in eastern Nova Scotia using a GIS. In *Proceedings of Remote Sensing for Exploration Geology: Calgary, Alberta*, p. 233-249.

Harris, J.R., Wilkinson, L., Heather, K., Fumerton, S., Bernier, M.A., Ayer, J., Dahn, R., 2001. Application of GIS processing techniques for producing mineral prospectivity maps – A case study: Mesothermal Au in the Swayze greenstone belt, Ontario, Canada. *Natural Resources Research* 10, 91-124.

He, S., Chen, Z., 2002. The zoning of surface tectonic geochemistry in Guizhou and its significance. *Guizhou Geology* 19, 148-155 (in Chinese with English abstract).

Hemley, J.J., Cygan, G.L., Fein, J.B., Robinson, G.R., d'Angelo, W.M., 1992. Hydrothermal ore-forming processes in the light of studies in rock-buffered systems; I, iron-copper-zinc-lead sulfide solubility relations. *Economic Geology* 87, 1-22.

Hodgson, C.J., 1990. Uses (and Abuses) of ore deposit models in mineral exploration. *Geoscience Canada* 17, 79-89.

Horel, J.D., 1984. Complex principal component analysis: theory and examples. *Journal of Climate and Applied Meteorology* 23, 1660-1673.

Hou, G., Tang, H., Liu, C., 2006. Geochemical characteristics of the Late Paleozoic volcanics in Jueluotage tectonic belt, eastern Tianshan and its implications. *Acta Petrologica Sinica* 22, 1167-1177 (in Chinese with English abstract).

Hron, K., Templ, M., Filzmoser, P., 2010. Imputation of missing values for compositional data using classical and robust methods. *Computational Statistics and Data Analysis* 54, 3095-3107.

Hua, L., Yang, X., Zhong, H., 2002. Geochemical characteristics and ore-finding forecast of "Shaquanzi" area, eastern Tianshan, Xinjiang. *Mineral Resources and*

Geology 16, 291-296.

Jiang, F., Qin, K., Fang, T., Wang, S., 2002. Types, geological characteristics, metallogenic regularity and exploration target of iron deposits in eastern Tianshan Mountains. *Xinjiang Geology* 20, 379-384 (in Chinese with English abstract).

Jiang, J., Cheng, J., Qi, S., Xiang, W., 2006. Applied geochemistry, first ed. China University of Geosciences Press, Wuhan, China (in Chinese).

Jolliffe, I.T., 2002. Principal component analysis, second ed. Springer, New York.

Kaiser, H.F., 1960. The application of electronic computers to factor analysis. *Educational Psychological Measurement* 20, 141-151.

Kassoy, D.R., Zebib, A., 1978. Convection fluid dynamics in a model of a fault zone in the earth's crust. *Journal of Fluid Mechanics* 88, 769-792.

Kerrich, R., 1986. Fluid infiltration into fault zones: chemical, isotopic, and mechanical effects. *Pageoph* 124, 225-268.

Li, S., Zhao, Z., Xie, M., Wang, Y., 2010. Investigating spatial non-stationary and scale-dependent relationships between urban surface temperature and environmental factors using geographically weighted regression. *Environmental Modelling & Software* 25, 1789-1800.

Li, W., Ren, B., Yang, X., Li, Y., Chen, Q., 2002. The intermediate-acid intrusive magmatism and its geodynamic significance in Eastern Tianshan region. *Northwestern Geology* 35, 41-64 (in Chinese with English abstract).

Liu, D., Tang, Y., Zhou, R., 1996. Metallogenic series types of deposits in Xinjiang. *Mineral Deposits* 15, 207-215 (in Chinese).

López, D.L., Smith, L., 1995. Fluid flow in fault zones: analysis of the interplay of convective circulation and topographically driven groundwater flow. *Water Resources Research* 31, 1489-1503.

Loughlin, W.P., 1991. Principal component analysis for alteration mapping. *Photogrammetric Engineering & Remote Sensing* 57, 1163-1169.

Lu, D., Ji, J., Lv, R., Tao, H., 1995. Geochemical characteristics and genesis of Yamansu iron deposit of Xinjiang. *Northwestern Geology* 16, 15-19 (in Chinese).

Ma, R., Shu, L., Sun, J., 1997. The tectonic deformation, evolution and metallization in the Eastern Tianshan Belt, Northwest China, first ed. Geological Publish House, Beijing (in Chinese).

Ma, R., Wang, C., Ye, S., 1993. Tectonic framework and crustal evolution of Eastern

Tianshan mountains, first ed. Nanjing University Press, Nanjing (in Chinese).

Mandelbrot, B.B., 1972. Possible refinement of the lognormal hypothesis concerning the distribution of energy dissipation in intermittent turbulence. In: Rosenblatt, M., Van Atta, C. (Eds.), *Statistical Models and Turbulence*, Lecture Notes in Physics, vol. 12. Springer, New York, pp. 333-351.

Mao, J., Goldfarb, R.J., Wang, Y., Hart, C.J., Wang, Z., Yang, J., 2005. Late Paleozoic base and precious metal deposits, East Tianshan, Xinjiang, China: characteristics and geodynamic setting. *Episodes: Journal of International Geoscience* 18, 23-36.

Mao, J., Yang, J., Han, C., Wang, Z., 2002. Metallogenic Systems of Polymetallic Copper and Gold Deposits and Related Metallogenic Geodynamic Model in Eastern Tianshan, Xinjiang. *Earth Science - Journal of China University of Geosciences* 27, 413-424 (in Chinese with English abstract).

Misra, K., 2000. *Understanding mineral deposits*. Kluwer Academic Publishers. 845pp.

Moon, C., Whateley, M., & Evans, A. M., 2009. *Introduction to mineral exploration*. Second ed. Wiley-Blackwell.

Nomikos, P., MacGregor, J.F., 1994. Monitoring batch processes using multiway principal component analysis. *AICHE Journal* 40, 1361-1375.

Páez, A., Uchida, T., Miyamoto, K., 2002. A general framework for estimation and inference of geographically weighted regression models: 1. Location-specific kernel bandwidths and a test for locational heterogeneity. *Environment and Planning A* 34, 733-754.

Pan, G.C., Harris, D.P., 2000. *Information Synthesis for Mineral Exploration*. first ed. Oxford University Press, New York. 461 p.

Panahi, A., Cheng, Q., Bonham-Carter, G.F., 2004. Modelling lake sediment geochemical distribution using principal component, indicator kriging and multifractal power-spectrum analysis: A case study from Gowganda, Ontario. *Geochemistry: Exploration, Environment, Analysis* 4, 59-70.

Pawlowsky-Glahn, V., Egozcue, J.J., 2006. Compositional data and their analysis: an introduction. *Compositional Data Analysis in the Geosciences: From Theory to Practice*. Geological Society, London, Special Publications 264, 1-10.

Qian, J., 2009. Tectono-geochemical prospecting method and its application in searching for sediment-hosted, disseminated gold deposits. *Geology and Exploration* 45, 60-67 (in Chinese with English abstract).

Qin, K., Fang, T., Wang, S., Zhu, B., Feng, Y., Yu, H., Xiu, Q., 2002. Plate tectonics

division, evolution and metallogenic settings in eastern Tianshan mountains, NW-China. *Xinjiang Geology* 20, 302-308 (in Chinese with English abstract).

Qin, K., Xiao, W., Zhang, L., Xu, X., Hao, J., Sun, S., Li, J., Tosdal, R.M., 2005. Eight stages of major ore deposits in northern Xinjiang, NW-China: Clues and constraints on the tectonic evolution and continental growth of Central Asia. In: Mao, J.W., Bierlein, F. (Eds.), *Mineral Deposit Research: Meeting the Global Challenge*. Berlin, Heidelberg, New York: Springer 2, 1327-1330

Ranjbar, H., Honarmand, M., 2004. Integration and analysis of airborne geophysical and ETM+ data for exploration of porphyry type deposits in the Central Iranian Volcanic Belt using fuzzy classification. *International Journal of Remote Sensing* 25, 4729-4741.

Ren, T., Zhao, Y., Zhang, H., Yang, S., 1989. Regional geochemical surveys in arid and semiarid regions in the middle and western part of Inner Mongolia. *Journal of Geochemical Exploration* 33, 11-26.

Rencz, A.N., Klassen, R. A., Moore, A., 2002. Comparison of geochemical data derived from till and lake sediment samples, Labrador, Canada. *Geochemistry: Exploration, Environment, Analysis* 2, 27-35.

Rollinson, H., 1992. Another look at the constant sum problem in geochemistry. *Mineralogical Magazine* 56, 469-475.

Rollinson, H., 1993. *Using geochemical data: evaluation, presentation, interpretation*, first ed. Longman, London.

Rose, A.W., Hawkes, H.W., Webb, J.S., 1979. *Geochemistry in Mineral Exploration*, second ed. Academic, London.

Ryan, T.S., 2009. *Modern Regression Methods*, 2nd ed. Wiley, New Jersey.

Saemundsson, K., Axelsson, G., Steingrímsson, B., 2009. Geothermal systems in global perspective. United Nations University, Geothermal Training Program, Santa Tecla, El Salvador, Short Course on Surface Exploration for Geothermal Resources, Oct. 2009.

Shu, L., Ma, R., Guo, L., Sun, J., 1997. Research on the thrust tectonics of the eastern Tianshan belt, Xinjiang. *Scientia Geologica Sinica*. 32, 337-350 (in Chinese with English abstract).

Sibson, R.H., 1994. Crustal stress, faulting and fluid flow. *Geological Society* 78, 69-84.

Sibson, R.H., 1996. Structural permeability of fluid-driven fault-fracture meshes. *Journal of Structural Geology* 18, 1031-1042.

Singer, D.A., Kouada, R., 1997. Use of a neural network to integrate geoscience information in the classification of mineral deposits and occurrences, in Guibins, A.G., (eds.), *Proceedings of Exploration 97: 4th Decennial International Conference on Mineral Exploration*. p. 287-298.

Singh, A., Harrison, A., 1985. Standardized principal components. *International Journal of Remote Sensing* 6, 883-896.

Su, B., Qin, K., Sakyi, P., Li, X., Yang, Y., Sun, H., Tang, D., Liu, P., Xiao, Q., Malaviarachchi, S., 2011. U-Pb ages and Hf-O isotopes of zircons from Late Paleozoic mafic-ultramafic units in the southern Central Asian Orogenic Belt: Tectonic implications and evidence for an Early-Permian mantle plume. *Gondwana Research* 20, 516-531.

Su, S., Xiao, R., Zhang, Y., 2012. Multi-scale analysis of spatially varying relationships between agribultural landscape patterns and urbanization using geographically weighted regression. *Applied Geography* 32, 360-375.

Tan, K., Xie, Y., Yang, J., Hu, E., 2004. Reaction-transport-mechanical coupling and self-organization in rock faulting. *Journal of Nanhua University (Science & Engineering Edition)* 18, 1-6 (in Chinese with English abstract).

Thomas, C.W., Aitchison, J., 2006. Log-ratios and geochemical discrimination of Scottish Dalradian limestones: a case study. *Compositional Data Analysis in the Geosciences: From Theory to Practice*. Geological Society, London, Special Publications 264, 25-41.

Thornton, I., Farago, M., 1997. The geochemistry of arsenic. *Arsenic*. Springer Netherlands, 1-16.

Tu, J., Xia, Z., 2008. Examining spatially varying relationships between land use and water quality using geographically weighted regression I: Model design and evaluation. *Science of The Total Environment* 407, 358-378.

Verma, S., Guevara, M., Agrawal, S., 2006. Discriminating four tectonic settings: five new geochemical diagrams for basic and ultrabasic volcanic rocks based on log-ratio transformation of major-element data. *Journal of Earth System Science* 115, 485-528.

Wang, C., Ma, R., Shu, L., Zhu, W., 1994. Study on the regional metamorphism and the tectonic settings in the eastern Tianshan orogenic belt. *Journal of Nanjing University (Natural Science Edition)* 30, 494-503 (in Chinese with English abstract).

Wang, H., Liu, T., Wang, Q., Zheng, Q., 2007. Geochemical character in ore-forming belt of Tianshan-Beishan mineralization zone, Xinjiang. *Journal of Earth Sciences and Environment* 29, 141-144 (in Chinese with English abstract).

Wang, J., Wang, Y., He, Z., 2006. Ore deposits as a guide to the tectonic evolution in

the East Tianshan Mountains, NW China. *Geology in China* 33, 461-469 (in Chinese with English abstract).

Wang, W., Cheng, Q., 2008. Mapping mineral potential by combining multi-scale and multi-source geoinformation. *Geoscience and remote sensing symposium, IGARSS '08*. In: *Proceedings of the IEEE International Geoscience & Remote Sensing Symposium*, 7-11 July 2008, 1321-1324.

Wang, W., Zhao, J., Cheng, Q., 2011. Analysis and integration of geo-information to identify granitic intrusions as exploration targets in southeastern Yunnan District, China. *Comput. Geosci.* 37, 1946-1957.

Wang, W., Zhao, J., Cheng, Q., 2013. Application of singularity index mapping technique to gravity/magnetic data analysis in southeastern Yunnan mineral district, China. *Journal of Applied Geophysics* 92, 39-49.

Wang, W., Zhao, J., Cheng, Q., Liu, J. 2012. Tectonic-geochemical exploration modeling for characterizing geo-anomalies in southeastern Yunnan district, China. *Journal Geochemical Exploration* 122, 71-80.

Wang, X., 1998. Leaching of mobile forms of metals in overburden: development and application. *Journal of Geochemical Exploration* 61, 39-55.

Wang, X., 2005a. Analysis of the geology and genesis of Yamansu Fe deposit. *Contributions to Geology and Mineral Resources Research* 20, 125-128 (in Chinese with English abstract).

Wang, X., 2005b. Conceptual model of deep-penetrating geochemical migration. *Geological Bulletin of China* 24, 892-896 (in Chinese with English abstract).

Wang, X., Chi, Q., Sun, H., 2001. Wide-spaced geochemical survey in arid desert terrain, a case history from the eastern Tianshan regions, northwestern China. *Xinjiang Geology* 19, 200-206 (in Chinese with English abstract).

Wang, X., Liu, Z., Ye, R., Cheng, Z., Fu, Y., 2003. Deep-penetrating geochemistry: a comparative study in the Jinwozi gold ore district, Xinjiang. *Geophysical & Geochemical exploration* 27, 247-254.

Wang, Y., Wang, J., Wang, L., 2006. Comparison of host rocks between two vanadic titanomagnetite deposit types from the eastern Tianshan mountains. *Acta Petrologica Sinica* 22, 1425-1436.

Windley, B., Allen, M., Zhang, C., Zhao, Z., Wang, G., 1990. *Geology* 18, 128-131.

Woodall, 1994. Empiricism and concept in successful mineral exploration. *Australian Journal of Earth Sciences* 41, 1-10.

- Xiao, F., Chen, J., Zhang, Z., Wang, C., Wu, G., Agterberg, F.P., 2012. Singularity mapping and spatially weighted principal component analysis to identify geochemical anomalies associated with Ag and Pb-Zn polymetallic mineralization in Northwest Zhejiang, China. *Journal of Geochemical Exploration* 122, 90-100.
- Xie, X., Mu, X., Ren, T., 1997. Geochemical mapping in China. *Journal of Geochemical Exploration* 60, 99-113.
- Xie, X., Ren, T., Xi, X., Zhang, L., 2009. The implementation of the Regional Geochemistry-National Reconnaissance Program (RGNR) in China in the past thirty years. *Acta Geoscientica Sinica* 30, 700-716.
- Xie, X., Wang, X., 2003. Recent developments on deep-penetrating geochemistry. *Earth Science Frontiers* 10, 225-238 (in Chinese with English abstract).
- Yang, S.X., Blum, N., 1999. Arsenic as an indicator element for gold exploration in the region of Xiangxi Au-Sb-W deposit, NW Hunan, PR China. *Journal of Geochemical Exploration* 66, 441-456.
- Yang, X., Tao, H., Luo, G., Ji, J., 1996. Basic features of plate tectonics in east Tianshan of China. *Xinjiang Geology* 14, 221-227 (in Chinese with English abstract).
- Yuan, J., Zhu, S., Zhai, Y., 1979. *Mineral Deposits*, first ed. Geological Publishing House, Beijing (in Chinese)
- Zhai, Y., Deng, J., Li, X., 1999. *Essentials of metallogeny*, first ed. Geological Publishing House, Beijing, China. 286pp (in Chinese with English abstract).
- Zhang, H., Xie, L., 2001. New views on origin of Yamansu iron deposit in Xinjiang autonomous region. *Journal of Changchun Institute Technology (Nature Science Edition)* 2, 26-29 (in Chinese with English abstract).
- Zhang, L., Qin, K., Xiao, W., 2008. Multiple mineralization events in the eastern Tianshan district, NW China: Isotopic geochronology and geological significance. *Journal of Asian Earth Science* 32, 236-246.
- Zhang, L., Xiao, W., Qin, K., Qu, W., Du, A., 2005. Re-Os isotopic dating of molybdenite and pyrite in the Baishan Mo-Re deposit, eastern Tianshan, NW China, and its geological significance. *Mineralium Deposita* 39, 960-969.
- Zhang, X., Zheng, Y., Ni, L., 2004. Characteristics of middle Devonian Kanguertage formation volcanic from Kaerlike of east Tianshan. *Xinjiang Geology* 22, 296-299 (in Chinese with English abstract).
- Zhao, D., Lin, Z., Tang, X., 2007. Laplacian PCA and its applications. In: *IEEE Conference on Computer vision and Pattern Recognition (CVPR2007)* October 14-21 2007, 2007, pp. 1-8.

Zhao, J., Wang, W., Dong, L., Yang, W., Cheng, Q., 2012. Application of geochemical anomaly identification methods in mapping of intermediate and felsic igneous rocks in eastern Tianshan, China. *Journal of Geochemical Exploration* 122, 81-89.

Zhao, P., 1999. Theory and practice of Geoanomaly in mineral exploration, 1st ed. China University of Geosciences Press, Wuhan, China. 150pp. (in Chinese with English abstract).

Zhou, D., 1998. Geological compositional data analysis: difficulties and solutions. *Earth Science-Journal of China University of Geosciences* 23, 147-152 (in Chinese with English abstract).

Zhou, J., Cui, B., Xiao, H., Chen, S., Zhu, D., 2001. Kangguertag-Huangshan collision zone of bilateral subduction and its metallogenic model and prognosis in Xinjiang, China. *Volcanology & Mineral Resources* 22, 252-263 (in Chinese with English abstract).

Zhou, J., Zhang, B., Zhang, C., 1996. Geology of the silver, rhenium-molybdenum, gold and copper deposits in the eastern Tianshan and its adjacent regions. Geological Publishing House, Beijing (in Chinese).

Zhuang, D., Liu, T., Hu, J., Wang, X., 2003. The review and prospect of regional geochemical exploration in Xinjiang. *Geophysical & Geochemical Exploration* 27, 425-427 (in Chinese with English abstract).

Zuo, R., Cheng, Q., Agterberg, F. P., Xia, Q., 2009a. Application of singularity mapping technique to identify local anomalies using stream sediment geochemical data, a case study from Gangdese, Tibet, western China. *Journal of Geochemical Exploration* 101, 225-235.

Zuo, R., Cheng, Q., Xia, Q., 2009b. Application of fractal models to characterization of vertical distribution of geochemical element concentration. *Journal of Geochemical Exploration* 102, 37-43.

Zuo, R., Xia, Q., Wang, H., 2013. Compositional data analysis in the study of integrated geochemical anomalies associated with mineralization. *Applied Geochemistry* 28, 202-211.